JAEA-Review
2005-001

JP0650155

JAEA-Review

TIARA Annual Report 2004

Advanced Radiation Technology Department

Takasaki Advanced Radiation Research Institute

January 2006

Japan Atomic Energy Agency

日本原子力研究開発機構

JAEA-Review 2005-001

TIARA Annual Report 2004

Advanced Radiation Technology Department

Takasaki Radiation Chemistry Research Institute
Japan Atomic Energy Agency
Watanuki-machi, Takasaki-shi, Gunma-ken

(Received October 24, 2005)

This annual report describes research and development activities which have been performed with the TIARA (Takasaki Ion Accelerators for Advanced Radiation Application) facilities from April 1, 2004 to March 31, 2005. Summary reports of 121 papers and brief descriptions on the status of TIARA in the period are contained. A list of publications, the type of research collaborations and organization of TIARA are also given as appendices.

On 1st October 2005, Japan Atomic Energy Research Institute combined with Japan Nuclear Cycle Development Institute and establishes a new organization, Japan Atomic Energy Agency (JAEA).

This report describes the research and development activities which have been performed with JAERI (Japan Atomic Energy Research Institute).

Keywords: JAERI TIARA, Ion Accelerators, Solid State Physics, Radiation Effects in Materials, Materials for Space, Semiconductors, Organic Materials, Inorganic Materials, Nuclear Fusion Reactor, Functional Materials, Radiation Chemistry, Radiation Biology, Nuclear Medicine, Biotechnology, Radioisotope Production, Nuclear Chemistry, Radiation Shielding, Materials Analysis, Microbeam Technology, Accelerator Technology, Accelerator Operation, Safety Control

---

(Eds.) Yoshihiro OHARA, Kazuo ARAKAWA, Shigeru TANAKA, Kazumasa NARUMI, Masaru YOSHIDA, Hisayoshi ITOH, Masato YOSHIKAWA, Atsushi TANAKA, Yasuhiko KOBAYASHI, Mitsuhiro FUKUDA, Michiro OTSUBO, Watalu YOKOTA, and Yoshiteru NAKAMURA

イオン照射研究施設（ＴＩＡＲＡ）平成１６年度年次報告

日本原子力研究開発機構高崎量子応用研究所
放射線高度利用施設部

(2005年10月24日受理)

本年次報告は、イオン照射研究施設で、2004年4月1日から2005年3月31日までの間に行われた研究活動の概要をまとめたものである。１）宇宙用半導体、２）バイオテクノロジー、３）放射線化学および有機材料、４）無機材料、５）材料解析、６）核科学およびラジオアイソトープ製造、７）マイクロビーム応用、８）加速器施設の放射線遮蔽、９）加速器技術の９部門にわたる１２１編の研究報告に加えて、施設の運転保守・利用状況、公表された文献、企業・大学等との研究協力関係、研究開発・施設運営組織を収録する。

(本報告は、旧日本原子力研究所において行われた研究活動の概要をまとめたものである。)

高崎量子応用研究所：〒370-1292 群馬県高崎市綿貫町 1233

PREFACE

This report covers research and development activities which have been conducted with TIARA(Takasaki Ion accelerators for Advanced Radiation Application) during the period from April 2004 to March 2005, and also gives an outline of the operation of TIARA in the same period.

All accelerators in TIARA, the AVF cyclotron, the 3MV tandem accelerator, the 3MV single-ended accelerator and the 400kV ion implanter, have been operated steadily since the start of operation in 1993. The beam-time has been allocated to the research programs as evaluated in advance by the Subcommittee of TIARA of Advisory Council for JAERI's Research Facilities. In the meantime, available ion species and their energy ranges have been widened to meet the requirements from users, and the quality of ion beams have been improved intensively.

In the research on semiconductors used in space, radiation degradation of solar cells, single event phenomena (SEP) in integrated circuits, and development of radiation resistant devices have been investigated using TIARA. In radiation effects in solar cells, the electrical performance of InGaP/GaAs/Ge triple junction solar cells irradiated with protons was found to be recovered due to forward current injection at around 150K. Regarding SEP, malfunctions like multiple-bit upsets (MBUs) in highly integrated memory devices were examined and plausible mechanisms explaining the observed phenomena were proposed. In the study of SEP caused in terrestrial LSIs by cosmic-rays (high energy neutrons), transient currents induced in Si diodes by monoenergetic (65MeV) neutrons were successfully observed and shown to be quite similar to those by 65MeV protons. In the R&D of radiation resistant devices, SiC-based p-channel metal oxide semiconductor field effect transistors (MOSFETs) were developed and confirmed to have high radiation resistance.

In the field of biotechnology, heavy-ion induced bystander effects were investigated by detection of a phosphorylation of histone H2AX, micronucleus formation, G1 arrest and apoptosis in cells of mammalian or *C. elegans*, *etc.*, to elucidate the effects of low dose of high-LET radiations. The foci formation of DNA repair proteins induced by heavy-ion microbeam was also examined using immunofluorescence techniques. For the positron emitting tracer imaging system (PETIS), production method of positron emitting nuclide of Cd was developed and applied for the visualization of transportation of Cd in an intact plant. Using ^{107}Cd, transportation of Cd in a young rice plant was first visualized by using the PETIS. For mutation induction of plants, the ion beam breeding technique has been widely applied to great deal of crop improvements including environmental resistance and phytoremediation. As ion beams induce large but minimum amounts of DNA damage and mutation, re-irradiation of ion beams can be useful to produce superior varieties without conspicuous deficiency.

In the field of radiation chemistry and organic materials, the five studies by different research groups have been continued, except for a new subject regarding the creation of nano-gel channels by ion beam irradiation. In the formation of carbon backbone polymer based-nanowires, it was found that the length and thickness of nanowires could be completely controlled by changing film thickness and molecular weight of used polymers like the LET effect by ion beams. By using a new-type poly(*p*-phenylene terephthalamide) film belonging to nylon polymers, it was successfully found out for the first time in the world that it was possible to control the geometry of the etched tracks in the film from the funnel to cylindrical shape by varying the parameters such as ion species, energy, and track formation sensitivity.

In the field of nuclear fusion and advanced fission reactor materials, various kinds of experimental studies were performed. In order to simulate the effects of He and/or H produced through transmutation reactions, dual or triple ion-beams were irradiated onto the candidate fusion/fission reactor materials (reduced activation ferritic steel F82H, austenitic stainless steels, 316SS with laser alloying surface treatment, SiC/SiC composites, Li_2TiO_3). Effects of implanted helium and/or hydrogen atoms on thermo-mechanical properties (swelling, radiation hardening, stress-strain curves) as well as microstructural change in composition, by irradiation damage were investigated.

In the field of inorganic materials, the nitriding transformation mechanisms of Titanium thin films by nitride-implantation were clarified using in-situ TEM observations. The defects produced in single-crystal ZnO wide band-gap semiconductor by B^+ and O^+-implantations were studied using positron annihilation measurements and the formation and recovery mechanisms during high-temperature annealing were investigated. As for the formation of blisters in rutile TiO_2 (100) films by helium ion implantation, the suitable condition of helium implantation energy and fluence were determined and the helium blisters with ~100 nm in diameter were successfully fabricated.

Radiation effects of energetic electrons on phase transitions of metal and reversible deformation of Au foils have been investigated compared with those of energetic-ion irradiation in order to understand the nature of the effects. Spin coherence time of donors ion-implanted in SiC has been evaluated from a viewpoint of possible application to quantum computing; it has been concluded that the long spin coherence time of P donors in SiC relates to the large energy separation between the two electronic levels, $1s(A_1)$ and $1s(T_2)$, rather than the host material.

In the field of materials analysis, Rutherford backscattering spectrometry (RBS) and nuclear reaction analysis (NRA), well-established, conventional methods, are still powerful tools for the purpose. Optimal preparation of sulfur-concentration-controlled TiO_2 films has been explored with RBS. Analysis of hydrogen distribution which is crucial to properties of carbon materials was performed with NRA. Availability of cluster ions with wide range of energy has made it possible to apply low-energy C_{60} ions to the modification of a surface region as well as to study non-linear radiation effects of fast-cluster bombardment.

In the radioisotope production and nuclear science, production method of positron-emitting radiotracer of ^{107}Cd was developed for plant study. Applying the gradient-method to dissolve and separate ^{107}Cd from the ^{nat}Ag target, recovery yield of 93% was obtained. After the radiochemical separation, the ^{107}Cd was not contaminated by Ag. ^{107}Cd solution was supplied to an intact rice plant and succeeded in the visualization of transportation of ^{107}Cd.

In the field of microbeam applications, in-air micro-PIXE(Particle Induced X-ray Emission) and micro-PIGE(Proton Induced Gamma-ray Emission) techniques with high spatial resolution have been widely used for the research in medical, dental, environmental and materials sciences. Imaging of boron blocks, produced by segregation of boron atoms doped in steel, has succeeded first by the micro-PIGE technique. Characteristics of cloud have been investigated by the micro-PIXE analysis of Cl in a single cloud droplet to understand the cloud scavenging mechanism and the Earth's radiation budget. In the development of a 260 MeV $^{20}Ne^{7+}$ microbeam for investigation of cell radiation response, the beam spot size has reached to 2 micrometers by the precise re-alignment of beam transport elements and the improvement of a coil current power supply of a beam scanning magnet.

In the field of shielding for accelerator facilities, three experiments have been conducted aiming

to contribute to the radiation safety of accelerator facilities. The first one is on a characterization of various radioactive aerosols and gases formed by 50MeV proton irradiation. It was found that ^{38}Cl and ^{39}Cl exist as aerosol, acidic gas and non-acidic gas. The second one is on a measurement of secondary heavy charged particle spectrum produced by 75MeV neutron induced reactions. The energy spectrum of fragments has been obtained by using a Bragg curve spectrometer. The third one is on an evaluation of the property for quasi-monoenergetic neutron calibration fields of high energies at TIARA. The neutron beam profile has been measured by using the imaging plate.

In the field of accelerator technology, various developments have been carried out to improve the accelerator performance. In the cluster ion beam research, the secondary ion emission from a HOPG target bombarded by carbon cluster ions (Cn, n=1～8) were measured with a TOF mass spectrometer, and a considerable difference between the positive and negative ion yields was observed. The average charge state of the constituent atoms of a carbon cluster was measured, showing a clear dependence of the charge state on the cluster structure. In the development of a flat-top acceleration system for the cyclotron, a new probe has been mounted at the beam extraction region to measure the turn-separation. This probe enables us to tune the single turn extraction in a short time, which contributes to reduce the beam loss and the subsequent radio-activation of the cyclotron. A beam writing function has been combined with the microbeam scanning system of the single-ended accelerator, which allows preset pattern irradiation on a sample for micro-machining.

The TIARA accelerators have been utilized smoothly in the 2004 fiscal year and the operation time of each accelerator was 3455 hours, 1915 hours, 2491 hours and 1845 hours for the AVF cyclotron, the tandem accelerator, the single-ended accelerator and the ion implanter, respectively. The TIARA accepted 129 experimental subjects, whose number is the largest so far. The radiation safety controls and radioactive waste managements were also steadily carried out.

The reception of the users, the supports on utilizations of the experimental apparatus, and safety management of the radiation controlled area have been conducted smoothly.

The Fourteenth TIARA Research Review Meeting was held on June 23 and 24, 2005 in Takasaki, of which subjects were reported in this issue. Thirteen oral and one hundred and eight poster papers, and one invited lecture were presented. Three hundred and twenty seven persons participated in the meeting.

We owe the progress mentioned above to the advice of the Consultative Committee for Joint Research Project and the Subcommittee of TIARA of Advisory Council for JAERI's Research Facilities.

Yoshihiro Ohara, Director
Advanced Radiation Technology Center
Takasaki Radiation Chemistry Research Establishment

This is a blank page.

Contents

This is a blank page.

1. Semiconductor for Space

1.1 Electrical Characteristics of III-V Compound Solar Cells Irradiated with Protons at Low Temperature

M. Imaizumi,* T. Sumita,* S. Kawakita,* K. Shimazaki,* K. Kibe,*
T. Ohshima** and H. Itoh**
Institute of Space Technology and Astronautics, JAXA*
Department of Material Development, JAERI**

1. Introduction

Multi-junction solar cells based on III-V compounds are regarded as promising space solar cells due to their superior high efficiency. At present, an efficiency of 31.5 % (AM1.5, 1 sun) has been achieved by using InGaP/(In)GaAs/Ge triple-junction (3J) solar cells[1]. In addition, such multi-junction solar cells possess high radiation resistance[2]. For space applications, it is necessary to accurately predict the degradation of the electrical performance of solar cells due to irradiation by charged particles such as electrons and protons. Generally, the electrical performance of solar cells degrades as a function of particle fluence. However, it was reported that the electrical performance of electron-irradiated InP solar cells was recovered by using current injection [3-4]. Because the lifetime of solar cells is affected by the recovery of electrical performance, it is very important to understand their recovery mechanism. Defects created by irradiation are expected to play an important role in the recovery mechanism, and the annealing of the defects might be affected by temperature. Therefore, to study the effects of temperature on radiation degradation is very important. In particular, because thermal-annealing effect can be suppressed at low temperature, it is very informative to observe change in performance of solar cells irradiated at low temperatures.

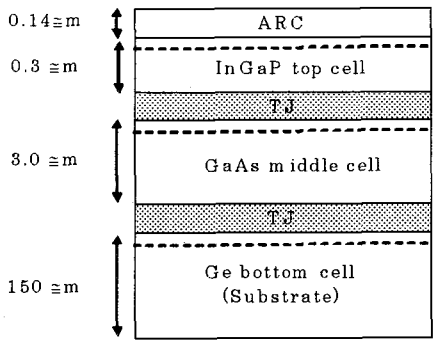

Fig.1 Schematic cross section of the 3J solar cell used in this study.

2. Experimental

The solar cells used in this study are InGaP/GaAs/Ge 3J space solar cells. The thicknesses of the InGaP top cell and the GaAs middle cell is 0.3 and 3.0 μm. Each subcell is connected using tunnel-junction (TJ) diodes. An anti-reflection coating (ARC) with a thickness of 0.14 μm is applied to the cells. The schematic cross section of the cell is shown in Fig. 1. The conversion efficiency of the cells (2cm×2cm) under AM0, 1-sun is about 27 %. The cells were irradiated with 10 MeV protons at the ion irradiation facility (TIARA) of the Japan Atomic Energy Research Institute, Takasaki. The proton irradiation was performed at 175 K under dark condition to avoid both current generation and thermal annealing effects. Since the projection range of 10-MeV protons is longer than the thickness of the cells, incident protons passed through the entire cells. After irradiation, light irradiation using an AM0 solar simulator (1-sun) was carried out at the same temperature. In this case, solar cells were kept under short circuit conditions, and the electrical performance was measured every five minutes. Besides, the current injection effect on the electrical performance of the irradiated cells was also studied. To avoid thermal-annealing effects, the current injection was done at 155 K. For the injection, a forward bias of ~3V was applied under dark conditions in order to inject a forward current of ~0.5 A/cm^2 into the cells. The electrical characteristics of the cells were measured *in situ* in the irradiation chamber. The details of this simultaneous measurement technique are described in ref[6].

3. Results and Discussion

Figure 2 shows the 10 MeV proton fluence dependence of short circuit current, Isc, (squares), open circuit voltage, Voc, (circles) and maximum power, Pmax, (triangles). The proton irradiation and the measurement were performed at 175 K. The closed symbols depict the results obtained from the low-temperature experiment. For comparison, the results for solar cells irradiated with protons at room temperature (RT) are also plotted with open symbols in the figure (The measurement was also done at RT). The Isc, Voc, and Pmax values plotted in the figure are normalized by the value before irradiation. The three values decrease with increasing proton fluence. At proton fluences of 1×10^{13} cm^{-2}, the Isc and Voc become about 87 and 80 % of the initial values. In the case of space Si solar cells, Isc and Voc become 70 and 75 % at 10 MeV-proton fluences of 3×10^{13} cm^{-2} [7]. Therefore, the results obtained in this study indicate that the 3J cells have higher radiation

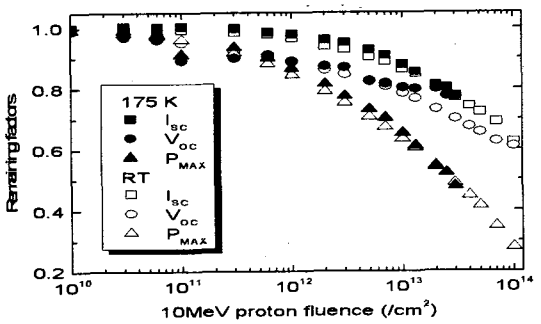

Fig. 2 10 MeV-proton fluence dependence of remaining factor of I_{SC} (squares), V_{OC} (circles) and P_{MAX} (triangles). The proton irradiation and the measurement were performed at

resistance than the Si cells. No significant difference in degradation behavior can be observed between low-temperature and RT irradiations. Since the electrical performance of solar cells is degraded by defects created by irradiation, the obtained result suggests that the type and the concentration of defects created at 175 K are similar to those created at RT.

Following the proton irradiation until the fluence of 3×10^{13} cm^{-2} at 175K, light illumination was carried out at the same temperature. Figure 3 presents changes in Isc and Voc for the proton-irradiated 3J cells at 175 K as a function of light-illuminated time by an AM0 solar simulator. Squares and circles represent the results of Isc and Voc. The plotted values are normalized by the values right after the proton irradiation. The values of both Isc and Voc do not change after 370 minutes of the AM0 illumination, meaning that no effect of light-soak annealing effect on the electrical performance of the 3J cells is observed. Thus, the obtained results suggest that the defects created in the 3J cells by the proton irradiation are not affected by AM0 light-illumination at 175 K. Throughout this study, light illumination using an AM0 simulator (1 sun) was performed. The results obtained in this study also indicate that no significant thermal

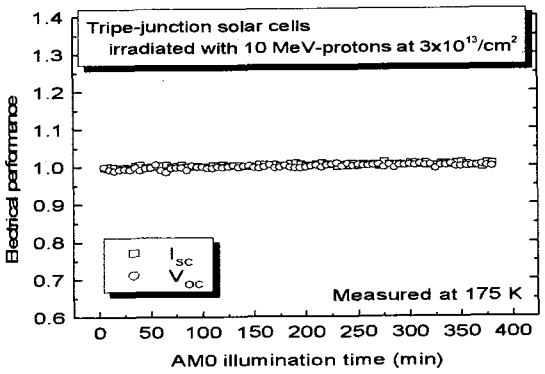

Fig. 3 I_{SC} and V_{OC} for 3J solar cells irradiated with protons at 175 K as a function of illumination time by an AM0 solar simulator. The plotted values of I_{SC} and V_{OC} are normalized by the values after proton irradiation.

annealing effect on the electrical performance is observed at 175 K.

Next, the effects of current-injection are described. The values of Isc and Voc for the 3J cells irradiated with protons at 175 K as a function of current-injection time are shown in Fig. 4. The electrical performance of the solar cells was measured at 155 K. Open and closed symbols depict the values of Isc and Voc, respectively. The values plotted in the figure are normalized by their values after the proton irradiation with fluence of 3×10^{13} cm^{-2}. Since the Isc and Voc decrease to approximately 80 % of their initial values right after the irradiation (*cf.* Fig. 2), the value "1.25" on the y-axis corresponds to the value before the proton

irradiation. Although the current injected into the cells was not controlled but forward bias of ~3 V was applied to the cells during the experiment, the current was nearly constant at approximately 0.5 A/cm^2. Both the Isc and Voc increase with increasing current-injection time, and the values become ~1.10 after the injection of 4500 seconds. Since the measurement temperature was kept at 155 K, this recovery of the electrical performance is thought to be due to carrier-injection annealing rather than thermal annealing. Yamaguchi et al[4]. reported that defects in InP showed a recovery by current-injection at around 200 K. Khan et al.[5] also reported that radiation-induced defects in InP (labeled H2 and H3) decreased by the

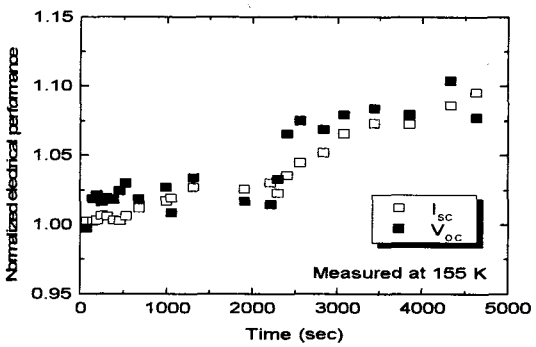

Fig. 4 The values of I_{SC} and V_{OC} of 3J solar cells irradiated with protons until fluence of 3×10^{13} cm^{-2} at 175 K as a function of current injection time. The values of I_{SC} and V_{OC} plotted in the figure are normalized by the value after proton irradiation. The measurement was carried out at 155 K.

minority-carrier injection and that the electrical performance of InP solar cells was recovered at RT. Therefore, the results obtained in this study suggest that the recovery of the electrical performance of InGaP and/or GaAs sub-cells occurs by carrier-injection. Since the value of the injected current was not controlled, the annealing rate cannot be estimated in this study. In order to determine the annealing rate, we intend to study the carrier injection effects using an external constant-current source.

4. Summary

Triple-junction solar cells designed for space applications were irradiated with 10 MeV protons at 175 K. The electrical performance of the cells was measured at 155 K. The output electrical performance decreased with increasing proton fluence, and at the fluence of 1×10^{13} cm^{-2}, Isc and Voc became 87 and 80 % of their initial values. No significant difference in degradation behavior of the electrical performance was observed between low temperature and RT irradiations. The effect of light illumination on the cells irradiated with 10 MeV protons was investigated using an AM0 solar simulator at 175 K. The electrical performance did not change after 370 minutes of illumination. With current injection at 155 K, the electrical performance of the proton-irradiated cells showed ~10% recovery after the current injection of 4500 seconds. However, because the effect of light illumination on the electrical performance of solar cells may depend on the intensity and wavelength-spectrum of the light source, further investigations are necessary to clarify the effects.

References

1) T. Takamoto, T. Agui, K. Kamimura, M. Kaneiwa, M. Imaizumi, S. Matsuda, M. Yamaguchi, Proc. of 3rd World Conference on Photovoltaic Energy Conversion, Osaka (2003), 3PL-C2-01.

2) M. Imaizumi, T. Takamoto, T. Sumita, T. Ohshima, M. Yamaguchi, S. Matsuda, A. Ohi, T. Kamiya, Proc. of 3rd World Conference on Photovoltaic Energy Con-version, Osaka (2003), 3O-D6-02.

3) M. Yamaguchi, K. Ando, A. Yamamoto, C. Uemura, Appl. Phys. Lett. 44 (1984), 432-434.

4) M. Yamaguchi, T. Takamoto, E. Ikeda, H. Kurita, M. Ohmori, K. Ando, C. Vargas-Aburto, Jpn. J. Appl. Phys. 34 (1995) 6222-6225.

5) A Khan, M. Yamaguchi, N. Dharmaso, J. Bourgoin, K. Ando, T. Takamoto, Jpn. J. Appl. Phys. 41 (2002) 241-1246.

6) S. Kawakita, M. Imaizumi, M. Yamaguchi, K. Kushiya, T. Ohshima, H. Itoh, S. Matsuda, Jpn. J. Appl. Phys. 41 (2002) L797-L799.

7) Y. Morita, T. Ohshima, I. Nashiyama, Y. Yamamoto, O. Kawasaki, S. Matsuda, J. Appl. Phys. 81 (1997) 6491-6493.

1.2 Development of Electrical Performance Measurement Technique for Space Solar Cells under Proton Irradiation at Low Temperature

T. Ohshima*, T. Sumita**, M. Imaizumi**, S. Kawakita**,
K. Shimazaki**, K. Kibe** and H. Itoh*
Department of Material Development, JAERI*
Japan Aerospace Exploration Agency (JAXA)**

1. Introduction

Multi-junction solar cells based on III-V compounds are suitable for space applications because of their high photoelectric conversion efficiency as well as high radiation resistance. At present, an efficiency of 31.5 % (AM1.5, 1 sun) has been achieved for triple-junction (3J) solar cells (InGaP/(In)GaAs/Ge). For the development of space solar cells, it is very important to understand degradation mechanisms of the electrical performance of solar cells due to irradiation of high-energy particles such as electrons and protons. In general, the electrical performance of solar cells degrades with increasing particle fluence.

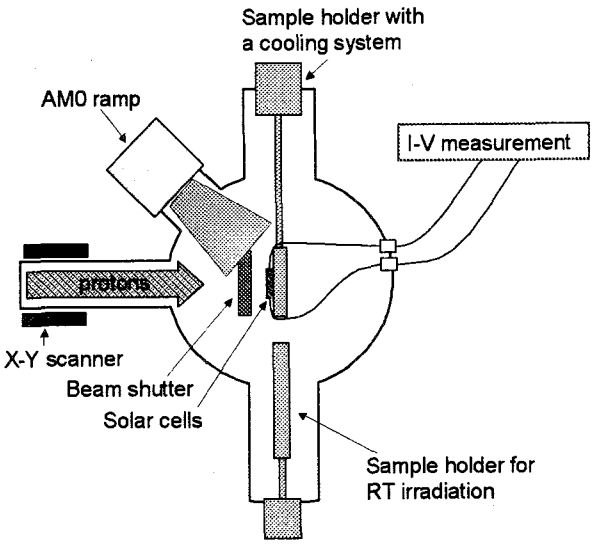

Fig. 1 Schematic top view of the vacuum

On the other hand, it was reported that the electrical performance of electron-irradiated InP solar cells was recovered by current injection[1, 2]. This result suggests that annealing behavior of residual defects is influenced by injected carriers, e.g., partial annealing of irradiation induced defects or their transformation into the other defects that do not act as carrier scattering centers. However, mechanisms of such a current injection effect have not been clarified yet. Since the annealing behavior of defects is strongly dependent on temperature, temperature control under proton irradiation and current injection is very important. In order to suppress thermal annealing of defects, it is very useful to lower temperature of solar cells during proton irradiation.

In this study, we have developed *in situ* measurement technique of the electrical performance of solar cells at low temperatures.

2. Proton Irradiation Chamber

The irradiation chamber was installed at the LD1 port at the ion irradiation facility (TIARA) of the Japan Atomic Energy Research Institute, Takasaki. In this chamber, solar cells can be irradiated with protons at energies of 10 to 90 MeV. Figure 1 shows the schematic top view of the chamber, which has two sets of sample holders. One is a sample holder for proton irradiation at room temperature (RT). The other one, which was

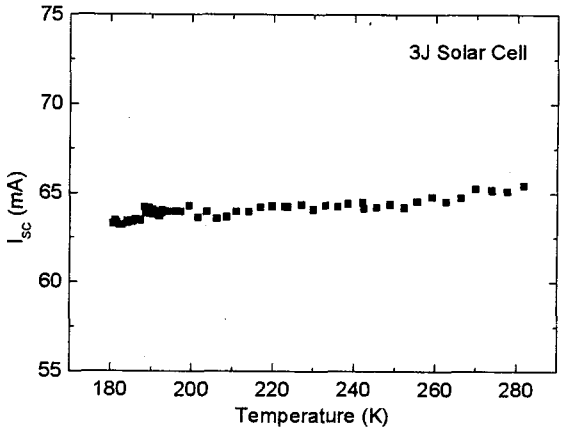

Fig. 2 Temperature dependence of I_{SC} for 3J solar cells before irradiation.

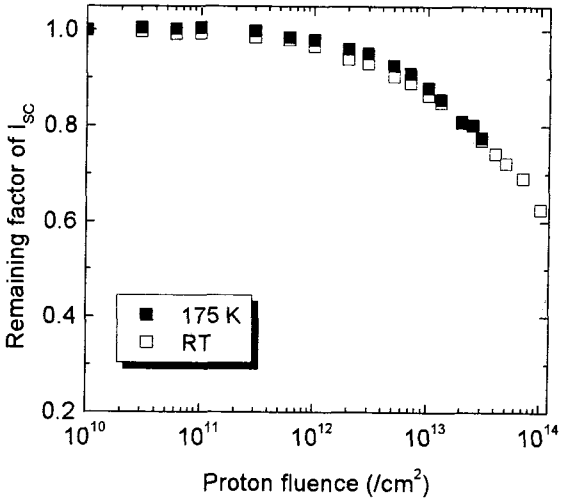

Fig. 3 Remaining factor of I_{SC} for 3J solar cells as a function of 10 MeV-proton fluence. Closed and open symbols represent the results obtained at 175 K and RT irradiation, respectively.

installed in this year, is connected with a cooling system. Since an AM0 solar simulator ramp is also installed in this chamber, the electrical performance of solar cells can be measured *in situ* under proton irradiation at RT or low temperatures. The current (I) – voltage (V) characteristics were immediately collected using a measurement system controlled using a computer. Scanned proton beams (maximum size 10 cm x 10 cm, the fluctuation of beam uniformity within 5%) can be formed by an X-Y scanner.

3. Results and Discussion

Figure 2 shows the temperature dependence of short circuit current (I_{SC}) for the 3J solar cells before irradiation. The cell temperature was swept from RT to 180K. The value of I_{SC} decreases with decreasing temperature. This behavior can be interpreted in terms of a change in hysical properties of semiconductors *i.e.* bandgap.

Figure 3 shows the remaining factor of I_{SC} for the 3J solar cells as a function of 10 MeV-proton fluence. The proton irradiation and the I-V measurements were performed at 175 K(closed symbols). For comparison, the results obtained for solar cells irradiated with protons at RT are also plotted as open symbols in the figure (The I-V measurements were also done at RT). The value of I_{SC} decreases with increasing proton fluence. At a proton fluence of $1x10^{13}$ /cm^2, I_{SC} becomes approximately 87 % of that before irradiation. In the case of Si solar cells developed for space application, it was reported that I_{SC} became 70 % at 10 MeV-proton fluences around $1x10^{13}$ /cm^3[3]. Therefore, the results obtained in this study indicate that the 3J solar cells have higher radiation resistance than Si solar cells. No significant difference in degradation behavior is observed between low temperature and RT irradiations. In addition, the electrical performance of the 3J solar cells irradiated with 10 MeV-protons at $3x10^{13}$ /cm^2 did not change even after keeping 370 min at 175K. This result indicates that thermal annealing does not occur at around this temperature. Thus, the current injection effects in the 3J

solar cells can be separated from thermal annealing effects at around 175K. At the next stage, we will examine the current injection effects in the 3J solar cells irradiated with protons at low temperatures around 180K.

4. Summary and Future plan

Proton irradiation and I-V measurement technique at low temperatures for space solar cells were developed. The degradation of electrical performance of the InGaP/(In)GaAs/Ge 3J solar cells due to 10 MeV proton irradiation was successfully measured at 175 K.

For the next step, we intend to study current injection effects on the electrical performance of the 3J solar cells. In addition, the degradation of the electrical performance of $CuInGaSe_2$ (CIGS) solar cells will be investigated to reveal mechanisms behind anomalous recovery found in the CIGS solar cells.

References

1) M. Yamaguchi, K. Ando, A. Yamamoto, C. Uemura, *Appl. Phys. Lett.* **44** (1984) 432-434.
2) A Khan, M. Yamaguchi, N. Dharmaso, J. Bourgoin, K. Ando, T. Takamoto, *Jpn. J. Appl. Phys.* **41** (2002) 1241-1246.
3) Y. Morita, T. Ohshima, I. Nashiyama, Y. Yamamoto, O. Kawasaki, S. Matsuda, *J. Appl. Phys.* **81** (1997) 6491-6493.

1.3 Analysis of Angular Dependence of Multiple-Bit Upsets in a Synchronous SRAM

H.Shindou*, N.Ikeda*, S.Kuboyama*, S.Matsuda*,
T.Hirao** and H.Itoh**
Japan Aerospace Exploration Agency (JAXA) *
Depertment of Materials Development, JAERI**

1. Introduction

Radiation tolerance of recent memories has been decreasing because up-to-date devices have fine structures and low critical charges for operation. A decrease in the critical charge raises the rate of Single Event Upsets (SEUs). It also leads to the fact that SEUs occur in highly integrated devices even by protons having low linear energy transfer (LET). Down sizing of the memory cell structure also facilitates the occurrence of Multiple Bit Upsets (MBUs) because of small separation between the adjacent cells. Since artificial satellites and spacecrafts fly in proton-rich environments around the earth, it is very important to evaluate the susceptibility of MBUs in state-of-the-art memories by protons as well as heavy ions.

It was reported that upsets caused by protons were isotropic[1]. On the other hand, Koga et al. reported an anisotropy of proton-induced upsets for the first time.[2] Reed predicted the angular dependence of proton-induced upsets by using computer simulation and experimentally demonstrated it[3]. Buchner et al. also observed the angular dependence of MBUs caused by protons in DRAMs and clarified three key factors to determine the dependence, which were proton energy, cell geometry and critical charge of the cell[4].

In this paper, we report the experimental results of MBUs caused in SRAMs by irradiation of protons and heavy ions. The dependence of the MBU susceptibility on incident ion angle, which is hereafter called the angular dependence of MBU, was examined. The relation between the MBU susceptibility and the arrangement of sensitive transistors in adjacent cells was also analyzed.

2. Experimental

A test structure of synchronous 9 Mbit (18 bit x 512k Word) SRAM was used in this study (Fig.1). This sample consisting of six-transistor memory cells was fabricated by 0.18 μm CMOS/Bulk technology. The cell pitch was 2.47 μm along the bit lines and 1.99 μm along the word lines. Schematic image of the cell layout in a basic cell unit (2 x 2 bit) is shown in Fig.2. Two sensitive (OFF-state) transistors, one was n-type and the other p-type, were located diagonally in each cell. The arrangement of transistors in each cell was symmetrical to its adjacent cells.

We used 30 and 70MeV protons and 450MeV Xe ions in the MBU tests. The device was operated in a static mode during irradiation, i.e., initial data was written

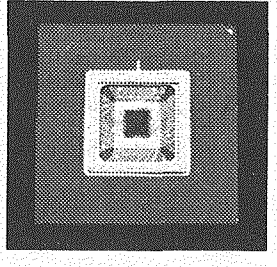

Fig. 1 Test sample. (9Mbit synchronous SRAM)

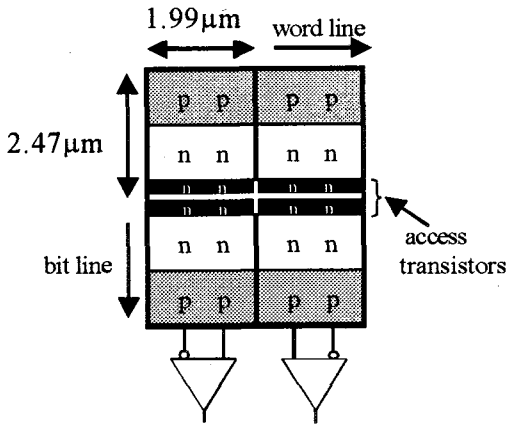

Fig.2 Schematic image of the cell layout

before irradiation and read back and checked after the irradiation. The device was irradiated from three directions, which were normal (0°), 80° along the bit lines, and 80° along the word lines, to examine the angular dependence of the MBU sensitivity. Each cell memorized "0" or "1" by controlling the ON/OFF state of a diagonally located transistor pair. There are several patterns in location of the closest sensitive transistors in adjacent cells. Figure 3 shows all the possible arrangements for 2 bit MBUs and their mnemonic codes. Either "0" or "1" was written in each cell so that the device included all these patterns.

3. Results and discussion

Figs.4 and 5 show the dependence of the MBU cross-section on the MBU pattern when irradiated with 70MeV protons and 450MeV Xe ions, respectively, at different angles. On the whole, the cross sections obtained for the p-transistor- related patterns were larger than those for n-transistor-related patterns. It is attributable to the fact that the sensitive area (the drain region) of p-transistors is smaller than that of n-transistors and that the critical charge for upsetting p-transistors is low compared with that for n-transistors. In the case of proton irradiation along the word line, the pattern "PN" was dominant. It seems consistent because the "PN" is a lateral MBU and the two adjacent cells upsetting simultaneously are aligned along the incident proton direction. On the other hand, the "PN" MBU also exhibited large cross sections even in the cases of irradiation along the bit line and normal, as shown in Fig.4. It can be explained by the assertion that the pattern "PN" is caused by an ordinary SEU and the following electrical propagation to adjacent cell takes place under the condition of the specific layout of sensitive transistors. This type of MBU can occur under normal SEU conditions. Thus it can be caused by protons with relatively low energies and its cross section is independent of the incident angle of protons. Although this MBU mechanism is quite different from that of the usual MBUs, it is very interesting and may be

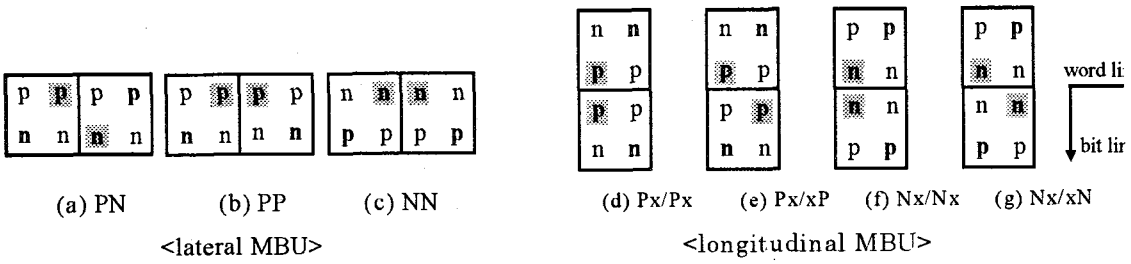

Fig.3 MBU test patterns

Sensitive transistors are shown in bold letters, and the closest pair of the sensitive transistors is colored in gray.

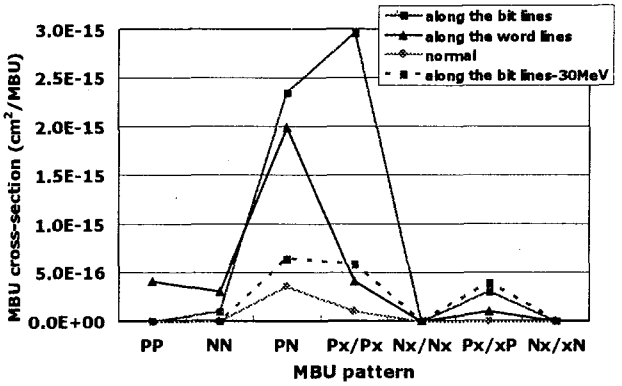

Fig.4 Dependence of the MBU cross section on the test pattern for the sample irradiated with 70MeV protons at different incident ion angles.

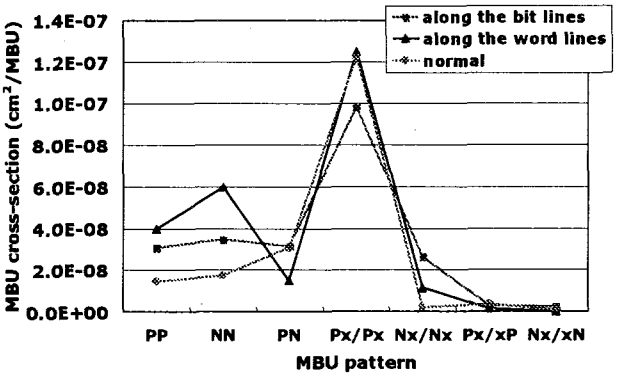

Fig.5 Dependence of the MBU cross section on the test pattern for the sample irradiated with 450MeV Xe ions at different incident ion angles.

common to many SRAM designs.

For the MBU patterns excepting the "PN", it is expected that the cross section of the MBUs in which sensitive transistors in the adjacent cells were aligned along the incident ion track (e.g.,"PP" and "NN" for irradiation along the word lines, "Px/Px" and "Nx/Nx" for irradiation along the bit lines) shows high values in comparison with that of the other patterns. However, the experimental results indicate that only the pattern "Px/Px" exhibited a considerably large cross section. This result can be related to the in-between structure of the two sensitive areas (drain regions) in concern.

In the case of Xe irradiation, the cross-section was much higher than that of the proton case, because LET of 450MeV Xe ions is very large (69 MeV/(cm^2/mg)). The cross-section of the pattern "PN" was not dominant in the case of Xe irradiation.

4. Summary

The angular dependence of MBU cross section was found for the first time in synchronous SRAMs fabricated with CMOS/Bulk technology when irradiated with high-energy protons and Xe ions. The pattern "PN" showed large MBU cross sections in the case of proton irradiation but not in Xe ion irradaition. Careful MBU examinations should be performed for highly integrated memory devices in order to apply those devices for space use.

References

1) S.D.K. Nichols, W.E. Price, L.S. Smith and G.A. Soli, IEEE Trans. Nucl. Sci. NS-31 (1984) 1565-1567.
2) R. Koga, W. A. Kolasinski, J. V. Osborn, J. H. Elder and R. Chitty, IEEE Trans. Nucl. Sci., NS-35 (1988)1638-1643.
3) R.A. Reed, IEEE Trans. Nucl. Sci. NS-49 (2002) 3038-3044.
4) S. Buchner, A. Campbell, R. Reed and S. Kuboyama, IEEE Trans. Nucl. Sci. NS-51 (2004) 3270-3277.

1.4 Single Event Effects on SRAMs

K. Ohnishi*, Y. Takahashi*, T. Abe*, T. Hirao**, S. Onoda** and H. Itoh**
Dept. of Electronic and Computer Science, College of Sci. and Tech., Nihon University*
Department of Material Development, JAERI**

1. Introduction

One of the most detrimental effects of radiation on semiconductor devices is single-event effects (SEEs). When a high-energy heavy ion strikes a memory device, electron-hole pairs are generated along the ion-track and they can induce sufficient transient current to cause a malfunction called single-event upset (SEU). In this work, heavy-ion induced SEUs in SRAMs have been investigated.

2. Experimental procedure

1Mbit CMOS SRAM (HM628128DLP-5, 128kwords×8bits) devices were irradiated with heavy-ions using an AVF cyclotron in JAERI Takasaki. Figure 1 shows the experimental setup.

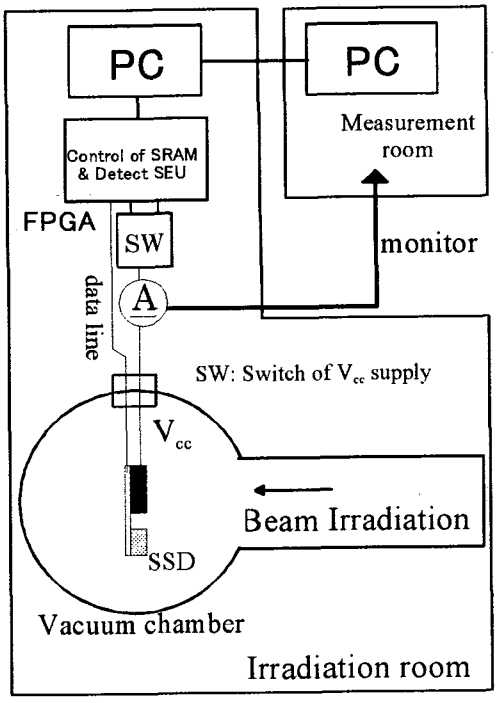

Fig.1 Experimental setup.

Table 1 Irradiation conditions

Ion	Energy [MeV]	LET [MeV/(mg/cm^2)]	Project Range [μm]
$^{15}N^{3+}$	53	3.423	50.09
$^{12}C^{3+}$	75	1.823	114.96
$^{20}Ne^{4+}$	75	6.329	42.47
$^{16}O^{4+}$	100	3.107	95.23
$^{40}Ar^{8+}$	150	15.11	38.55
$^{84}Kr^{17+}$	322	39.92	40.86

The semiconductor chip was bared by removing a part of plastic package, and irradiated with ion beams in a vacuum chamber. Table 1 shows the linear energy transfer, LET, and the project range of each heavy ion used in this experiment.

Data reading and writing from/to the memory were controlled by FPGA. Data of [00]h or [FF]h were written into all addresses before irradiation. After irradiation, the read-out data were compared with the initial data by FPGA. When unmatched data were detected, FPGA send the error information to PC as SEU detection report. We also measured the current of power supply during irradiation.

3. Experimental results

Figure 2 shows the number of upset bits as a function of ion beam fluence. The number of upset bits is in proportion to the fluence. It was also found that the number did not depend on the initial data ([00]h or [FF]h). The number of upset bits at the ion fluence of 1cm^{-2}, SEU cross-section, increases with LET of irradiated ions, as shown in Fig. 3. The SEU cross section

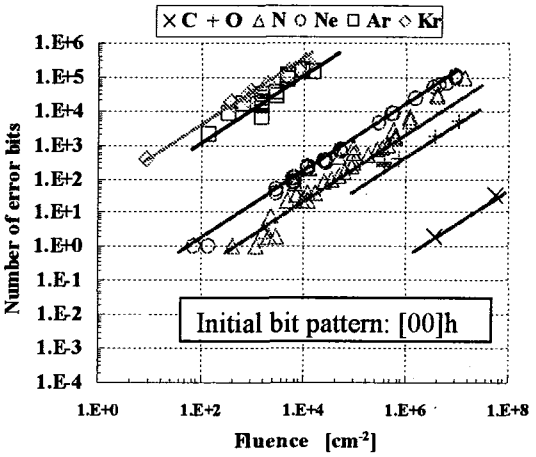

Fig.2 Number of upset bits as a function of fluence.

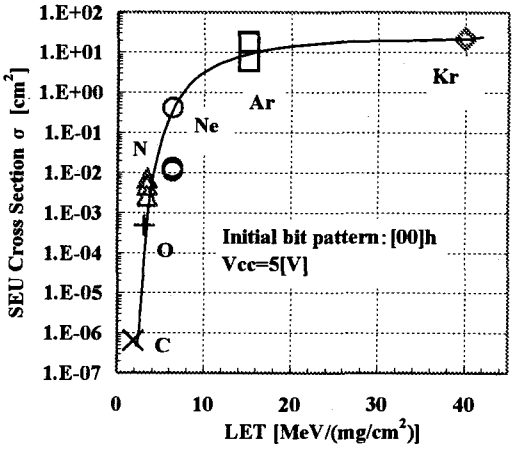

Fig.3 SEU cross section as a function of LET.

is saturated at about 15 MeV/(mg/cm^2), and the saturated cross-section is larger than 10 cm^2. Because the chip size is about 0.25 cm^2, the obtained large values of the saturated cross-section suggest that more than 40 bits are simultaneously upset by hitting a single ion with such high LETs. It was reported that the multi-bit (several bits) upsets were observed in high density ICs.

Figures 4 and 5 show the changes in the supplied current during Ar ion irradiation with ion fluxes of 11 and 480 cm^{-2}s^{-1}, respectively. The current decreases as a series of pulses. It was also found that the amount of the current fluctuation and its frequency increase with the flux and LET of irradiated ions.

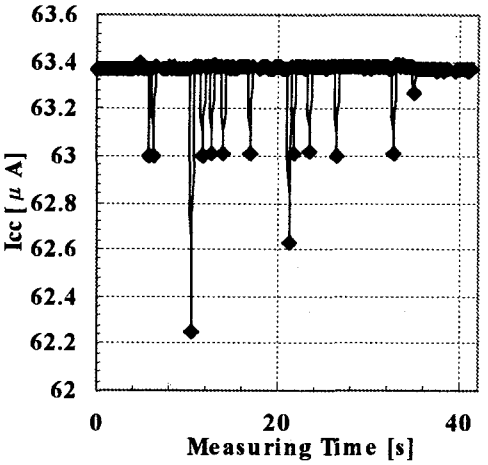

Fig.4 Supplied current during Ar irradiation (Flux = 11 cm^{-2}s^{-1}).

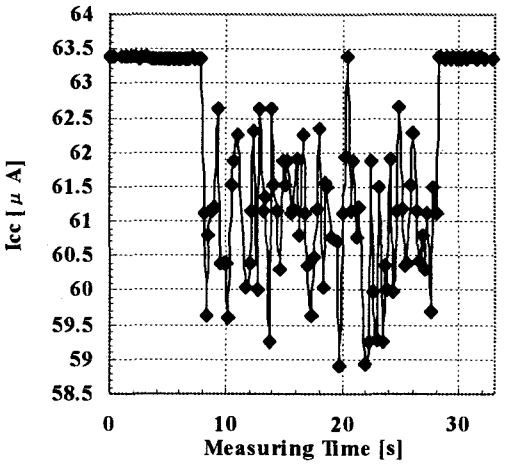

Fig.5 Supplied current during Ar irradiation (Flux = 480 cm^{-2}s^{-1}).

4. Discussion

In order to clarify the mechanism of the observed multi-bit upsets, we analyzed the address bits and the data bits of all upset data. Figures 6 and 7 show the data after Ne and Ar ion irradiations, respectively, as a function of memory address when the initial data was set [00]h. The pattern of upset data bit(s) induced by low LET ion (Ne) is independent of address. On the other hand, in the case of high LET ion (Ar) irradiation, the pattern changes every 1.6x10^4 =

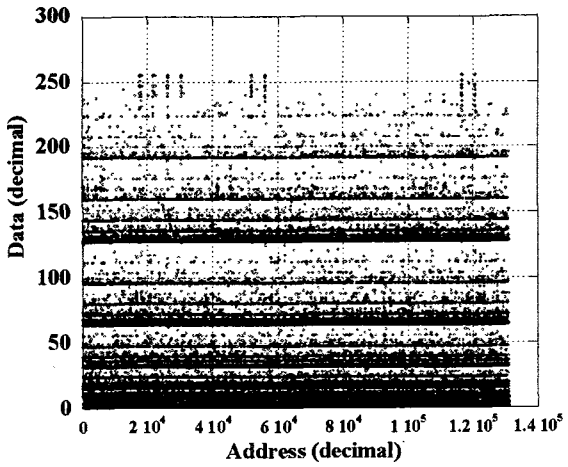

Fig.6 Address dependence of error data bits due to Ne irradiation.

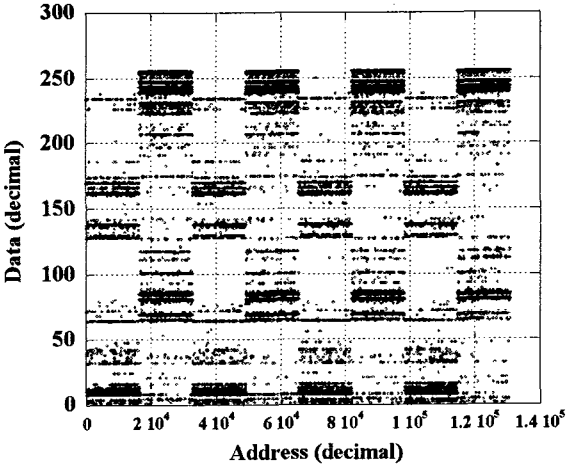

Fig.7 Address dependence of error data bits due to Ar irradiation.

2^{14} in memory address. It means the upset data bit depends on the state of 15th address bit (AD14). According to the data sheet, the AD14 is assigned as the least significant bit, LSB, of address column, and the column decoder is connected with I/O circuit. It was also found that the change of upset bit pattern was observed whenever a decrease of the supplied current was induced by irradiation, and that the change of the current was a multiple of 0.4 μA.

From these results, it can be concluded that the observed multi-bit upset is due to the incorrect action of column decoder that is caused by radiation induced transient current.

5. Summery

The heavy-ion induced SEUs in SRAMs have been investigated. From ion irradiation tests of 1Mbit CMOS SRAMs, it was found that unusual multi-bit upsets and decreases of supplied current were induced by irradiation of high LET ions like 150MeV-Ar. By analyzing the address bits and the data bits of all upset data, it was found that the pattern of upset data bit(s) induced by high LET ions depends clearly on the state of the specific address bit. It suggests the multi-bit upset is caused by incorrect action of column decoder.

JP0650160

1.5 Study on Layout Dependence of Soft Errors in CMOS Latch Circuits Fabricated by 65 nm CMOS Process

H. Fukui*, M. Hamaguchi*, H. Yoshimura*, H. Oyamatsu*, F. Matsuoka*, T. Noguchi*, T. Hirao**, H. Abe**, S. Onoda**, T. Wakasa** and H. Itoh**
TOSHIBA CORPORATION Semiconductor Company*
Department of Materials Development, JAERI**

1. Introduction

CMOS LSIs are widely used in various fields and become one of the most important elements constructing the infrastructure because both their characteristics and cost can be improved by shrinking the dimensions of CMOS devices. However, scaling of devices involves many serious problems. Increasing Single Event Upset (SEU) is one of the most serious problems, because it causes the operational errors of the system. It has been reported that when the gate length of MOSFETs becomes smaller than 50 nm, SEU caused by cosmic rays will affect the system operation even at the ground level[1]. Therefore, for mass production utilizing them, it is required to develop the method to suppress SEU induced by cosmic rays.

Our objective in this work is to develop the guideline to design the soft-error immune circuits utilizing CMOSFETs with the gate length below 50nm. We have performed accelerated soft error testing with proton beam for latches fabricated by 65nm CMOS process and clarified the dependence of SEU cross section on the physical layout.

2. Experiment

We have prepared the shift register with 80,000 flip-flop stages fabricated by 65nm CMOS process as shown in Fig. 1. It was composed of CMOSFETs with the gate length of 50 nm. Each flip-flop cell was connected in series. After 80,000 cycles of clock signal, data was output.

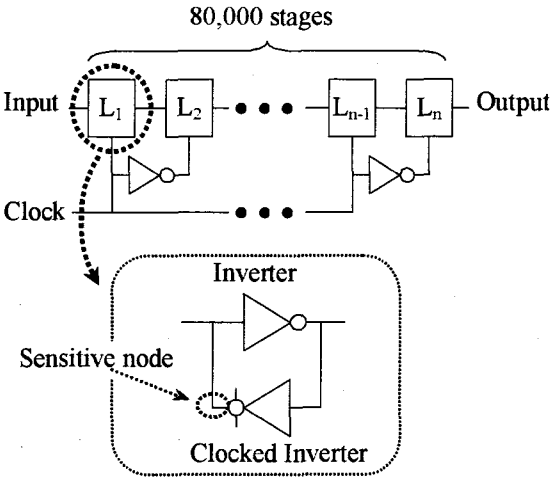

Fig. 1 Test circuit.

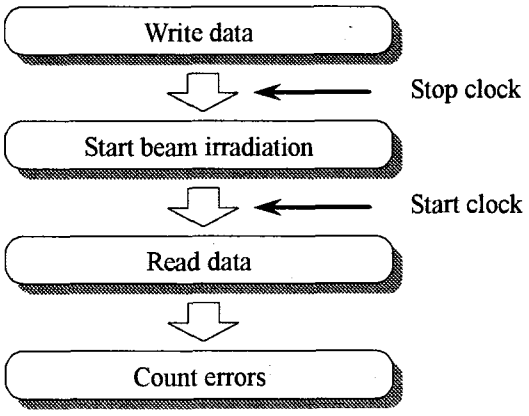

Fig. 2 Measurement procedures.

Figure 2 shows the measurement procedures. At first, initial data was written into each flip-flop cell. After that, the clock was stopped. Next proton beam irradiation started. Irradiation was kept in a constant time. Next, we started the clock and read the output. We compared the

output with the input and considered that SEU occurred when the output was different from the input. We have checked if SEU occurred for each flip-flop cell and summed up the error count. We have estimated the SEU cross section by the total error counts and the proton fluence.

Accelerated soft error testing was performed utilizing AVF Cyclotron at JAERI Takasaki. The test circuits were irradiated directly by a scanning proton beam in 5 minutes. The scanning frequency was 50Hz (X-axis) and 2.5Hz (Y-axis). The proton flux was measured by Faraday cup. The SEU measurements were done at the energies of 20, 30, 45, 55 and 75 MeV.

3. Results and Discussion

Figure 3 shows the relationship between the SEU cross section and the critical charge Q_{crit} at the radiation energy of 45 MeV. Q_{crit} was calculated by SPICE code. In Fig. 3, "High" or "Low" means that high or low level was initially written into all cells, respectively. It is shown that the SEU cross section decreases exponentially with increasing Q_{crit} in spite of the written data. This tendency was also observed at the other radiation energies. Figure 4 shows the SEU cross section as a function of the area of the sensitive node. Here, "sensitive" means that SEU is easy to occur. Closed and opened squares represent the SEU cross section in the n- and p-type sensitive nodes, respectively. It is found that the SEU cross section increases linearly with increasing the area of the node. Enlargement of the area of the node leads to an increase in the number of particles penetrating through it, which results in an increase in the SEU cross section. Figure 5(a) shows the relationship between the width w_n of nFET in the circuit and Q_{crit}. Closed and opened squares indicate Q_{crit} for electron and hole injection cases, respectively. It is shown that while Q_{crit} in the electron injection case is independent of w_n,

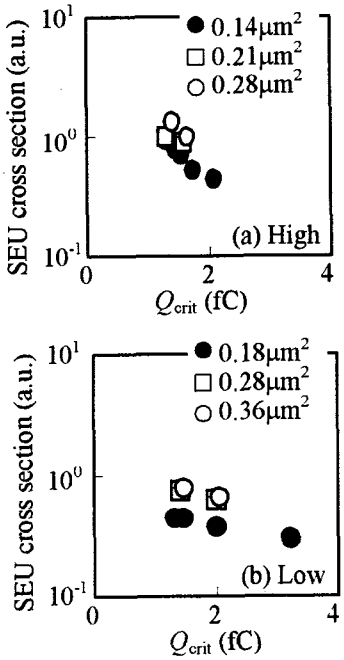

Fig. 3 SEU cross section as a function of the critical charge, Q_{crit}.

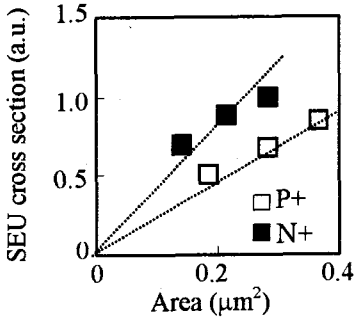

Fig. 4 SEU cross section as a function of the area of the sensitive node.

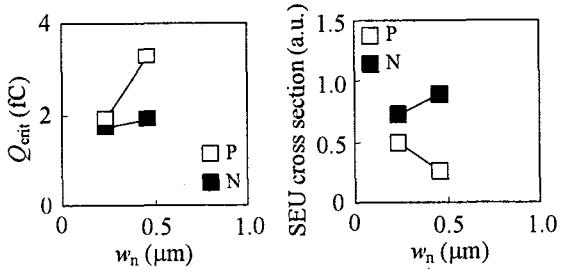

Fig. 5 (a) Q_{crit} as a function of w_n. (b) SEU cross section as a function of w_n.

Q_{crit} in the hole injection case increases with increasing w_n. As shown in Fig. 5(b), while the SEU cross section in n-type sensitive node increases with increasing w_n, the SEU cross section in p-type sensitive node decreases. This is explained as follows. In the n-type sensitive node, the SEU cross section increases because of the increase in the area of the node. In the p-type sensitive node, the SEU cross section decreases because of the increase in Q_{crit}.

4. Summary

In this work, we have performed accelerated soft error testing with proton beam for latches fabricated by 65nm CMOS process. We have clarified the dependence of the SEU cross section on the layout. It was found that the SEU cross section linearly increases with increasing the area of the sensitive node. The experimental results demonstrated that the SEU cross section depends on the width of MOSFET in the circuit. Therefore, in order to minimize the SEU cross section, it is necessary to optimize it.

References

1) R. Baumann, Technical Digest of IEDM (2002) 329-332.

1.6 Evaluation of Collected Charge Induced in Si PIN Diodes by Neutrons and Protons

T. Hirao*, H. Abe*, Su. Tanaka*, S. Onoda*,**, T. Wakasa*,**, T. Sanami***, H. Hirayama*** and H. Itoh*
Depertment of Material Development, JAERI*
Graduate School of Engineering, Tokai university**
High Energy Accelerator Research Organization, KEK***

1. Introduction

It is well known that when an energetic heavy ion passes through semiconductor devices in space, dense electron-hole plasma is generated along the ion track, leading to an assortment of single event phenomena (SEP) [1]. In recent years, as scaling down of the device size proceeds, neutron induced soft errors have become a serious problem in highly integrated devices used at the ground level [2-4]. In order to solve this problem and develop soft error free devices, it is necessary to clarify mechanisms behind neutron induced SEP. In this paper, we report experimental and theoretical investigations of single event transient (SET) currents, which play an important role in causing SEP, induced in Si devices by neutron irradiation. Proton induced SET currents are also shown and compared with neutron induced ones to consider the possibility of substituting protons for neutrons in SEP tests.

2. Experiments

The samples used in this study were commercial 1.5 GHz Si pin photodiodes with a diameter of 450 μm. The p^+-layer thickness was ~0.2 μm and the depletion layer thickness was ~15 μm at a bias of -20 V [5]. During all SET current measurements, a constant reverse bias of 20 V was applied to the samples.

A quasi-monoenergetic 65 MeV neutron beam was generated by using the ^{7}Li(p,n) neutron source facility[6]. The energy of primary protons accelerated by an AVF cyclotron was 70 MeV. For comparison, irradiation of 65 MeV protons was also performed. The fluxes of neutrons and protons were about 1×10^4 and 2×10^6 $cm^{-2}s^{-1}$, respectively. The SET current waveforms induced by neutrons were measured using a 3 GHz Tektronix 694C digital sampling oscilloscope (DSO) and time to amplitude converter (TAC) [7]. The SET currents induced by protons were also measured using 3 GHz DSO. Details of the measurement system have been described in the previous report [8].

3. Results and discussion

Figure 1 shows typical SET current waveforms induced by 65MeV neutrons in the Si pin photodiode under reverse bias at 20 V. A variety of SET current waveforms were observed. This variation is explained by the generation of secondary particles and fragments due to nuclear reactions of neutrons with Si nuclei. In order to compare the neutron and proton induced SEP, the normalized distributions of the collected charges obtained by integrating SET currents in the neutron and proton irradiated samples are shown in Fig. 2. As a result, the both distributions were found to be well agreed.

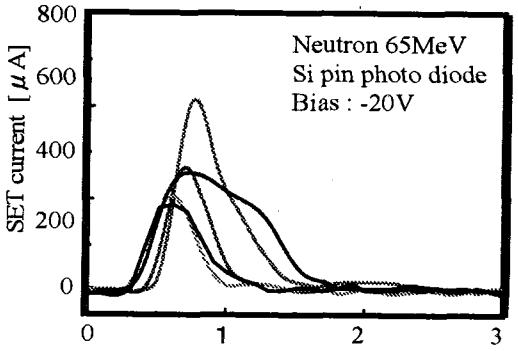

Fig. 1 Typical SET current waveforms induced in the Si pin photodiodes by 65 MeV neutrons at an applied bias of -20V.

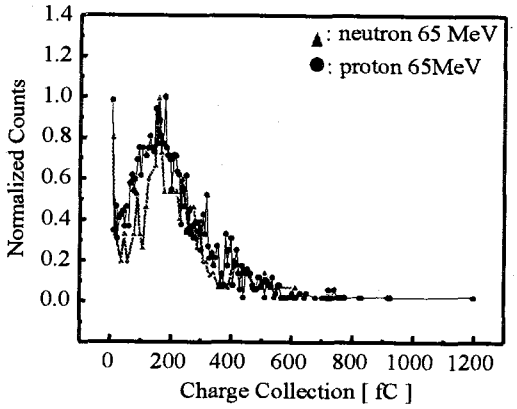

Fig.2 Normalized charge distributions induced in the Si pin photodiodes by 65 MeV neutrons and protons.

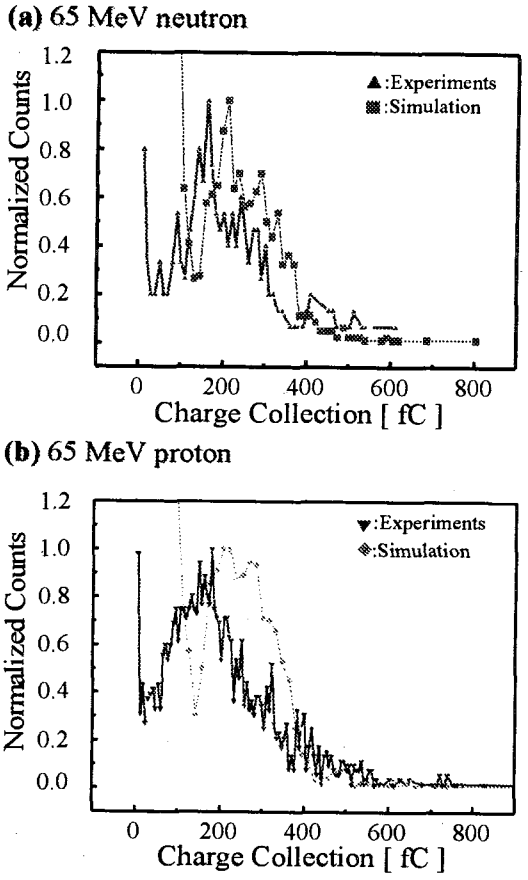

Fig.3 Normalized charge distributions derived from simulations and experiments for (a) 65MeV neutron and (b) 65MeV proton irradiations.

To discuss the charge distribution, we have simulated the nuclear reactions between nucleons and lattice Si using a PHITS (Particle and heavy ion transport code system) code [9] combined with a cross section library LA150 [10]. As a result of the PHITS simulation, the species of secondary generated nuclei, their positions, directions, and energies were obtained. From the obtained information, we derived the amount of charges collected in the Si pin photodiode samples.

Figure 3(a) shows the normalized distributions of the collected charges derived from the PHITS simulations and experiments for the neutron irradiation. On the other hand, the results obtained for the proton irradiation are displayed in Fig. 3(b). In both cases, the experimental results are well represented by the PHITS simulations, supporting that the collected charges are produced primarily by nuclear reactions of neutrons or protons with Si.

When neutrons and protons pass through electronic devices, several kinds of particles are secondarily generated due to nuclear reactions. These secondary particles containing proton, alpha, and heavy ions induce charges in the devices. Since neutrons and protons cannot induce charges directly, these secondary particles are the dominant causes of SEP. The similarity between the charge distribution in the neutron irradiated samples and that in the proton irradiated ones,

which is shown in Figs. 3(a) and 3(b), suggests that the similar kinds of secondary particles contribute to the charge generation and collection in both the 65 MeV neutron and 65 MeV proton irradiations. This fact suggests that in an energy range around 65MeV, protons can be substituted for neutrons in testing cosmic-ray induced SEP at the ground level. Since nuclear reactions depend strongly on energy of neutrons or protons, further investigations are necessary to determine the energy range in which protons can be substituted for neutrons in SEP tests.

4. Summary

We have successfully measured 65MeV neutron and 65MeV proton induce SET currents in Si pin photodiodes. The charge distribution obtained in the proton irradiation was found to be in good agreement with that observed in the neutron irradiation. From the simulation using a PHITS code, charges collected in the neutron and proton irradiated samples were confirmed to be caused by secondary particles produced via nuclear reactions. The similarity of proton induced SET currents to neutron induced ones also indicated the possibility that protons are used as a substitute for neutrons in testing SEP in the energy range around 65MeV.

References

1) T.Hirao et al., Nucl. Instrum. and Methods, B210, 227-231 (2003).
2) E. Normand et al., IEEE Trans, Nucl. Sci., NS-45(6) 2904 (1998).
3) C. S. Guenzer et al., IEEE Trans. Nucl. Sci., NS-26 (6) 5048 (1979).
4) C. A. Gosset et al., IEEE Trans. Nucl. Sci., NS-40 (6) 1845 (1993).
5) J. S. Laird et al., IEEE Trans. Nucl. Sci., NS-50, 2003 (2003).
6) M.Baba et al., Nucl. Instr. Meth. Phys. Res.A., 428, 454 (1999).
7) T. Wakasa et al., Proc. of the 6th Internat. Workshop on Radiation Effects on Semiconductor Devices for Space Application (2004) p.213.
8) T.Hirao et al., Nucl. Instr. Meth. Phys. Res. B. 130, 486 (1997).
9) H.Iwase et al., J. Nucl. Sci. & Tech., 39, 1142 (2002).
10) R. C. Little, "Readme_LA150N," (July 2000, revised May 2002).

1.7 Comparison of Heavy Ion and Laser Microbeams for Investigating Single Event Transient Currents

J. S. Laird*, T. Hirao*, S. Onoda*, ** and H. Itoh*
Department of Material Development, JAERI*
Graduate School of Engineering, Tokai University**

1. Introduction

For space applications, photodetectors based on III–V semiconductors are preferred over Si based devices due to their higher absorption coefficients and therefore thinner active regions[1]. Although III-V devices have advantage of displacement damages due to thinner active region, high energy heavy ions can cause Single Event Transient (SET) currents resulting in the errors such as Single Event Upsets (SEUs). Hence, SET currents induced by high-energy heavy ions are an important avenue of investigation.

MeV ion and laser microbeams are the two most common means of evaluating SET currents[2),3)]. Although the ion beam based experiments have been partially replaced by the simpler laser based technique[4),5)], the laser technique cannot fully replace accelerator testing as pointed out by Melinger et al.[6]. In fact, fundamental differences between ion-solid and photon-solid interactions in devices can result in the laser method being inappropriate. However, for the case of SET current generation in photodetectors, the nature of the device and its simple structure mean that lasers can enormously simplify SET testing. In this paper we demonstrate that the use of a laser microbeam can simplify SET testing for photodetectors.

2. Experimental

The devices used in this work were commercial InGaAs p-i-n photodiodes with a diameter of 250μm. A constant reverse biases ranging from 0 to 10V were applied during all tests.

The Transient Laser Beam Induced Current (TLBIC) system used a 788nm picosecond laser diode with a Gaussian pulse (FWHM of 46ps) and peak optical power of 167mW. The laser output was collimated, circularized and passed through a Neutral Density Filter (NDF) wheel for controlling the laser intensity. A 1.5GHz Si p–i–n diode, optimized for the 800nm region, measured the full laser power to be 1.85pJ per pulse at the sample. An aspherical lens inside the chamber focused the beam with an XYZ stage (1μm step). By stage scanning a Cu grid (1000mesh), a spot size of 2μm was measured. The sample was mounted on a double microstripline waveguide with both signals passed to separate 50Ω 40GHz semi-rigid transmission lines onto Picosecond Labs bias tees (5542-2). The signal then passed to a CSA803 sampling oscilloscope equipped with a SD-32 50GHz sampling head. The CSA803 trigger was provided by the laser controller with a timing jitter of less than 10ps[7].

To compare the laser with heavy ions, the Transient Ion Beam Induced Current (TIBIC) system described elsewhere[8] was used to collect transient currents induced by O-15MeV, C-15MeV and Au-10MeV. This system was similar to the TLBIC, except that a Tektronix 694C 3GHz Digitizing Sampling Oscilloscope (DSO) was substituted for the CSA803 and DSO triggering is provided by the substrate signal.

3. Results

TLBIC data was then collected from the centre of the sample as a function of both bias and laser transmission intensity (10–80% of 1.85pJ) in steps of 1V and 10%, respectively. Shown in Fig. 1 is the transient response versus bias averaged over 256 passes in the case of 50% transmission. Laser induced transients also exhibited space-charge dependent charge collection, apparent as an increase of the risetime with intensity and a saturation of the peak current at higher intensities. Charge collection characteristics as a function of laser power will be discussed later.

The bias dependence for ions were all collected for 0 to 10V. After each bias series, single ion transients were collected for doses of up to 10^{13} cm^2. No significant decrease in either the charge or peak current was noted within the dose range required for these experiments. For brevity, these results are not shown here. Figure 2 shows the integrated charge curves (solid lines) for the total 20ns of the transient. On the right side of the same figure (dashed lines),

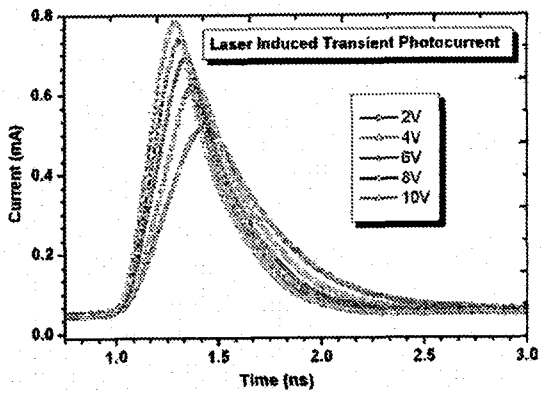

Fig. 1 Transient LBIC bias dependence at 50% of the full laser power.

the peak currents are represented as a function of bias. In this case, charge collection efficiencies have not been used due to the ambiguities regarding electron-hole pair (EHP) formation energies. In the case of Au ion injection, high-injection spacecharge screening effects are apparent by both the amount of charge collected (<30% of that collected by C and O after correcting for its energy) and its bias dependence (a flat response followed by a gradual rise). In the flat response region, the external field is unable to penetrate the dense plasma, and high-injection levels greater than $10^{21}cm^{-3}$ (over less spatial extent than for C and O) result in shorter high-injection lifetimes due to Auger recombination. O and C injection does not produce the same behavior since most of the charge is collected by

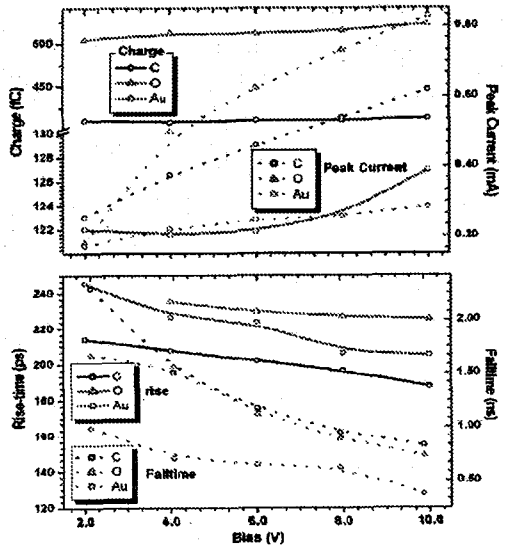

Fig. 2 Top: integrated charge (—) and peak current (…) for the three ions as a function of bias. Bottom: corresponding rise (—) and fall (…) times.

diffusion from the InP region below. The non-ionizing energy loss fraction for Au is also considerably higher than for both O and C. As an indicator of similar charge collection dynamics, the rise and fall times are also compared and shown in Fig. 2.

4. Discussion

At appropriate laser intensity, charge collection dynamics for laser and 10MeV Au ions should be similar if the laser technique can successfully simulate heavy ion induced currents. Shown in Fig. 3 is the collected charge versus bias for all laser intensities and ions. Although the charge collected with C and O ions are within the range accessible by laser, these transients differ markedly due to differing penetration depths. To make a direct comparison, a point of reference between the two sets must be found. Deposited energy or effective dE/dx can not be used since (a) EHP formation energies are different for ions and photons and (b) reflection losses at the surface are unknown. Here we decided to use the total charge as the point of comparison on the grounds that the peak current or rise time would differ if at the same total charge, the collection processes differed. As indicated in Fig. 3, charge collected by 10MeV Au strikes corresponds closely to that of 20% laser intensity (9% difference).

The laser charge characteristics are now compared to those of 10MeV Au. This comparison is shown in Fig. 4. After correcting for the 9% difference in average charge over the bias range, a reasonably close agreement was found between the two cases as shown in the top of the figure. The bottom of the figure confirms that the corrected rise times also agree within error. The fall times, not shown here for brevity, indicate a small deviation between the

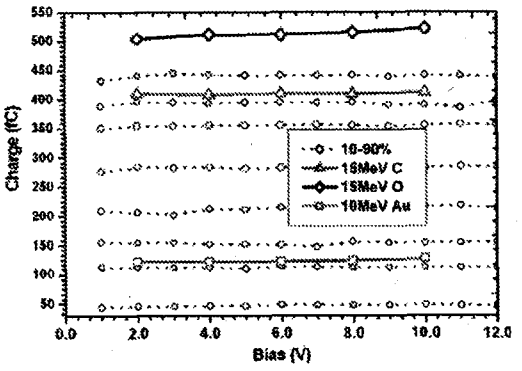

Fig. 3 Plots of charge collected versus bias for all laser intensities (10–80%) and the three ions.

laser and ion induced transients, particularly at higher biases where a second peak appears. We believe the appearance of a second peak is related to the fraction of charge generated in the InP gap and InGaAs regions. For the laser case, only 10% of energy loss occurs in the InGaAs region, as opposed to over 50% in the case of ions. Ignoring the negative differential due to high electric fields, the respective electron and hole mobilities in near intrinsic $In_{0.53}Ga_{0.47}As$ are 15000 and 280 cm^2/Vs. Since electrons are 50 times faster than holes (a similar ratio exists in InP), electron and hole contributions to the measured current can be differentiated. For charge generated in the top InP, band bending only allows electrons diffusion into the junction. Hence in the case of Au, the transient current is dominated by a fast electron current with a smaller 2nd peak due to holes. For 15MeV O and C, the larger the amount of charge generated in the InGaAs, the larger the leading peak current. In these cases, the 2nd peak current is approximately the same magnitude and likely contains a hole current from the InP substrate. In summary then, although the initial EHP plasma generation volumes are markedly different for MeV heavy ions and pulsed laser beams, the charge collection dynamics for both situations remain quite similar. By an appropriate choice of laser power and wavelength we have been able to reproduce the charge collection dynamics of 10MeV Au ion induced transient currents using a focused pulsed picosecond laser. Hence, even though the radial extent of the initial EHP distribution is markedly different, overall the charge collection dynamics of the two are found to be similar. This is most likely due to rapid ambipolar expansion of the Au induced EHP plasma in the first few picoseconds leading to similar transient currents over the longer duration measured. For simple devices where the lateral uniformity of the active region is considerably larger than the radial extent of the EHP plasma, both laser and ion transient currents are expected to be similar. We therefore believe the laser technique to be a suitable means of simulating heavy ion strikes in InGaAs on InP photodetectors. However, such experiments can commence, detailed calculations of the plasma volume must be compared to those predicted for the laser beam and a suitable spot size and wavelength chosen.

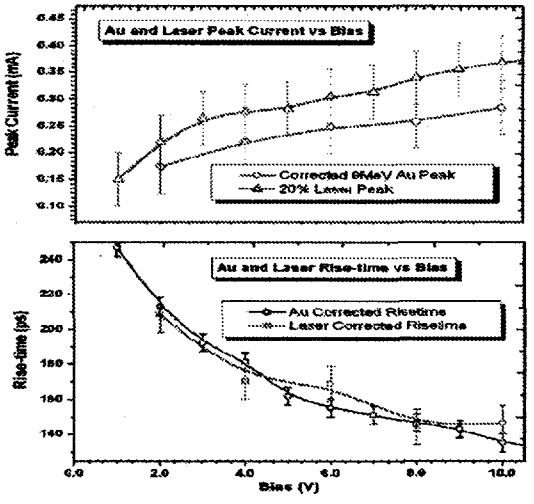

Fig. 4 Comparison of 10MeV Au and 20% laser intensity data.

5. Conclusion

We have compared basic charge collection characteristics of InGaAs on InP p–i–n photodiodes using laser and ion beam induced currents, to ascertain whether laser beam techniques can simulate the generation of EHP plasmas by heavy ions. We found that by a careful choice of the laser intensity, we were able to show reasonable agreement between the ion and laser generated SETs. In the case of 10MeV Au, very good agreement was found. We believe that after careful consideration of the laser wavelength and intensity, SET generation from single heavy ions can be simulated.

References

1) B.E. Anspaugh, GaAs Solar Cell Radiation Handbook, JPL Publication 96-9 (NASA, 1 July 1996).

2) S. Buchner, et. al., IEEE Trans. Nucl. Sci. NS-35 (6) (1988) 1517.

3) I. Nashiyama, et. al., IEEE Trans. Nucl. Sci. 40 (6) (1993) 1935.

4) K. Kang, et. al., IEEE Trans. Nucl. Sci. 39 (6) (1992) 1295.

5) A.H. Johnston, IEEE Trans. Nucl. Sci 40 (1993) 1694.

6) J.S. Melinger, et. al., IEEE Trans. Nucl. Sci. 41 (6) (1994) 2574.

7) Hamamatsu Picosecond Laser Manual.

8) J.S. Laird, et. al, Nucl. Instr. and Meth B 181 (2001) 87.

1.8 Studies of Charge Collection Mechanism in MOS Capacitor using a Heavy-ion Microbeam

T. Hirao*, S. Onoda*,**, J. S. Laird*, T. Wakasa*,** and H. Itoh*
Department of Material Development, JAERI*
Graduate School of Engineering, Tokai University**

1. Introduction

Single-event phenomena (SEP) such as soft-error, latch-up, and burn-out are the most serious problem in applying highly sophisticated modern electronic devices in space environments. In order to develop single-event tolerant devices, it is indispensable to understand the transportation mechanisms of electric charges induced in a device subjected to energetic ion irradiation. Several attempts have been made for the direct measurements of extremely fast transient currents induced by single ion strikes on a silicon p^+n junction diode or schottky diode, and charge collection mechanisms such as drift, funneling, and diffusion effects have been studied [1-4].

Silicon-on-insulator (SOI) technology has been used for a long time in niche application such as spacecraft electronics and devices operating in a high-temperature or radioactive environment. The SOI structure is regarded as one of the most promising methods to provide large-scale integrated circuits with higher single-event tolerance as well as higher performance. It has been believed that the amount of single-event charges is reduced significantly by applying the SOI structure, because the charge collection through the funneling mechanism is suppressed by the existence of an electric insulation layer in the SOI structure [5]. In recent years, an anomalous charge collection in SOI devices has been observed when high-energy charged particles traverse their active regions. This fact suggests that dense charges generated under a buried oxide contribute to the charge collection. To investigate the charge collection mechanisms in SOI devices, we have measured transient currents induced in metal oxide semiconductor (MOS) capacitors by high-energy heavy ions.

2. Experimental Approach

Experiments were performed on three low capacitance Si MOS capacitors with a cross-sectional structure as indicated in Fig. 1. The oxide layer thickness for these devices ranged over 50, 100 and 200 nm. The front Al-electrode of each sample was 100 μm in diameter and 50 nm in thickness.

Each device was mounted onto a ceramic chip carrier containing a double-ended micro-strip line. The geometry of the chip carrier was designed to achieve a 50 Ω impedance for high bandwidth current transient measurements. Both ends of the micro-strip line launched onto 50 Ω transmission lines and passed out of the chamber to bias tees and the recording oscilloscope. Transient current waveforms were recorded with a 3 GHz

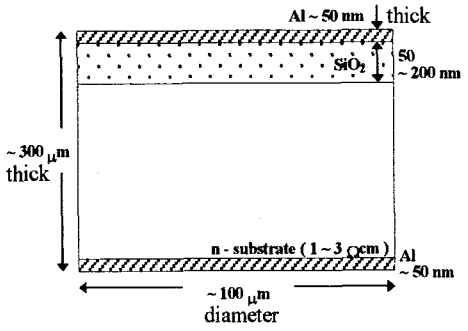

Fig.1 Schematic structure of Si MOS capacitor samples.

Tektronix model TDS 694C. In order to reduce the effect of radiation damage, we have used the transient ion beam induced current (TIBIC) measurement system in conjunction with the single ion hit (SIH) system.

3. Results and Discussion

3.1 Transient Current Waveform

Figure 2 shows transient current waveforms as a function of bias from -3 to -10 V when 18 MeV O ions were irradiated to the MOS capacitor with a 50 nm thick oxide. The peak height of the transient current increases with increasing bias voltage whereas the fall-time decreases.

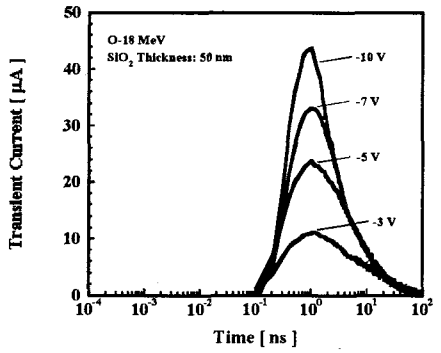

Fig.2 Transient current waveforms as a function of bias voltage in the Si MOS capacitors irradiated with 18 MeV O ions.

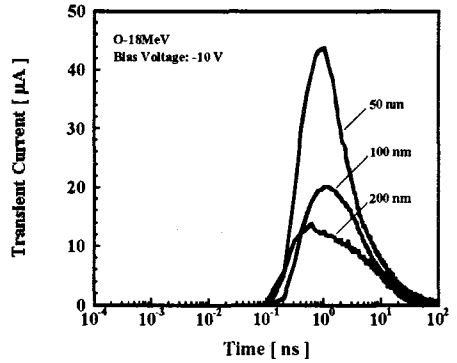

Fig.3 Transient current waveforms as a function of oxide thickness in the Si MOS capacitors irradiated with 18 MeV O ions.

In order to estimate the influence of oxide thickness, we performed the measurements of transient current induced in the samples with different oxide thicknesses under reverse bias at 10 V. As shown in Fig.3, the current transient peak height decreases with increasing the thickness of oxide layer. The peak height observed for the 50 nm oxide sample is two to three times as large as that of the other oxide layer diodes. In addition, the fall-time and the full-width at half maximum (FWHM) of the transient current waveform become longer with increasing oxide thickness.

3.2 Collected Charge

Figure 4 shows the relationship between the bias voltage and the amount of collected charge derived from the transient current waveforms observed. The collected charge increases with increasing bias voltage as expected. Additionally, in the 50 nm oxide sample, the collected charge is two to three times as large as that of the 200 nm oxide sample. Although the depletion width was estimated to be saturated at a reverse bias of 0.7 V,

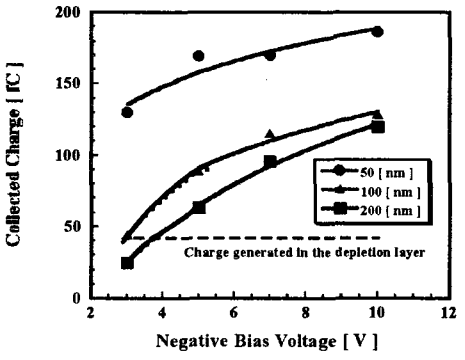

Fig.4 Dependence of the amount of charge collected in the Si MOS capacitors on reverse bias voltage when irradiated with 18 MeV oxygen ions. The dashed line indicates the calculated result for the amount of charge generated in a depletion layer. The solid lines represent the bias dependence of the amount of collected charge obtained experimentally for the samples having different oxide thicknesses.

the collected charge continues to be a strong function of bias well beyond the saturation point (42 fC).

3.3 Simulation

Figure 5 shows transient current waveforms calculated with the simulation code VENUS-2D/B for the sample applied at a reverse bias of 10 V when irradiated with 18 MeV O ions. In the simulation, the oxide was considered as an ideal insulator and thus only displacement current is assumed to flow in the sample. In order to compare the properties of simulated

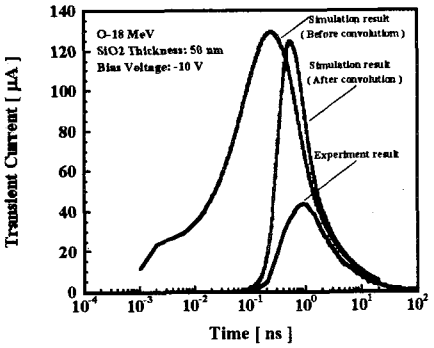

Fig.5 Transient current waveforms simulated using VENUS-2D/B and that obtained experimentally for the Si MOS capacitors with the oxide thickness of 50 nm when irradiated with 18MeV-Oions.

current transients with those of measured, we convoluted the simulated transients with the system response function using the following formula:

$$i(t) = \int_{-\infty}^{\infty} i(t) \times g(t) \qquad (1)$$

$$g(t) = \frac{1}{\sigma\sqrt{2\pi}} e^{-(t^2/2\sigma^2)} \qquad (2)$$

where g(t) indicates a Gaussian distribution with a standard deviation σ that relates to the system rise time[6]. The system rise time of 141 ps was used in the simulation, and as a result, we have extracted a convoluted transient waveform as shown in Fig. 5. Whereas the peak height of the simulation result shows 2 to 3 times as large as that obtained experimentally, the simulated current waveform is similar to the experimentally obtained waveform.

By using the TIBIC technique combined with the SIH system, we have successfully observed transient currents induced by MeV ions in MOS capacitors, and obtained the influence of oxide thickness and bias voltage on the transient current. Further investigations are necessary to clarify all the implications of charge generation and transportation in MOS structures irradiated with energetic ions.

References

1) R.S. Wagner, J. M. Bradley, Nicole Bordes, D. N. Sinha, C J. Maggiore, and R. B. Hommond, IEEE Trans. on Nuclear Science, NS-34, No.6 (1987) 1240.

2) R.S. Wagner, J. M. Bradley, Nicole Bordes, D. N. Sinha, C. J. Maggiore, A. R. Kundson, and A.B. Campbell, IEEE Trans. on Nuclear Science, NS-35, No.6 (1988) 1578.

3) T. Hirao, I. Nashiyama, T. Kamiya, T. Suda, T. Sakai, T. Hamano, Nuclear Instruments and Methods in Physics Research B130 (1997) 486.

4) I. Nashiyama, T. Hirao, T. Kamiya, H.Yutoh, T.Nishijima, H. Sekiguti, IEEE Trans,Nucl. Sci., Vol. NS-40, No.6(1993) 1935.

5) T. Hirao, T. Hamano, T. Sakai, I. Nashiyama, Nuclear Instruments and Methods in Physics Research B 158 (1999) 260.

6) J. S. Laird, T. Hirao, H. Mori, S. Onoda, T. Kamiya, H. Itoh, Nuclear Instruments and Methods in Physics Research B 206 (1993) 36.

JP0650164

1.9 Development of TIBIC System using Collimated High Energy Heavy Ion Beam with Diameter of 20μm

S. Onoda[*, **], T. Hirao[*], T. Wakasa[*, **], H. Abe[*] and H. Itoh[*]
Department of Material Development, JAERI[*]
Graduate School of Engineering, Tokai University[**]

1. Introduction

High energy heavy ions in harsh radiation environments like space cause Single Event Effects (SEEs) in Integrated Circuits (ICs). To understand the mechanisms of SEEs and estimate the on-orbit SEE hardness, a lot of experiments using accelerators have been performed[1]. As a result, it is found that Linear Energy Transfer (LET) is one of the most important physical terms to estimate SEEs, such as the cross section curve of Single Event Upsets (SEUs). Once the LET dependence of SEU cross section was determined, the SEU cross section due to any ions can be predicted without additional experiments.

Another common term of SEE tests is the ion energy. Early researchers have tried to clarify whether the charge collection in ICs depends on the ion energy. As a result, no remarkable difference in the charge collection was obtained [2]. Some recent studies also led to similar results. However, other recent tests have indeed suggested a difference in SEU response to ions with different energies exhibiting the same LET [1,3].

At a given LET, the high energy ion track has a much larger radius and a longer range than the low energy ion track. This fact leads to different charge collection and SEU response. For example, high energy ions cause more Multiple Bit Upsets (MBUs) than low energy ions because of expanding radial track distributions.

The influence of ion energy on Single Event Transient (SET) current contributing the earliest stage of SEEs is required to understand SEEs induced by the real space radiations having extremely high energies [4,5]. We have developed Transient Ion Beam Induced Current (TIBIC) system combining with collimated high energy ion beams accelerated by an AVF Cyclotron at JAERI Takasaki. Here, TIBIC images induced by extremely high energy heavy ions are shown and discussed.

2. Development of TIBIC system

Figure 1 shows the schematic diagram of the chambers designed here. Ion beams from the AVF Cyclotron were collimated using a pair of double (X-Y) slits placed along the beam line with about 11m distance each other. The beams entered the left of the profiling chamber containing the

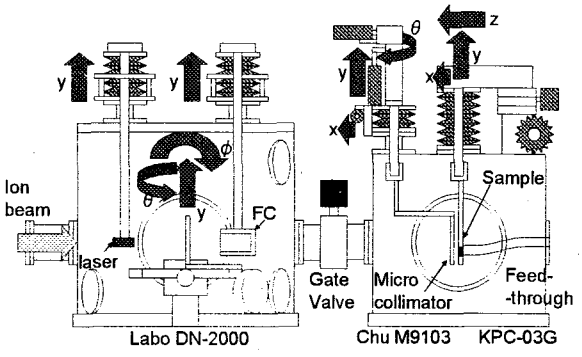

Fig. 1 Schematic diagram of chambers for newly developed TIBIC system.

beam characterization tools; (a) a laser and lens for aligning the micro-collimator and sample with the beam, (b) a scintillater chip for confirming beam position, and (c) a Faraday Cup (FC) for monitoring the beam current. The scintillater chip was mounted on the y-θ-φ stage (Labo DN-2000), on which other equipments for beam characterizations such as Silicon Surface-barrier Detector (SSD) could also be mounted. All of them were y-shifted away from the center of beam line after laser alignment and beam positioning. Next, the beams were transported into the irradiation chamber containing the micro-collimator on the x-y-θ stage (Chu M9103) and the sample on the x-y-z stage (KPC-03G). The micro-collimator with a diameter of 20μm was made of Mo. Samples were mounted on a ceramic chip carrier with double-ended microstrip lines with 40GHz RF transmission line feedthroughs at the end of the irradiation chamber. All stages were fully automated for adjusting the best locations and angle of the micro-collimator and sample so as to minimize the ion scattering at the inner wall of the micro-collimator. Details of the procedures to form the collimated beams and the estimation methods of the beam quality have been described in the previous paper [6].

The devices used in this work were commercial Si pin photodiodes with a diameter of 450μm as shown in Fig. 2 (a). A constant reverse bias of 20V was applied to the device during all irradiations. Two Bias-Tees were used for sample biasing. Where necessary, the fast amplifiers (Picoseconds Pulse Lab.) could be used for trigger and signal amplification. SET currents were recorded with a 3GHz 4-channel single-shot digital storage oscilloscope (Tektronix Model TDS694C). More detailed information on the measurement system has been described elsewhere [7].

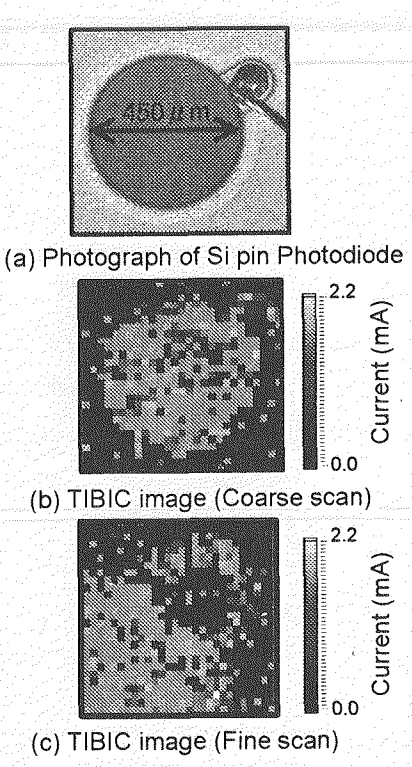

Fig. 2 Photograph of Si pin photodiode with the circular electrode (a). TIBIC peak images with coarse scan (b) and fine scan (c).

3. TIBIC Images

The TIBIC method gives us the two-dimensional maps of SET currents characterized by the peak current, rise time, fall time and total collected charge. Figures 2 (b) and 2(c) show TIBIC peak images with the coarse scan (800x800μm^2, 40x40steps) and the fine scan (300x300μm^2, 30x30steps) induced by Ar-150MeV. Both images indicate that the diode region covered with the circular electrode is SEE sensitive except the bonding wire. Because of the wire with a diameter of 30μm, ions

don't reach the sensitive region, thus any SET currents are observed.

It is likely that SET currents outside the electrode are introduced by scattering ions. Although not shown here, these signals are typically slow and small compared with that inside the electrode because of relatively lower energies. This fact underestimates the averaged SET current. To reduce the scattering effects, we have optimized the scanning method and Z-direction which is restricted by the geometry of the sample holder design. Although SET currents due to scattering still exist in images, the resolution of TIBIC image is enough to evaluate SEE in the devices having several tens μm.

4. Summary

SET current is the most interesting issue for understanding and predicting SEEs in space environments. Since the space radiations consist of high energy heavy ions, the energy dependence of SET current has to be considered. In order to estimate this effect, we have developed TIBIC system combining with collimated high energy ion beams accelerated by the AVF Cyclotron. Using newly developed TIBIC system, we have demonstrated the performance of TIBIC system.

References

1) P. E. Dodd, *Basic mechanisms for single-event effects*, section II, IEEE NSREC Short Course (1999).

2) W. J. Stapor, P. T. McDonald, A. R. Kundson, A. B. Campbell and B. G. Glagola, IEEE Trans. Nucl. Sci., 35, 6 (1988) 1585-1590.

3) P. E. Dodd, O. Musseau, M. R. Shaneyfelt, F. W. Sexton, C. D'hose, G. L. Hash, M. Martinez, R. A. Loemker, J.-L. Leray and P. S. Winokur, IEEE Trans. Nucl. Sci., 45, 6 (1998) 2483-2491.

4) R. S. Wagner, J. M. Bradley, N. Bordes, C. J. Maggiore, D. N. Sinha and R. B. Hammond, IEEE Trans. Nucl. Sci., 34, 6 (1987) 1240-1245.

5) I. Nashiyama, T. Hirao, T. Kamiya, H. Yutoh, T. Nishijima and H. Sekiguti, IEEE Trans. Nucl. Sci., 40, 6 (1993) 1935-1940.

6) I. Nashiyama, T. Hirao, T. Hamano, H. Itoh and T. Ohshima, JAERI-Review, 97-015, (1997) 3-4.

7) J. S. Laird, T. Hirao, H. Mori, S. Onoda, T. Kamiya and H. Itoh, Nucl. Instr. and Meth. B, 181, (2001) 87-94.

1.10 Single Event and Total Dose Synergy Effects in SOI Devices

H. Mori*, S. Satoh*, T. Hirao**, H. Abe** and H. Itoh**
Graduate School of Engineering, University of Hyogo*
Department of Material Development, JAERI**

1. Introduction

It is well known that malfunctions in semiconductor devices, which are called a single event (SE) effect, in artificial satellites are caused by cosmic rays in space. Such cosmic rays also raise a total dose (TD) effect, by which devices are degraded significantly. It is most probable that these two effects simultaneously occur in semiconductor devices in space. However, very little is known about the SE and TD synergy effect.

In this study, we aim at clarifying the SE and TD synergy effect in SOI (silicon on insulator) devices, which have received considerable interest recently because of their excellent performance, e.g., high speed and low power operation, required for space application. In the first stage of our investigations, we have examined the TD effects in metal- oxide-semiconductor (MOS) capacitors irradiated with high energy protons. In this paper, we report flat band voltage (V_{FB}) shifts observed in the MOS capacitors due to proton irradiation and discuss mechanisms behind the V_{FB} shift based on the defect introduction.

2. Experimental

The samples used in this study were p-type Si-MOS capacitors, which were fabricated using a Si substrate with the resistivity of 9-12 Ω cm. The oxide layer with the thickness of about 300 nm was grown thermally. The Pt electrode with the diameter of 1 mm and the thickness of about 50 nm was deposited on the oxide layer. Proton irradiation was performed using a 400 keV ion implanter at JAERI Takasaki TIARA facility. Proton energy was chosen to be 40 and 80 keV to form different damage profiles in the MOS capacitors. In 40keV irradiation, the damage peak was estimated to be located near the interface between the oxide layer and the Si substrate. On the other hand, the damage peak was derived to be located in the substrate when protons were irradiated at 80keV. The fluence of protons ranged from $2x10^9$ to $2x10^{10}$ cm^{-2}. High-frequency C-V measurements were performed to obtain the electrical characteristics of the samples before and after irradiation.

3. Results and discussion

Figure 1 shows the C-V curves observed for the samples irradiated with 40 and 80keV-protons. The C-V curves obtained for the unirradiated samples are also shown for comparison. The C-V curve was found to shift toward the negative voltage side by the irradiation. This result indicates that positive fixed charges are produced in the oxide of the MOS capacitors by proton irradiation. It is also shown from Fig.1 that the C-V curve shift in 40keV-proton irradiation is wider than that in 80keV irradiation, indicating that a large number of positive charges are generated in the oxide by 40keV irradiation compared with 80keV irradiation.

Next, we have estimated the vacancy profiles in the irradiated MOS capacitors by using a SRIM code[1], and the results are shown in Fig.2. In this figure, the interface between the Pt electrode and the oxide layer and that between the oxide layer and the Si substrate are represented by vertical lines. It was derived from the SRIM calculation that the vacancy production rates in the oxide layer by 40 and 80 keV-proton irradiations were 9.38 and 2.83 / ion, respectively. Assuming that one vacancy creates one positive fixed charge in the oxide layer, the V_{FB} shift can be given by

$$V_{FB} = -\int_0^{t_{ox}} \frac{qN_{ox}(x)}{\varepsilon_S} x dx, \qquad (1)$$

where t_{ox}, q, $N_{ox}(x)$, ε_S are the thickness of the oxide layer [cm], the elementally charge [C], the vacancy density in the oxide layer [cm^{-2}], the permittivity of oxide [F/cm], respectively. Table 1 shows the experimentally and theoretically obtained V_{FB} shifts. The calculated values of the V_{FB} shift are small compared with the experimentally obtained values, as shown in the Table. It suggests that positive charges in the oxide are also produced by electronic excitation due to proton irradiation. Further investigations are necessary to clarify the mechanisms behind the V_{FB} shift. For clarification of the SE and TD synergy effect in SOI devices, we plan to investigate the TD effect in buried oxide layers of SOI devices irradiated with proton beams, and then measure single event transient currents induced in the SOI devices using ion microbeams.

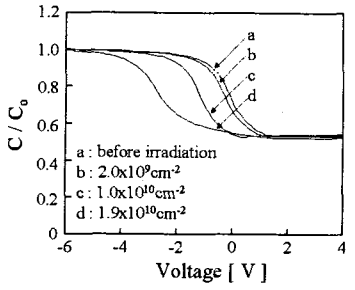

(a) 40keV proton irradiation

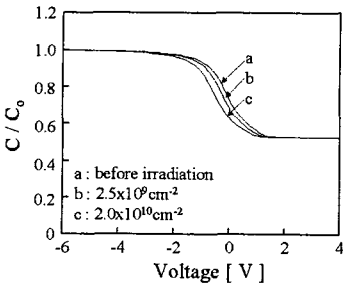

(b) 80keV proton irradiation

Fig. 1 C-V curves observed at 1MHz for MOS capacitors irradiated with (a) 40 keV and (b) 80 keV protons. C-V curves for the unirradiated sample are also shown for comparison.

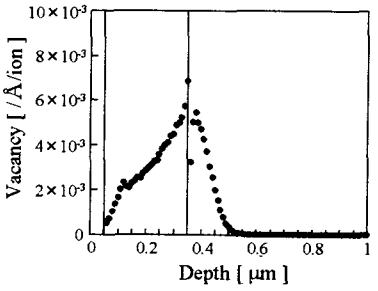

(a) 40keV proton irradiation

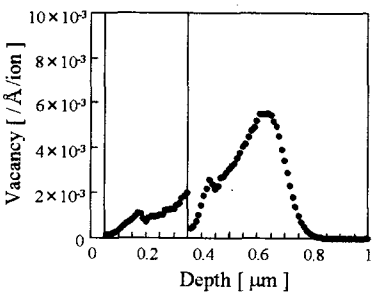

(b) 80keV proton irradiation

Fig. 2 Calculated vacancy profiles using SRIM code for MOS capacitors irradiated with (a) 40 keV and (b) 80 keV protons.

Table 1 V_{FB} shifts derived from the C-V measurements and calculation using eq.(1).

Proton Energy	Dose cm^{-2}	V_{FB} V	Vacancy cm^{-2}	V_{FB} from Not V
40keV	$2.0x10^9$	-0.2	$1.88x10^{10}$	-0.17
	$1.0x10^{10}$	-1.1	$9.38x10^{10}$	-0.83
	$1.9x10^{10}$	-2.7	$1.78x10^{11}$	-1.57
80keV	$2.5x10^9$	-0.2	$7.06x10^9$	-0.06
	$2.0x10^{10}$	-0.5	$5.65x10^{10}$	-0.50

Reference

1) J. F. Ziegler, Stopping and Range of Ions in Solids, Pergamon, 1985.

1.11 Degradation of Electrical Performance of P-Channel 6H-SiC MOSFETs by Gamma-ray Irradiation

T. Ohshima and H. Itoh
Department of Material Development, JAERI

1. Introduction

Since silicon carbide (SiC) was found to have strong radiation resistance[1-3], SiC is expected to be applied to electric devices used in harsh radiation environments. Especially, p-channel SiC MOSFETs are regarded as a promising candidate for dosimeters with extremely high radiation resistance[2]. For applying SiC to dosimeters, it is very important to understand the change in the electrical characteristics by irradiation. In previous studies [2,3], the threshold voltage (V_T) of p-channel SiC MOSFETs was reported to shift toward the negative voltage side. In addition, Lee et al.[3] reported that a decrease in channel mobility of SiC MOSFETs can be described as a function of interface traps generated by irradiation. However, the type and value of interface traps depend on the fabrication process of SiC MOSFETs, and the effects of such defects on the electrical characteristics of SiC MOSFETs have not yet fully understood. In this article, we describe changes in the electrical characteristics of p-channel SiC MOSFETs by gamma-ray irradiation.

2. Experimental procedures

The MOSFETs used in this study were fabricated on n-type epitaxial 6H-SiC films (5μm thick) grown on 6H-SiC substrates (3.5° off, Si-face). The net donor concentration of the epitaxial films was 6.9×10^{15} /cm^3. The source and drain of the MOSFETs were formed using aluminum (Al) ion implantation at 800 °C and subsequent annealing at 1800 °C for 10 min in an Ar atmosphere. For Al introduction, three-fold implantation (110, 75, 50 keV) was carried out to form the box profile of Al at a mean concentration of 5×10^{19}/ cm^3. The gate oxide of 33 nm thick was fabricated by pyrogenic oxidation (H_2:O_2 = 1:1) at 1100 °C for 30 min. The gate length and width of the MOSFETs were 10 μm and 200 μm, respectively. Al electrodes were formed using lift-off method. The electrodes for source and drain were sintered at 850 °C for 5 min in Ar. Gamma-ray irradiation was performed up to 530 kGy (SiO_2) at a rate of 0.9 kGy/h at RT. No electrical bias was applied to the gate, the drain and the source during the irradiation. The electrical characteristics were measured at RT in a shielded probe station under dark conditions to minimize external supurious noises. The V_T was determined as the value at the intersection between the V_G-axis and the line extrapolated from the curve of the square root of I_D versus V_G in the saturation region. The value of V_T before irradiation was –3.7 V. The channel mobility (μ) of the MOSFETs was derived as follows; First, the values of μ were estimated from the linear region of the drain current (I_D) versus drain voltage (V_D) curves (the slope of I_D-V_D curves between V_D = 0 and 0.2 V) in various gate voltage (V_G). Then, the maximum value obtained from the V_G dependence of μ was used as the value of μ in this study. The value of μ before irradiation was estimated to be 6.7 cm^2/Vs.

3. Results and Discussion

Figure 1 shows the shift of V_T for p-channel 6H-SiC MOSFETs due to gamma-ray irradiation (closed squares). The result reported for p-channel 6H-SiC MOSFETs in ref. 2 is also plotted as open squares in the figure for comparison. The gate oxide of reported MOSFETs was also formed using pyrogenic oxidation. The value of V_T shifts to the negative voltage side by irradiation. The shift of V_T obtained in this study is larger than the reported value. Since the shift of V_T occurs by the generation of charge trapped in oxide and interface traps, the result obtained in this study suggests that oxide-trapped charges and interface traps are generated by irradiation and that the number of such defects for the MOSFETs in this study is larger than that for the reported MOSFETs. For evaluating the number of oxide-trapped charges and interface traps generated by irradiation, I_D-V_G curves in the subthreshold region (subthreshold-current curves) were analyzed.

According to McWhorter and Winokur[4], the entire subthreshold-current curve is simply transferred by the generation of oxide-trapped charge because the contribution of trapped-oxide charge to the shift of threshold voltage is independent of gate bias. On the other hand,

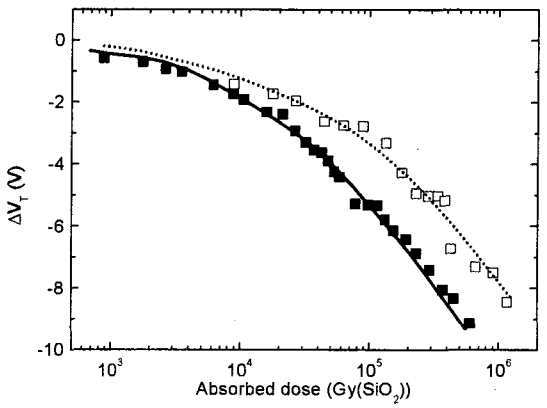

Fig. 1 Shift of V_T for p-channel 6H-SiC MOSFETs due to gamma-ray irradiation (closed squares). The result reported for p-channel 6H-SiC MOSFETs in ref.2 is also plotted as open squares in the figure for comparison.

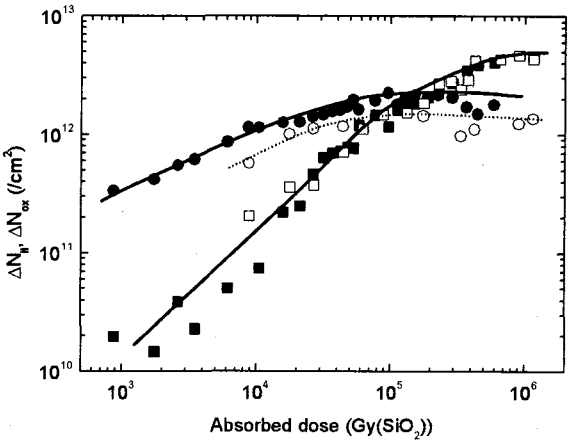

Fig. 2 Absorbed dose dependence of ΔN_{OX} (closed circles) and ΔN_{IT} (closed squares) for the 6H-SiC MOSFETs. The data reported for p-channel 6H-SiC MOSFETs in ref.2 are also plotted in the figure for comparison, (ΔN_{OX} (open circles) and ΔN_{IT} (open squares)).

interface traps interact with carriers in semiconductor, and the density of interface traps capturing carriers depends on the Fermi level (thus, the value of gate bias). Therefore, the subthreshold-current curve is stretched by the generation of interface traps. As a result, the shift of V_T by irradiation (ΔV_T) is explained to be $\Delta V_{OX}+\Delta V_{IT}$, where ΔV_{OX} and ΔV_{IT} are the voltage shifts due to the generation of oxide-trapped charges and interface traps, respectively. The shift of the midgap voltage (ΔV_{MID}) due to irradiation represents the formation of trapped-oxide charges only (ΔV_{OX} = ΔV_{MID}). Because the subthreshold-current curve between the midgap (V_{MID}) and the threshold voltages is stretched by the generation of interface traps, ΔV_{IT} can be determined from ΔV_{IT} = $(V_T - V_{MID})_{POST}$ - $(V_T - V_{MID})_{PRE}$, where "POST" and "PRE" denote after and before irradiation, respectively. For MOS capacitors fabricated on n-type substrates, information on interface traps with energy levels located in the upper half of the band gap is obtained mainly from capacitance-voltage curves. On the other hand, information on interface traps in the lower half of the bandgap can be derived from the relationship between V_{MID} and V_T measured from the MOSFET subthreshold-current curve.

In order to separate the contributions of radiation-induced interface traps from that of trapped-oxide charges, the drain current corresponding to the midgap condition (I_{MID}) is obtained by the following analysis. In the subthreshold region, I_D is represented by the formula [5]

$$I_D = \sqrt{2}\mu(W/2L)\,(qN_DL_B/\beta)(n_i/N_D)^2\exp(\beta\phi_s)(\beta\phi_s)^{-1/2}, \quad (1)$$

where W, L, N_D, n_i, ϕ_s and L_B are the gate width, the gate length, the donor concentration in the channel, the intrinsic carrier concentration, band bending at the surface and the Debye length given by $L_B = [\varepsilon_s/(\beta q N_D)]^{1/2}$, respectively. Here, β is equal to q/kT, where q and k are the electron charge and the Boltzmann constant, respectively. Since ϕ_s at the midgap condition is equal to $(kT/q)\ln(N_D/n_i)$, I_{MID} is derived from the substitution of ϕ_s for $(kT/q)\ln(N_D/n_i)$ in eq. (1). Using the obtained value of I_{MID} and the subthreshold-current curve, V_{MID} can be determined. Since I_{MID} tends to be of the order of 10^{-30} A in 6H-SiC, it is necessary to linearly extrapolate the lower position of the subthreshold-current curve down to the lower part of the curve, for the determination of V_{MID}. As a result of the analysis of p-channel SiC MOSFETs, both ΔV_{OX} and ΔV_{ox} show negative voltage shifts. This result indicates that positive charges are generated in the gate oxide and negatively charged interface traps are produced by irradiation. Since donor-like interface traps falling above the Fermi level are charged positively, this result can be explained in terms of the formation of donor-like interface traps in the lower half of the band gap.

The net number of radiation-induced oxide-trapped charges (ΔN_{OX}) and interface traps (ΔN_{IT}) can be obtained from ΔV_{OX} and ΔV_{IT} using the following formulae;

$$\Delta N_{OX} = |\Delta V_{OX}| C_{OX}/q, \quad (2)$$
$$\Delta N_{IT} = |\Delta V_{IT}| C_{OX}/q, \quad (3)$$

where C_{OX} is equal to ε_{OX}/t_{OX}, and ε_{OX} and t_{OX} are the relative dielectric constant of SiO_2 and

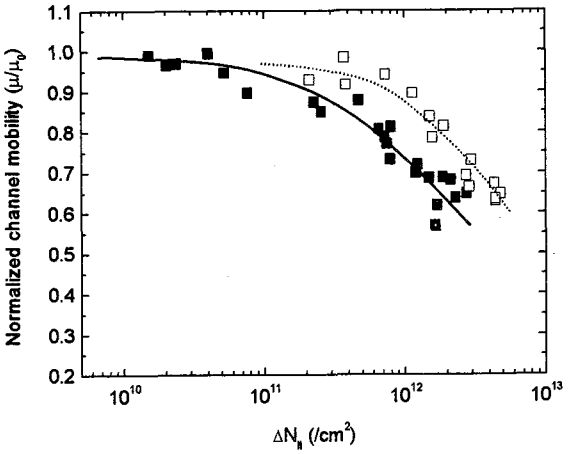

Fig.3 Relationship between the channel mobility and ΔN_{IT} obtained in this study (closed squares) and reported in ref.2 (open squares). The values of the channel mobility are normalized by that before irradiation (μ/μ_0).

the thickness of gate oxide, respectively. The absorbed dose dependence of ΔN_{OX} (closed circles) and ΔN_{IT} (closed squares) for the 6H-SiC MOSFETs is shown in Fig. 2. For comparison, the data reported for p-channel 6H-SiC MOSFETs in ref. 2 are also plotted in the figure (ΔN_{OX} (open circles) and ΔN_{IT} (open squares)). For both SiC MOSFETs, the value of ΔN_{OX} increases with absorbed dose and the saturation of ΔN_{OX} is observed above 5×10^4 Gy. Although the gate oxide of both MOSFETs was formed using pyrogenic oxidation, the value of ΔN_{OX} obtained in this study is larger than the reported value. This result can be interpreted in terms that the characteristics of the gate oxide are affected by a small difference in the fabrication process and the control of the quality of oxide on SiC is very difficult. For interface traps, ΔN_{IT} for both MOSFETs increases with increasing absorbed dose and a saturation of the increase is observed above 4×10^5 Gy. No significant difference in the absorbed dose dependence of ΔN_{IT} between this study and the reported one is observed.

Figure 3 shows the relationship between the channel mobility and ΔN_{IT} obtained in this study (closed squares) and that reported in ref. 2 (open squares). The values of the channel mobility are normalized by that before irradiation (μ/μ_0). The μ/μ_0 for both MOSFETs decreases with increasing ΔN_{IT}. However, the decrease in μ/μ_0 in this study is larger than the reported value. The value of μ/μ_0 becomes 0.6 at around ΔN_{IT} of 2×10^{12} /cm^2 in this study although the reported μ/μ_0 becomes 0.6 at ΔN_{IT} of 4×10^{12} /cm^2. Lee et al.[6] reported that decreases of channel mobility in both n-channel and p-channel SiC MOSFETs were described as one expression and that they were independent of gate oxidation process. However, the result obtained in this study cannot be fitted by the expression. Yano et al.[7] reported that interface traps existing near the conduction band edge affect the channel mobility in n-channel SiC MOSFETs. If interface traps located near the midgap do not scatter carriers in the inversion layer, the discrepancy of our result from the reported expression can be explained in terms that a part of interface traps generated by irradiation does not affect channel mobility and that the concentration of such interface traps in the reported MOSFETs is higher than that obtained in this study. For SiC, scattering mechanisms of carriers in the inversion layer due to interface traps are not yet fully understood. To clarify this point, further investigations are necessary.

4. Summary

P-channel MOSFETs were fabricated on 6H-SiC epitaxial layers, and their electrical characteristics were examined before and after gamma-ray irradiation. The threshold voltage shifts toward the negative voltage side, and the channel mobility decreases with increasing absorbed dose. The densities of oxide-trapped charges and interface traps generated by irradiation were estimated from the change of subthreshold curves. The density of oxide-trapped charges increases with absorbed dose and the saturation of ΔN_{OX} is observed above 5×10^4 Gy. For interface traps, the density increases with absorbed dose, and saturation is observed above 4×10^5 Gy.

References

1) T. Ohshima, H. Itoh, M. Yoshikawa, J. Appl. Phys. **90** (2001) 3038.
2) K. K. Lee, T. Ohshima, H. Itoh, Mater. Sci. Forum **389-393** (2002) 1097.
3) K. K. Lee, T. Ohshima, H. Itoh, Mater. Sci. Forum **433-436** (2003) 761.
4) P. J. McWhorter, P. S. Winokur, Appl. Phys. Lett. **48** (1986) 133.
5) J. R. Brew, in *Applied Solid State Science*, edited by Dawon Kahhy (Academic, New York, 1981)
6) K. K. Lee, T. Ohshima, H. Itoh, IEEE Trans. Ncl. Sci. **50** (2003) 194.
7) H. Yano, T. Kimoto, H. Matsunami, M. Bassler and G. Pensl, Mater. Sci. Forum **338-342** (2000) 1109.

1.12 Development of Advanced Optoelectronic Devices based on Ion-implanted Wide-gap Semiconductors

A. Wakahara*, T. Fujiwara*, F. Oikawa*, H. Okada*, T. Ohshima**and H. Itoh**
Department of Electrical & Electronic Engineering, Toyohashi University of Technology*
Department of Material Development, JAERI**

1. Introduction

Light emission from rare-earth ions (REIs) in a semiconductor has been paid much attention in order to realize a temperature stable light emitting device for optoelectronic systems, because 4f-4f electron level transitions in REIs have narrow bandwidth and less temperature sensitive peak position[1]. Recently, some research groups reported on development of visible electroluminescent devices using REIs doped GaN[2]. Moreover, the luminescence of REIs in GaN shows good radiation tolerance. Therefore, REIs doped III-Nitride has a potential application for light emitting devices in radiation environment.

We have been investigating photoluminescence (PL) properties of REIs (Eu, Tb, Tm, and Er) in $Al_xGa_{1-x}N$, and the PL intensity is dramatically increased with the Al content[3-8]. However, there are only a few reports on the effects of AlN molar fraction on the REIs related photoemission, and thus the effect of AlGaN on the energy-transfer and/or back-transfer processes is not deeply understood.

In this study, we investigated time-resolved PL to clarify the energy-back- transfer process in AlGaN with various AlN molar fractions.

2. Experimental details

Eu and Tb were used in the present work. These were implanted into $Al_xGa_{1-x}N$ ($0 \leq x \leq 1$) epitaxial layers, which were grown on a sapphire (0001) substrate with a 2μm-thick GaN epitaxial template. The ion implantation was carried out at room temperature with the acceleration energy of 200keV. The dose of the implanted REIs was set to $1\times10^{15}cm^{-2}$. The project range and peak concentration estimated by using TRIM were 100nm and $3\times10^{20}cm^{-3}$, respectively. After the implantation, the samples were annealed in N_2+NH_3 mixture (3:1) at 1100°C for 120s.

The time-resolved PL measurement was done in the temperature range of 14K - 300K by using ArF excimer laser (λ=193nm) as the excitation light source. The excitation power density was approximately $100\mu J/cm^2$ and the pulse duration was about 100ns.

3. Results and Discussion

3.1 Luminescence properties of Eu^{3+}

Figure 1 shows PL spectra and the decay transient of $Al_xGa_{1-x}N$:Eu with various Al composition measured at room temperature. Luminescence from ^5D_I - ^7F_J (I=0 and 1, J=0-3) transitions of Eu is clearly seen, and the strongest emission is $^5D_0$ - $^7F_2$ transition. The Eu-related PL intensity increases with increasing the Al composition and the PL intensity of $^5D_0$ - $^7F_2$ transition for Al composition x~0.2 reaches maximum, at which the intensity is more than ten times stronger than that of Eu implanted GaN. As the Al composition is increased, the relative PL intensity between $^5D_1$ - ^7F_J and $^5D_0$ - ^7F_J transitions is also increased with the intensity of $^5D_1$ - ^7F_J becoming stronger. PL decay transients can be fitted by double-exponential

decay with the fast component of ~50μs and the slow component of 150 - 200μs, as can be seen in Fig.1(b). The decay characteristics do not seem to depend on the Al composition.

The increase of the PL intensity without the reduction of decay time suggests that it is caused by an increase of energy transfer efficiency rather than an increase of transition probability. In order to understand the effect of AlGaN, the energy transfer process from the host to Eu^{3+} and the energy back-transfer process were investigated. Figure 2 shows the temperature dependence of PL intensity and the fast component of decay time for $^5D_0$ - $^7F_2$ transition of AlGaN:Eu. The PL intensity does not depend on the temperature for T<200K and slightly decreases in the high temperature region, while the change in the decay time is vary small. Only $Al_xGa_{1-x}N$:Eu with x<0.3, for which thermal quenching is relatively large, indicating a slight decrease of the decay time at the high temperature region (T>200K).

3.2 Luminescence properties of Tb^{3+}

Figure 3 (a) shows room temperature PL spectra of AlGaN:Tb with various Al composition. Luminescence related to $^5D_4$ - ^7F_J (J = 3, 4, 5, 6) transitions of Tb^{3+} can be clearly seen. As we reported previously, $^5D_3$ - ^7F_J transitions are major emission lines at low-temperature (<100K). For higher temperatures $^5D_3$ - ^7F_J transitions disappear and $^5D_4$ - ^7F_J transitions become major emission lines at room temperature. When the Al composition is smaller than 0.1, thermal quenching of $^5D_4$ - ^7F_J transitions is very large and it is difficult to detect $^5D_4$ - ^7F_J transitions from GaN:Tb at room temperature. Transient decay of $^4D_4$-$^7F_6$ transition in Tb^{3+} shows non-exponential feature and can be fitted by double-exponential decay. The obtained fast component of the decay time becomes longer for a higher Al composition and is about a few tens μs. On the contrary, the slow component seems to be less dependent on Al composition and is about 200μs. Since the decay time of the Tb^{3+}-related PL has temperature dependence, we have to correct for that in order to discuss the luminescence process. Figure 4 shows the temperature dependence of both the normalized PL intensity and the fast component of the decay time. It is clearly seen that the PL intensity and

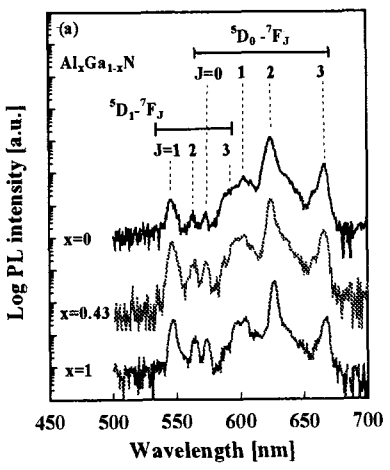

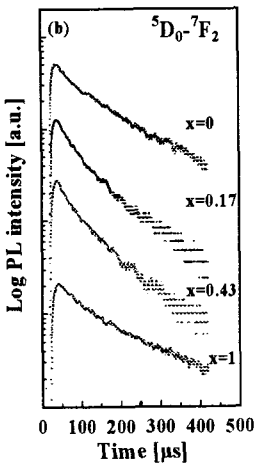

Fig. 1 (a) Room-temperature PL spectra of Eu-doped $Al_xG_{1-x}N$ with various Al composition. (b) PL decay transient of $^5D_0$ - $^7F_2$ transition measured at room temperature.

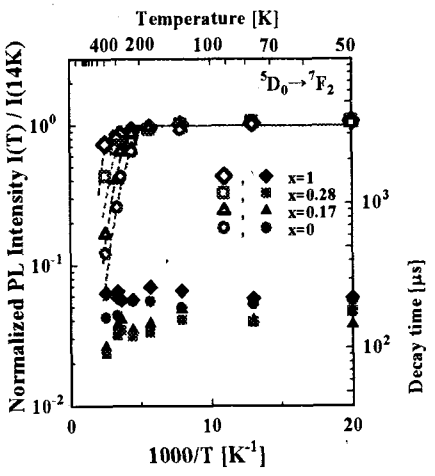

Fig. 2 Temperature dependence of the normalized PL intensity and the decay time for $^5D_0$-$^7F_2$ transition.

the decay time are constant at low temperatures. On the other hand, they rapidly decrease when the temperature exceeds a critical value, which is dependent on the Al composition but seems to be almost the same for the PL intensity and the decay time. Moreover, the fast component of decay slows down at low temperature and becomes equal to the slow component. For the Al composition x>0.7, no decrease in the decay time was observed in the present work. These results mean that non-radiative recombination and/or energy back-transfer rate become small at low temperature and/or for samples with high Al contents.

3.3 Discussion

To explain a luminescence mechanism of RE^{3+} in a semiconductor, such as Si:Er, GaAs:Er, and InP:Yb[9], an energy transfer model was proposed. According to this model, energy back-transfer from RE to impurities and/or trap levels is available via multi-phonon assisted processes. Activation energy for back-transfer 'E_{BT}' was estimated by using this model. In case of $Al_xGa_{1-x}N$:Eu, the E_{BT} is increased from 167meV for x=0 to 232meV for x=0.3, and for $Al_xGa_{1-x}N$:Tb, it is increased from 8meV for x=0 to 190meV for x=0.3. These results are also consistent with the results of numerical analysis of the decay time in GaN:Eu using rate-equation reported by Lee et. al.[10].

References

1) M. J. Weber, Phys. Rev., **171**, 283 (1968).
2) A. J. Steckl, M. Garter, D. S. Lee, J. Heikenfeld, and R. Birkhahn, Appl. Phys. Lett.**75**, 2184 (1999).
3) J. Heikenfeld, M. Garter, D. S. Lee, R. Birkhahn, and A. J. Steckl, Appl. Phys. Lett.**75**, 1189 (1999).
4) Y. Nakanishi, A. Wakahara, H. Okada, A. Yoshida, T. Ohshima, and H. Itoh, phys. stat. sol. (c) **0**, No.1, 461 (2002)
5) Y. Nakanishi, A. Wakahara, H. Okada, A. Yoshida, T. Ohshima, H. Itoh, T. Shibata, and M. Tanaka, phys. stat. sol. (c) **0**, No.7, 2623 (2003)
6) Y. Nakanishi, A. Wakahara, H. Okada, A. Yoshida, T. Oshima, and H. Itoh, phys. stat. sol (b) **240**, No.2, 342 (2003)
7) U. Hömmerich, Ei Ei Nyein, D. S. Lee, A. J. Steckl, and J. M. Zavada, Appl. Phys. Lett., **83**, 4556 (2003)
8) D. S. Lee and A. J. Steckl, Appl. Phys. Lett., **83**, 2094 (2003)
9) K. Takahei, A. Taguchi, and R. A. Hogg, J. Appl. Phys. **82**, 3997 (1997).
10) C. W. Lee, H. O. Everitt, D. S. Lee, A. J. Steckl, and J. M. Zavada, J.Appl. Phys., **95**, 7717 (2004).

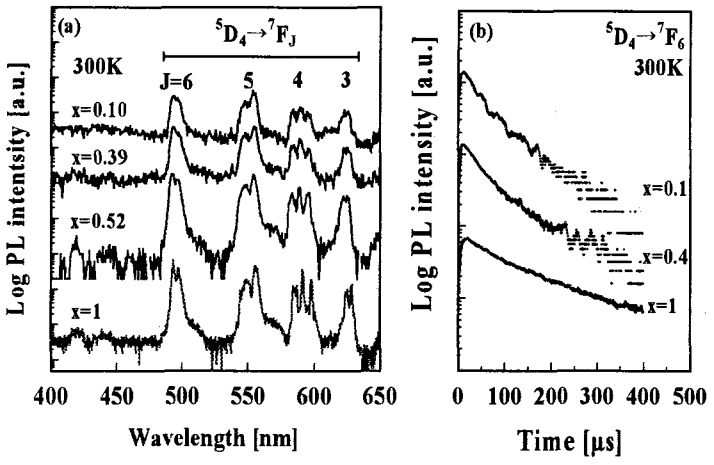

Fig. 3 (a) Room-temperature PL spectra of $Al_xG_{1-x}N$:Tb with various Al composition. (b) PL decay transient of $^5D_4$ - $^7F_6$ transition measured at room temperature.

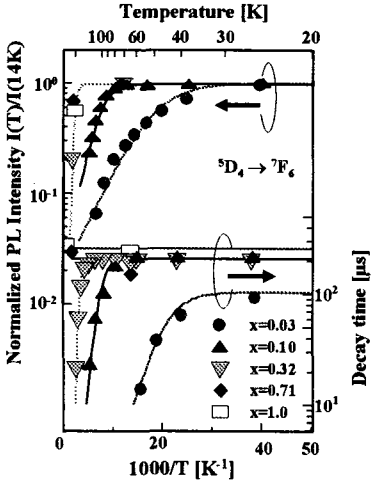

Fig. 4 Temperature dependence of the normalized PL intensity and the decay time of $^5D_4$-$^7F_6$ transition.

This is a blank page.

2. Biotechnology

This is a blank page.

2.1 Analysis of Radiation-induced DNA Double-strand Breaks in Tobacco BY-2 Cells

Y. Yokota*, M. Inoue**, N. Shikazono*, Y. Hase*, T. Funayama*, S. Wada*, S. Yamada** and A. Tanaka*
Department of Ion-beam-applied Biology, JAERI*
Graduate School of Agriculture, Kyoto Prefectural University**

Introduction

High-LET ions induce mutations accompanied with large-scale structural changes of chromosome efficiently, compared with low-LET radiations [1), 2)]. However, biological effects of high-LET ions are still unclear in plants. To develop an efficient procedure of ion beam irradiation for plant breeding, it is needed to evaluate biological effects of high-LET ions in plants at unicellular and molecular levels. We reported that single tobacco cells were 5 to 10 times more tolerant to radiation than mammalian cells, and that cell-killing effect per Gy of carbon ions with an LET of 230 keV/μm was 4.5 times higher than that of gamma rays [3)]. We also developed an ion microbeam system for irradiating single plant cells [4)]. DNA double-strand breaks (DSBs) are known to be a trigger of various kinds of biological effects led by radiation and the most serious type of DNA lesions. In this study, we analyzed DSBs induced by gamma-rays and high-LET ions in tobacco BY-2 cells by means of pulsed-field gel electrophoresis (PFGE) assay [5)].

Materials and Methods

Protoplasts were isolated from tobacco BY-2 cells and suspended in LSD medium supplemented with 0.75% agarose GB (Takara Bio), 0.4 M sorbitol and 5 mM MES. Protoplast suspension was gelled in a plug mold (1.5×5×10 mm^3, Bio-Rad) to make agarose plug. Agarose plugs were irradiated with gamma rays (LET = 0.2 keV/μm), and helium (9.4 keV/μm) and carbon (94.8 keV/μm) ions at ice temperature. Immediately after the irradiation, agarose plugs were transferred to protease buffer [1 mg/ml protease K, 1% sodium N-lauroyl sarcosinate in 0.5 M EDTA (pH 8.0)] and incubated for 1h at 4°C, then for 24h at 50°C. After the incubation, agarose plugs were washed for 30 min in 0.5×TBE buffer (pH 8.3) 4 times. Washed plugs were placed in an electrophoresis gel [1% Pulsed Field Certified Agarose in 0.5×TBE buffer], set in a contour-clamped homogeneous electric field (CHEF) DR-III apparatus (Bio-Rad) filled with 0.5×TBE buffer. PFGE was performed under the following conditions; initial switch time 60 sec, final switch time 120 sec, run time 24h, voltage 6 V/cm, angle 120°, temperature 14°C. *Saccharomyces cerevisiae* chromosomal DNA (1.9 Mbp to 220 kbp, Takara Bio) was run as a DNA size marker. After the run, electrophoresis gel was dried in a gel drier and re-hydrated in D.W. Then, the electrophoresis gel was stained with SYBR Green buffer [0.01% SYBR Green I (Takara Bio) in 0.5×TBE buffer] for 3h at 50°C. Electrophoresis pattern of DNA was visualized on a 302-nm UV transilluminator and recorded using an electric-cooled CCD camera. Number of DSBs induced by gamma rays was quantified according to the method reported by Blöcher [6)], which bases on the assumption of random distribution of DSBs. Chinese hamster (CHO-K1) cells were also irradiated with gamma rays as a reference. In tobacco cells irradiated with high-LET ions, the number and frequency of DSBs that were induced at intervals of 1.6 - 0.36 Mbp were quantified based on the method of Höglund [7)], since

high-LET ions induce DSBs non-randomly.

Nuclei were isolated from tobacco protoplasts using Galbraith's buffer and fixed with 70% ethanol at 4°C over night. Fixed nuclei were filtrated through a 30-μmϕ nylon mesh and mixed with two volumes of DAPI solution (High resolution kit for plant DNA, Partec). The mixture was run in a PAS flow cytometer. Rice (*Oryza sativa* ssp. *japonica* cv. Nipponbare, 860 Mbp DNA per diploid cell) nuclei isolated from the leaf were also run as a reference.

Results and Discussion

From the flow cytometry analysis, fractions of $G_{0/1}$, S and G_2/M phase of tobacco protoplasts were 76.9 ± 5.7, 13.4 ± 3.4 and 9.7 ± 2.5% (mean ± SD of 3 replications) respectively (Fig. 1a). DAPI intensity was 14.3 times greater in diploid tobacco BY-2 cells than in diploid rice cells (Fig. 1b). From this, DNA content per diploid tobacco BY-2 cell was calculated to be 12.3 Gbp.

In tobacco and CHO-K1 cells, the number of DSBs per Gbp DNA linearly increased with dose (Fig. 2). The number of DSBs per Gbp DNA at the same dose, however, was much different between both cell types. DSB yield per Gbp DNA per Gy was obtained from the slope of regression line (Table 1). It has been reported that DSB yields (Gbp DNA^{-1} Gy^{-1}) were around 6 in mammalian cells and yeasts irradiated with low-LET radiations [9]. DSB yield (Gbp DNA^{-1} Gy^{-1}) was 3-times lower in tobacco cells than in mammalian cells and yeasts. This is certainly one of causes for radiation tolerance found in tobacco cells [3]. Species and/or contents of radical scavengers that reduce biological effects of radiation might be different among tobacco cells, mammalian cells and yeasts. The number of DSBs per diploid cell at mean lethal dose (D_0) was 5 times more in tobacco cells than in CHO-K1 cells. In other words, tobacco cells could tolerate 5 times more DSBs than CHO-K1 cells (Table 1). Tobacco cells might repair DSBs efficiently and/or be tolerant un-/mis-repaired DSBs. Quantification of DSB repair is necessary to understand the radiation tolerance of plants.

Number of DSBs induced at intervals of 1.6 – 0.36 Mbp linearly increased with dose (Fig. 3). DSB yield (Gbp DNA^{-1} Gy^{-1}) was 1.92 and 1.86 times more in helium and carbon ions than in gamma rays, respectively (Table 2). DSB yield (Gbp DNA^{-1} ion $particle^{-1}$) was 10 times more in carbon ions than in helium ions. From these, it was found that high-LET ions induce DSBs in tobacco cells more efficiently than gamma rays. Frequency of DSB induction was higher in ion beams than in gamma rays through the investigated range (Fig. 4). The frequency of DSBs induced by gamma rays corresponded with the theoretical one assuming random distribution of DSBs. This means that the gamma-ray irradiation induces DSBs on tobacco genome randomly.

Table 1 DSB yields in tobacco BY-2 and CHO-K1 cells irradiated with gamma rays.

Cell type	DNA content per diploid cell (Gbp)	Mean lethal dose (Gy)	DSB yield* (Gbp^{-1} Gy^{-1})	Number of DSBs per diploid cell at mean lethal dose*
Tobacco BY-2	12.3	10.7 [3]	2.0±0.1	263.2±13.2
CHO-K1	6.0 [6]	1.4 [8]	6.6±0.2	55.4±1.7

*Mean ± SE of 2-6 replications.

Table 2 DSB yields in tobacco BY-2 cells irradiated with gamma rays, and helium and carbon ions.

Radiation	Mean LET (keV/μm)	DSB yield*,** (Gbp^{-1} Gy^{-1})	(Gbp^{-1} ion particle^{-1})	RBE***
Gamma rays	0.2	0.85±0.01	–	1
Helium ions	9.4	1.63±0.02	$2.45\times10^{-8}\pm2.72\times10^{-10}$	1.92
Carbon ions	94.8	1.58±0.01	$2.39\times10^{-7}\pm1.5\times10^{-9}$	1.86

*Mean±SE of 2-6 replications.
**DSBs induced at intervals of 1.6-0.36 Mbp.
***Based on the DSB yield (Gbp^{-1} Gy^{-1}) of gamma rays.

References

1) Shikazono et al. (2001) *Genetics* 157
2) Shikazono et al. (2003) *Genetics* 163
3) Yokota et al. (2003) *Int. J Radiat. Biol.* 79
4) Yokota et al. (2003) *Biol. Sci. Space* 17
5) Yokota et al. (2005) *Radiat. Res.* 163
6) Blöcher (1990) *Int. J. Radiat. Biol.* 57
7) Höglund et al. (2000) *Int. J. Radiat. Biol.* 76
8) Wada et al. (2003) *J. Vet. Med. Sci.* 65
9) Prise et al. (1998) *Int. J. Radiat. Biol.* 74

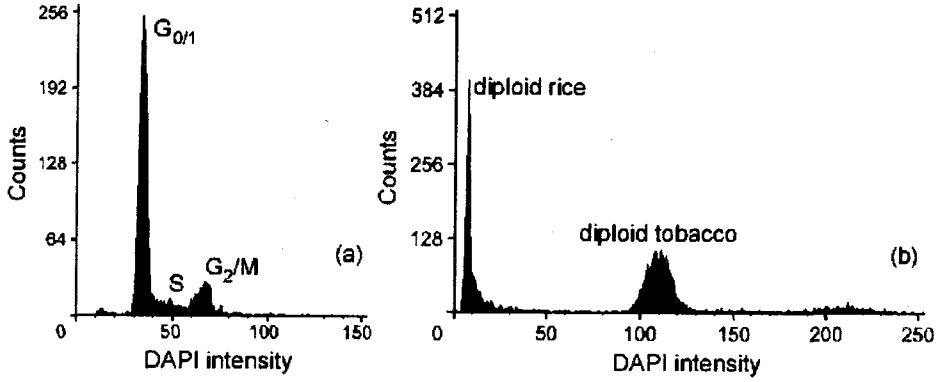

Fig. 1 Flow cytometry data.
(a) Analysis of cell cycle of tobacco BY-2 cells. The first and second peaks indicate $G_{0/1}$ and G_2/M phase of nuclei, respectively. The area between these peaks indicates S phase. (b) Estimation of DNA content per diploid tobacco BY-2 cell. The first and second peaks indicate diploid rice and diploid tobacco nuclei.

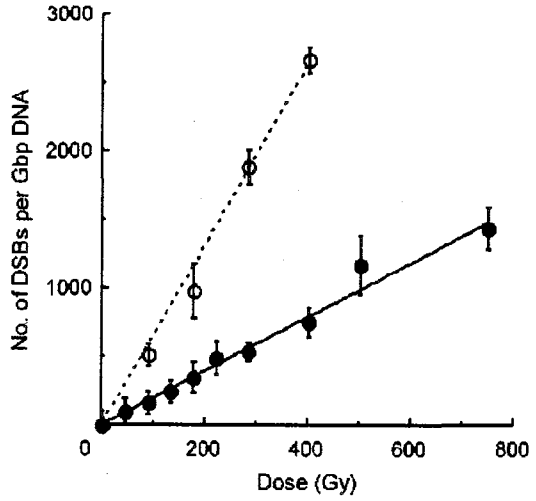

Fig. 2 Dose response of DSB induction in tobacco BY-2 (●) and CHO-K1 (○) cells irradiated with gamma rays.
The number of all DSBs is quantified. Each point indicates mean ±SE of 2-6 replications. Regression lines are fitted to the function Y = AX by a least-squares method weighted to SEs.

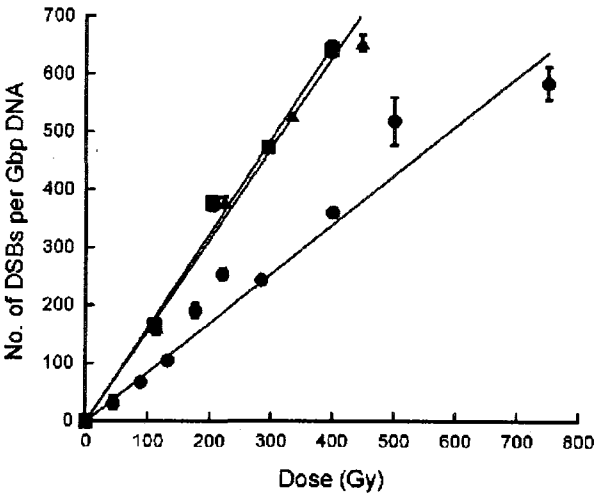

Fig. 3 Dose response of DSB induction in tobacco BY-2 cells irradiated with gamma rays (●), and helium (■) and carbon (▲) ions.
The number of DSBs that are induced at intervals of 1.6 to 0.36 Mbp is quantified. Each point indicates mean ± SE of 2-5 replications. Regression lines are fitted to the function Y = AX by a least-squares method weighted to SEs.

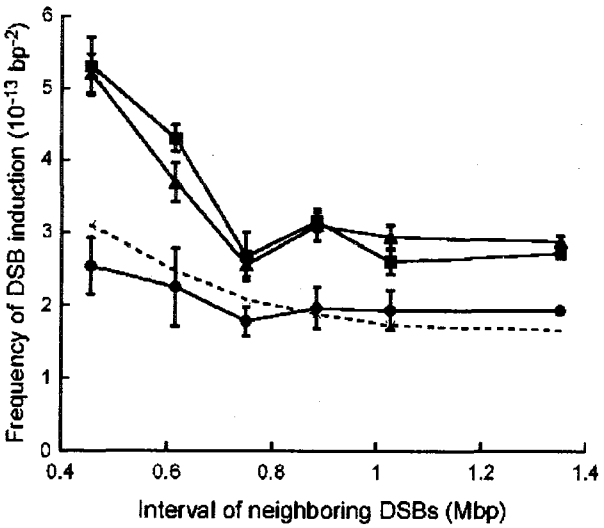

Fig. 4 Relationship between freaquency of DSB induction and interval of neighboring DSBs in tobacco cells irradiated with gamma rays (220 Gy, ●), and helium (203 Gy, ■) and carbon (223 Gy, ▲) ions.
Each point indicates mean ±SE of 2-5 replications. Theoretical values assuming random distribution of DSBs are also shown as a dotted line.

2.2 Plant Regeneration from Ion Beam-irradiated Microspores of *Solanum integrifolium*

K.Takata*, Y. Saiki*, K. Hirashima*, T. Nakahara*, Y. Hase**, Y. Yokota** and A. Tanaka**

Department of Agricultural Biotechnology, Fukuoka Agricultural Research Center*, Department of Ion-beam-applied Biology, JAERI**

1. Introduction

The ion beams have high linear energy transfer, so is widely used as one of the efficient mutagens to improve plants. Seeds, callus and leaf segments are widely used as the materials to irradiate, but we aimed at microspores. By using microspores, we are able to irradiate a large number of cells at a time without generating chimera compared with the multicellular tissues. In addition, we are able to obtain a recessive mutation in a short term because of the haploidy of the microspores.

In this study, we succeeded to regenerate plants through culture of ion beam-irradiated microspores of *Solanum integrifolium*.

2. Materials and Methods

Eggplant rootstock cultivar, *Solanum integrifolium* was used for the experiment. Flower buds of *S. integrifolium* were collected and surface sterilized for 10 min in 1% sodium hypochlorite and rinsed 3 times for 1 min each in sterile distilled water. The anthers collected from these flower buds were macerated in a sterile petri dish with sterile water using a syringe barrel.

After the maceration, microspore suspension was sieved through nylon mesh with 50 μ m pore size and the filtrate was centrifuged at 200 x g for 3 min. The pelletized microspores were then purified by stepwise Percoll gradient centrifugation at 150 x g for 5 min. The contain microspores interlayer was collected, and washed with sterile water at 200 x g for 3 min. The washed microspores were finally suspended in distilled water and pipetted into a petri dish (60 mm diameter), and incubated at 35℃ in darkness for 4 days after sealing with the Parafilm.

Then the microspores were diluted to 2 x 10^5 cells/ml with the microspore culture medium which kept warm at 40℃, composed of NN medium (Nitsch & Nitsch) containing half strength macronutrients, supplemented with 20 g/l sucrose, 0.5 mg/l NAA (Naphthalene acetic acid), 0.5 mg/l BA (Benzylaminopurine), 0.2% Gellan Gum. One ml of the microspore suspension was poured and solidified into petri dish (35 mm diameter), which was covered with Kapton film.

Prepared microspores were irradiated 320MeV $^{12}C^{6+}$ ions delivered from the AVF cyclotron in JAERI. After irradiation, 1ml of the fresh 1/2NN liquid medium was added to each dishes, and cultured at 25 ℃ in the dark. At 4 weeks after irradiation, to induce shoots, the calli derived from microspores were transferred to the MS medium (Murashige-Skoog) containing 20 g/l sucrose, 0.2 mg/l IAA, 4.0 mg/l Zeatin, and solidified with 0.8 % agar. The cultures were maintained at 25℃ under 16 h photoperiod (6,000 lux). Regenerated shoots were rooted in the 1/2MS medium containing 20 g/l sucrose and solidified with 0.2 % Gellan Gum. The rooted

plants were transferred into the plastic pots with soil, and cultivated at green house.

3. Results and Discussion

The dose response of callus formation derived from the microspores irradiated with $^{12}C^{6+}$ ion beam was shown in Fig.1 as a percent of the non-irradiated control (100%). The callus formation rate decreased according to increase the dose. Only few calli were observed at 10 Gy, and no callus at 20 Gy. The LD_{20} of callus formation was estimated around 2 Gy. In case of $^{12}C^{6+}$ irradiation to the leaf protoplasts of Chrysanthemum, a same single cell, a similar result has been obtained[1]. It wasn't observed a significant difference about shoot from the calli irradiated at 0 Gy to 2 Gy. We obtained about 300 regenerated plants from the irradiated microspores until now. Plant regeneration from the microspores is in progress, and we are performing the evaluation of its traits.

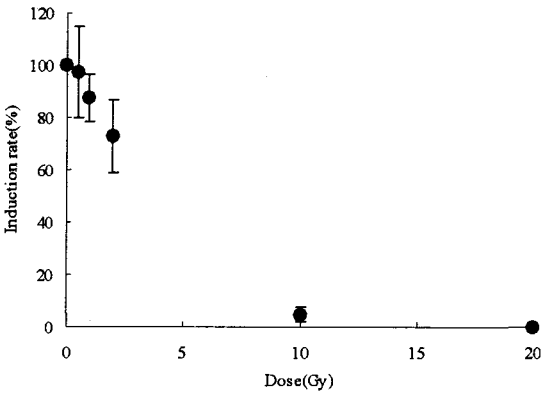

Fig.1 Effect of $^{12}C^{6+}$ ion beam on the formation of callus from microspores. The number of calli was counted at 4 weeks after irradiation. Average values of 7 replications were expressed as a percent of non-irradiated control.

References

1) H. Ikegami, K. Takata, H. Kai, K. Hirashima, T. Nakahara, Y. Hase, N. Shikazano and A. Tanaka, TIARA Annual Report 2003-033(2003), 40-41

2.3 Mutation Induction from Osteospermum Leaf Cultures with Ion Beam Irradiation

M.Iizuka*, Y.Kimura*, Y.Hase** and A.Tanaka**
Gumma Agricultural Technology Center*
Department of Ion-beam-applied Biology, JAERI**

Introduction

Ion beams, which have a higher linear energy transfer (LET) than X and gamma rays, are one of efficient mutagenic agents, and applicable to mutation breeding of many horticultural crops. However, there have been few studies on the effects of ion beam irradiation on induction of mutation in vegetables and ornamental crops. The lethal dose of the $^{4}He^{2+}$ and $^{12}C^{5+}$ ion beam irradiation to strawberry, hydrangea and spiraea seed became clear [1),2),3)].

In Gumma Prefecture, Osteospermam cultivation is prosperous and its quality has obtained high evaluation. We have wild out the mutation breeding of the Osteospermam that is important pot cultures. Ion beams were irradiated to Osteospermam for the purpose of getting variation of the flower color and character. Here examined effects of ion beam irradiation on germination of Osteospermam.

Materials and Methods

Osteospermam in greenhouse were used as plant materials. Young leaves were excised, and the surface was sterilized by immersing in 70% ethyl alcohol for 1 min, followed by 1%(W/V) sodium hypochlolite solution for 15 min and then rinsed three times in distilled water. The leaf segments were cultured on modified Murashige and Skoog's (MS) medium supplemented with 0.1 mg/l NAA and 1mg/l BA. The samples covered with Kapton film were irradiated with carbon ion beam (220 MeV $^{12}C^{5+}$ and 320 MeV $^{12}C^{6+}$) at various doses (2 to 150 Gy). After irradiation the leaf segments were transferred to the fresh medium and cultured at 25 °C and 16 hr-photoperiod. Rgeneration rate was investigated after 40-50 days of culture.

Results and Discussion

Osteospelmam leaf segments was not able to rgeneration irradiated with 20 Gy or more[4),5)].

Therefore, it was thought that the irradiation of 1～5Gy was effective.

More individuals of redifferentiation were induced from bladed that were irradiated with higher doses.

Hundreds of individuals grew, and three of them having a mutation in color of the flower on the other side of the petal have been selected so far (Table 1, Fig 1).

The selected mutants showed a form different from original stock in plant type and the leaf shape. It is thought that the change was given to the gene of Osteospelmam by the ion beam.

We are performing cytological studies to investigate horticultural values of the mutants and are screening flower

color-variation mutants out of the growing plants.

References

1) N. Kudo et al. TIARA Ann. Rep., 16:62-64. (1998)
2) M. Iizuka et al. TIARA Ann. Rep., 2.3:30-31. (1999)
3) M. Iizuka et al. TIARA Ann. Rep., 2.7:45-46. (2001)
4) M. Iizuka et al. TIARA Ann. Rep., 2.4:42-43. (2002)
5) M. Iizuka et al. TIARA Ann. Rep., 2.3:40-41. (2003)

Table 1. Mutants in Osteospelmam by the irradiation of 220 MeV $^{12}C^{5}$+ and 320 MeV $^{12}C^{6}$+ ion beams

Radiation	No. of hardening	No. of mutants	
$^{12}C^{5}$	540	petal	2(0.4)[z]
		plant type	3(0.6)
$^{12}C^{6}$	445	petal	3(0.7)
		plant type	1(0.2)

[z]The percent is shown in the parenthesis.

Fig.1 Mutants of back of petal in Osteospelmam by the irradiation of ion beams.
(A)Normal (B) Clear petal

2.4 Mutation Induction in Orchids using Ion Beam

A. Sakinah, *, A. H.Affrida,.*, A. Zaiton*, B. Mohd Nazir*, A. Tanaka**, N. Shikazono**, Y. Oono** and Y.Hase**
Agrotechnology and Biosciences Division, Malaysian Institute for Nuclear Technology Research (MINT)*
Department of Ion-beam-applied Biology, JAERI**

1. Introduction

Orchid is the largest income earner for Malaysia's floriculture industry. The orchids are mainly exported as pot plants and cut flowers. Due to the increasing demand for new commercial viable varieties, new characteristics such as flower of colour, shape and longer shelf life are needed to satisfy the consumers' preferences.

The use of conventional breeding methods to create variation in orchids is restricted by sexual incompatibility, sterility problems and long breeding time. Mutation induction by ionising irradiation provides an alternative for the improvement of orchids. Gamma irradiation has been successful in creating many *Dendrobium* 'Sonia' mutant varieties. In *Dendrobium* Ekapol and *Dendrobium* Sonia for examples, irradiation has resulted in changes of flower pigmentation and size [1,2].

Ion beams has been utilized widely as new mutagens because they can deposit high energy on a target densely and locally compared to low linear energy transfer radiations (electrons, X-rays and gamma rays)[3]. An ultraviolet-resistant mutant in Arabidopsis and the other novel mutants of chrysanthemum and carnation having various kinds of flower colors have been successfully isolated using ion beams[4,5,6]. In this study, experiments were carried out to induce mutation in orchids using ion beam.

2. Experimental procedure

2.1 Plant material

Dendrobium mirbellianum and *Dendrobium crumenatum* were used for this study. The seeds of *D.mirbellianum* and *D.crumenatum* were germinated *in vitro* and cultures were maintained on half-strength Murashige and Skoog (MS) medium [7] at 26°C with 12h photoperiod.

2.2 Ion beam irradiation

Protocorms that were uniform in size with approximately 2.0 mm diameter were chosen for ion beam irradiation. They were transferred into sterile 6 cm Petri dish containing MS. Samples were covered with sterile Kapton film (0.8μm in thickness) and were irradiated with 320 MeV $^{12}C^{5+}$ ion, accelerated by AVF cyclotron at JAERI, Takasaki at doses of 0, 0.2, 0.4, 0.8, 1.0, 2.0, 4.0, 6.0, 8.0, and 10.0 Gy for *D.mirbellianum*. Whilst, *D.crumenatum* was irradiated at 0.2, 0.4, 0.8, 1.0, 2.0, 4.0, 6.0, 8.0, 10.0, 12.0, and 15.0 Gy.

2.3 Propagation and Greenhouse screening

Irradiated protocorms were immediately transferred onto fresh MS medium and were allowed to proliferate and multiply for several months by subculturing onto fresh medium every four weeks. The frequency of shoots regeneration was examined every four weeks.

The regenerated plantlets were acclimatized in the greenhouse and their heights are recorded every four weeks. Any morphological changes are also observed and recorded.

3. Results and Discussion

3.1 *Dendrobium mirbelliannum*

From our previous report [8], it is assumed that the appropriate dose of irradiation for *D. mirbelliannum* is in the range of 0.8 to 1.0 Gy. The irradiation experiment for *D.mirbellianum* was repeated. Due to the difficulty in estimating the effective irradiation dose on protocorms [8], the survived protocorms were subcultured and allowed to regenerate into shoots. The number of regenerated shoots that are more than 1.0 cm in height and have at least 2 leaves, was recorded after 4 and 8 weeks (Table 1). More than 20 shoots were generated in each 0.4, 0.8 and 1.0 Gy treatment after 4 weeks. However, the number is decreasing at doses higher than 1.0Gy. Data was taken again after 4 weeks during the next subculture. There is an increase in the number of shoots for culture irradiated at 0, 0.2, 0.4, 0.8, and 1.0 Gy. However, the numbers of shoots at doses higher than 1.0 Gy remain the same. This result indicates that shoot regeneration was inhibited by the high irradiation dose.

A total of 99 plantlets from the earlier irradiation experiment were transferred into the glasshouse for screening. All of the plantlets were generated from the protocorms irradiated at dose 0, 0.2, 0.4, 0.8 and 1.0 Gy (Fig. 1). No plantlet was obtained for doses higher than 1.0 Gy because shoot regeneration was inhibited at tissue culture stage by the high irradiation dose.

Table 1 Number of regenerated shoots for *D.mirbellianum* after 4 and 8 weeks

Dose (Gy)	Regenerated shoots (Shoots with height >1cm and at least 2 leaves)	
	After 4 weeks	After 8 weeks
0	14	36
0.2	16	33
0.4	26	36
0.8	25	42
1.0	26	33
2.0	18	18
4.0	13	13
6.0	4	4
8.0	5	5
10.0	4	4

Figure 1 shows that more than 90% of the plantlets were less than 3.0 cm height one month after being transferred into the glasshouse. There were only 5 and 3 plantlets with height of more than 3.0 cm, from samples irradiated at 0.8 and 1.0 Gy respectively.

The distribution in the number of plantlet moved from range 0 to 3.0 cm height to range 3.0 to 4.5 cm after 2 months as shown in Fig. 2 indicating that the plantlets have grown normally. Treatment at 0.4 Gy has the highest number of plants with height 3.0 to 4.5 cm followed by treatment at 0.2 Gy.

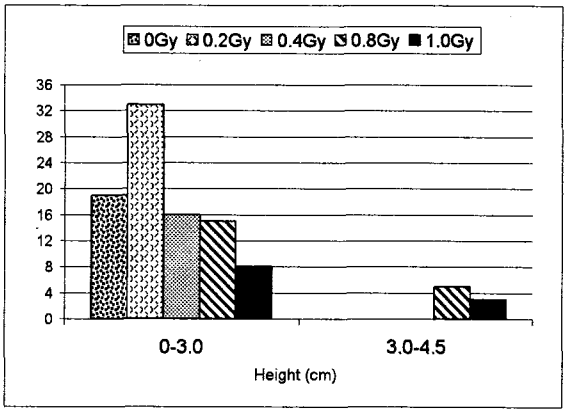

Fig. 1 Plant height after 1 month in the glasshouse

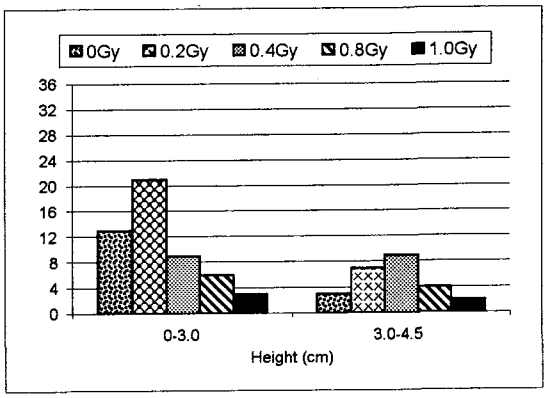

Fig. 2 Plant height 2 months in the glasshouse

After 4 months of planting, more plantlets reached more that 3.0 cm height (data not shown). Some plantlets with height of 0 to 3.0 cm in the previous month have grown to 3.0 to 4.5 cm height.

During this screening, no morphological change was observed on these plants. These may be observed when the plants have matured.

3.2 *Dendrobium crumenatum*

As the dosage of irradiation increasing, number of regenerated shoots decreasing (Table 2). The number of shoots was decreasing at doses higher than 0.4 Gy and at dose of higher than 1.0 Gy, the regeneration number decreased rapidly (Table 2). Whereas no shoot regeneration was observed for 15.0 Gy due to the high irradiation dose.

Table 2 Number of regenerated shoots for *D.crumenatum* after 8 weeks

Dose (Gy)	Regenerated shoots (shoots>1cm with 2 leaves)
0	27
0.2	23
0.4	34
0.8	28
1.0	29
2.0	15
4.0	22
6.0	17
8.0	11
10.0	2
12.0	3
15.0	0

References

1) Mohd. Nazir, B., and A.Sakinah (2001). Molecular techniques as complementary tools in orchid mutagenesis. *Proceedings of The 2001 FNCA Workshop on Agriculture: Plant Mutation Breeding & Biofertilizer, August 20-24, Bangkok, Thailand,* JAERI, 91-102.

2) Sakinah, A. and B.Mohd Nazir (2002). Increasing characteristic variations in Dendrobium orchid through acute irradiation. 17th World Orchid Conference and Show, Shah Alam, Malaysia, April 26-May 2, 2002.

3) Kraft, G., M.Kramer and M.Scholz (1992) *Radiat. Environ. Biophysics.* 31:161.

4) Tanaka, A., A.Sakamoto, Y.Ishigaki, O.Nikaido, G.Sun, Y.Hase, N.Shikazono, S.Tano and H.Watanabe, *Plant Physiol.* 129 (1) (2002) 64.

5) Nagatomi, S., A.Tanaka, A.Kato, H.Yamaguchi. H.Watanabe and S.Tano, *JAERI-Review 98-016 (1998) 41.*

6) Okamura, M., N.Yasuno, M.Ohtsuka, A. Tanaka, N.Shikazono and Y.Hase (2003) Wide variety of flower-color and –shape mutants regenerated from leaf cultures irradiated with ion beams. *Nucl. Instr. and Meth. in Phys. Res.* B 206:547-578.

7) Murashige, T. and F.Skoog (1962). A revised medium for rapid growth and bioassays with tobacco tissue cultures. *Physiol. Plant* 15: 473-497.

8) Mohd Nazir, B., A.Sakinah, A.H.Affrida, A.Zaiton, A.Tanaka, N.Shikazono, Y.Oono and Y.Hase (2004) TIARA Ann. Rep., 45-47.

2.5 Comparison of the Mutation Inducing Effect between Ion Beams and Gamma Rays

H. Yamaguchi*, T. Morishita*, M.Nishimura*, M. Kusaba*,
A. Tanaka** and Y. Hase**
Institute of Radiation Breeding, National Institute of Agrobiological Science*,
Department of Ion-beam-applied Biology, JAERI**

1. Introduction

Mutation induction is a useful method for plant breeding and the type of mutagenic treatment is an important factor for successful results.

One unique characteristic of ion beam irradiation is their high level of linear energy transfer (LET) and the potential to focus that high energy on a target site. As a consequence, ion beam irradiation can induce a high level of mutagenic effect. For this reason, there is an expectation for a higher degree of effect on DNA and a higher level of mutation induction when compared to gamma rays having a low level of LET[1),2)]. However, the use of ion beam irradiation as a mutagen for mutation breeding has not been examined. Therefore, we have investigated the nature of ion beams as a treatment for mutation breeding and compared it with gamma ray irradiation treatments.

2. Materials and methods

2.1 Plant material

The rice variety 'Hitomebore' was used as experimental material.

2.2 Irradiation treatment

Brown rice was placed on 6 cm diameter petri dishes with their embryos facing the irradiation source. The samples were irradiated with 220 MeV carbon-ion beams ($^{12}C^{5+}$, LET; 121 keV/μm), 320 MeV carbon-ion beams ($^{12}C^{6+}$, LET; 86 keV/μm) and 100 MeV helium-ion beams ($^{4}He^{2+}$, LET; 9 keV/μm) generated by an AVF-cyclotron. Gamma rays were applied to dry seed at dosage rate of 10 Gy per hour in a gamma-room.

2.3 Mutation frequency

The effect of mutation induction was investigated in the M_2 generation using the M_1-plant progeny method. Irradiated seed were sown to the field and M_2 seeds from the primary panicle of the M_1 plants were harvested and 25 seeds in each panicle were grown individually in greenhouse. The frequency of chlorophyll mutation was determined as the number of the M_1 spikes emerged chlorophyll mutation per the number of the M_1 spikes sown.

2.4 Spectrum of chlorophyll mutations

Chlorophyll mutations were classified into four groups, i.e. albino (white), xantha (yellow), viridis (light green) and others.

3. Results and Discussion

The effect of mutation induction was different among irradiation treatments (Table 1). Within the dose range irradiated in this experiment, the mutation frequency per M_1 spike in 100 MeV helium-ion beams was highest, 12.4 %. That was 10.4 % using 320 MeV carbon-ion beams, 9.0 % using carbon-ion beams and 8.4 % using gamma

Table 1 The effect of ion beam and gamma ray irradiation on mutation induction.

	Dose (Gy)	Chlorophyll mutation frequency per M1 spike (%)
220MeV carbon-ion beams	40	9.0
	30	8.5
	20	7.8
	10	6.0
320MeV carbon-ion beams	100	9.2
	80	10.4
	60	8.7
	40	5.4
100MeV helium-ion beams	250	12.4
	200	10.9
	150	8.4
	100	4.5
	50	2.1
gamma rays	300	8.4
	250	6.8
	200	7.7
	150	5.4
	100	4.3

rays, respectively.

The relative frequency and type of chlorophyll mutations generated by each treatment (albina, xantha viridis and others), were compared (Table 2). Among the irradiation treatments, the frequency of each mutant was similar and the differences were not observed. In an earlier study, Matsuo et al. (1958) reported that in rice, the types of chlorophyll mutants induced by X-rays and by thermal neutrons appeared similar[3]. In a similar study utilizing barley, the relative frequency of chlorophyll mutations induced by neutron and by X-ray irradiation also indicated little difference in treatments[4]. However, mutations induced by chemical mutagens, ethylene oxide etc., were different from those by radiation, that is to say, the frequency of viridis was higher than that of albina[4]. From these results, we supposed that the relative frequency of each type of chlorophyll mutation induced by radiation was same without regard to the type of radiation.

References

1) Y. Hirono, H. H. Smith, J. T. Lyman, K. H. Thompson, J. W. Baum, Radiation Research, 44(1970)204-223.
2) M. Mei, H. Deng, Y. Lu, C. Zhuang, Z. Liu, Q. Qiu, Y. Qiu, T. C. Yang, Adv. Space Res., 14(1994)363-372.
3) T. Matsuo, H. Yamaguchi, A. Ando, Jap J. Breeding, 8(1958)37-45.
4) A. M. van Harten, Mutation Breeding: Cambridge University Press,(1998)

Table 2 The relative frequency and type of chlorophyll mutant.

	(%) albina	xantha	viridis	others
220MeV carbon-ion beams	53.6	8.7	25.0	12.8
320MeV carbon-ion beams	50.4	11.7	25.1	12.8
100MeV helium-ion beams	47.7	15.0	24.6	12.6
gamma rays	52.5	8.2	30.6	8.7

2.6 Breeding of Stress Tolerant Variety Series in Ornamentals by Ion Beam Breeding; Comparison with Gamma-ray

M.Okamura*, N.Yasuno*, N.Fukaya*, A.Tanaka**, Y.Hase**, T.Morishita***, H.Yamaguchi*** and K.Degi***
Plant Laboratory, Agribio business company, Kirin Brewery Co., Ltd.*
Department of Ion-beam-applied Biology, JAERI**
Institute of Radiation Breeding, NIAS***

1. Introduction

Floriculture and ornamental business has been growing worldwide and the Japanese domestic market amounts to 1.2 billion yen. By the combined method of ion beam irradiation with tissue culture, new carnation varieties have been developed in 2002[1)]. Ion beams proved useful as new mutagen to obtain the commercial variety series with various flower colors in a short time[1, 2)].

In this study, we compared the efficiency of mutation generation between ion beams and gamma ray and their use for breeding stress tolerant varieties in carnation.

2. Materials and Methods

Standard carnation variety 'Star' (orange fancy), superior variety with a long vase life and high productivity, and spray carnation variety 'Nazareno' (deep purple), very popular variety with good color but without stem wax, were used for the experiment.

Ion beam irradiation; Small leaf segments with micro buds were placed in petri dish containing Murashige and Skoog medium supplemented with 0.1 mg/l NAA and 0.1 mg/l BA, 30 g/l sucrose and 7 g/l agar. The samples covered with Kapton film were irradiated with 220 MeV carbon ion beams from the TIARA AVF cyclotron (JAERI, Takasaki).

Gamma-ray irradiation; In vitro plants were irradiated with gamma rays from the Gamma room Co60 source (Institute of Radiation Breeding, NIAS) for 20 hours a day at 0.5 Gy/h. In acute irradiation samples were irradiated once of 30 to100 Gy. In chronic irradiation, samples were irradiated ten times for 3 weeks of 100 Gy in total.

After irradiation, the rate of shoot growth was examined. The irradiated plants were acclimatized in the greenhouse and cultivated to investigate flower color and shape.

3. Results and Discussion

The influence of irradiation on bud growth was examined. The median growth dose was estimated at 17 Gy, 20 Gy and 60 Gy for 220 Mev carbon ion, 320 MeV carbon ion and acute gamma-ray irradiations, respectively.

Various mutants of cv. Star in flower color and shape were obtained by ion, acute and chronic gamma irradiation. The mutation spectrum of

the flower color and shape induced by ion irradiation was wider as compared with acute-type gamma irradiation (Fig.1). Floral mutants with yellow petals were obtained both by ion and chronic gamma irradiation, but not by acute-type gamma irradiation (Fig.2). Promising mutants such as orange, yellow and striped flowers retained the stress tolerance of the parent to drought and had long vase life.

In ion beam irradiation of cv. Nazareno, floral mutants such as pure purple, pink, and bi-colored emerged and the new-type mutants with wax-rich stem were obtained (Fig.3). The wax-rich mutants are expected to reduce the amount of chemicals during cultivation, for stem wax plays the important role in disease and insect resistance in carnation.

In this study the spectra in floral mutants of carnation cv. Star by ion beams, acute-type and chronic-type gamma-ray irradiation were examined. The width of the spectrum was in the order; ion beams, chronic-type and acute- type gamma-rays. The results correspond with the reports in chrysanthemum.[3)]

In the process to develop the commercial carnation varieties[1)], mutants with various characteristics such as stem hardness, calyx breakage etc. were observed. Wax- rich mutants of cv. Nazareno showed the new potential of Ion beams for breeding stress tolerant variety series in ornamentals.

References

1) M.Okamura et. al., Nucl. Inst. and Meth. in Phys. Res. B 206 (2003), 574-578 S. A.
2) K.Ueno et. al., JAERI-Review 2003-033 (2003), 52-54
3) S.Nagatomi, et. al., Gamma Field Symposia, No.35 MAFF (1996), 51-69

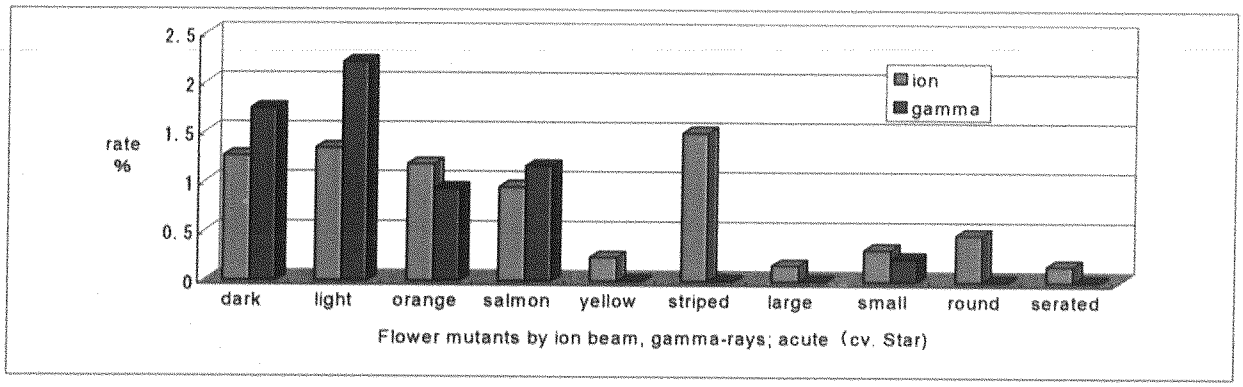

Fig.1 Rates of floral mutants in carnation obtained by the acute irradiation of ion beams and gamma-rays.

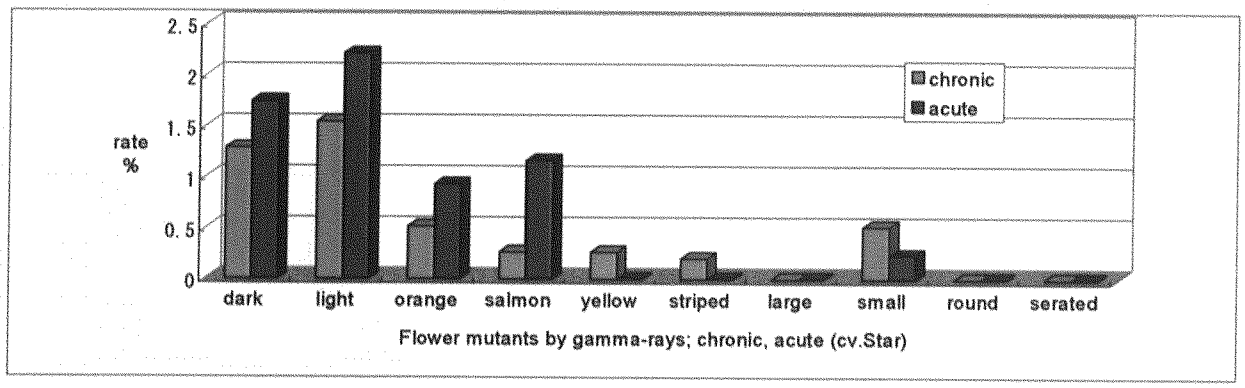

Fig.2 Rates of floral mutants in carnation obtained by the acute- and chronic- irradiation of gamma-rays.

Fig.3 Floral mutants of carnation cv. 'Nazareno' obtained by ion beam breeding. (left to right; up to bottom): Round mutant, Parent cv. Nazareno, Bi-colored mtant, Wax-rich mutant, Pure purple mutant.

2.7 Additional Improvement of *Chrysanthemum* using Ion Beam Re-irradiation

K. Ueno*, T. Shirao*, S. Nagayoshi*, Y. Hase** and A. Tanaka**
Kagoshima Biotechnology Institute*,
Department of Ion-beam-applied Biology, JAERI**

1. Introduction

Chrysanthemums have some agronomical traits to be improved such as reducing axillary buds to save farmer's labor and lower temperature flowering to save the cost of heating. We succeeded in the introduction of two new cultivars of chrysanthemum with reducing axillary buds in 2003 using ion beam irradiation[1), 2)]. The numbers of axillary buds were less than half to quarter, compared to the original cv. *"Jimba"*. They were named *"Imagine"* and *"Aladdin"*.

We are now going to prepare for selection of mutants which have both few axillary buds and low temperature flowering trait. In this paper, we describe the effects of re-irradiation of ion beam on the mutation induction from cultures of chrysanthemum.

2. Materials and Methods

2.1 Line breeding selection

The individually selected plants in 2003 were proliferated by vegetative propagation, and each selected plant was separated as a line. Then, they were grown in two different cropping systems; for selection either fewer axillary buds (flowering period in December) or lower temperature flowering type (flowering period in April).

2.2 Individual selection

Chrysanthemum (cvs. *"Jimba"*, *"Aladdin"* and selected line; B02-1-1) leaves were cultured on MS medium for plant regeneration by using 'line breeding system' [1), 2), 3)]. Then, they were grown in two different cropping systems in December or March.

2.3 Ion beam irradiation

Leaf discs of chrysanthemum were irradiated with 220 MeV or 320 MeV carbon ions, accelerated by AVF cyclotron at JAERI at doses of 1-5 Gy.

2.4 Analysis of DNA contents

DNA contents were estimated by the Ploidy Analyzer (PARTEC PA)[4)]. Sugar cane was used as genome size control. DNA contents of chrysanthemum were consistently determined by comparing with these of sugar cane.

3. Results and Discussions

3.1 Line breeding selection

Under low temperature, flowering period of *"Jimba"* or *"Aladdin"* are greatly delayed. Thus, in winter season, these cultivars are forced to culture under high temperature controlled at 15 to 20°C. As a result, we tried to select early flowering type to behave safety even under low temperature of 10 to 12°C.

The cropping systems for flowering in March and April were under low temperature for two and four months, respectively; although, that in December was only for several weeks. Therefore, the individually selected plants in December were flowering five to eight weeks after lighting stop. And those in March were flowering seven to eight weeks after lighting stop. The lines in April were flowering nine to 13 weeks after lighting stop (Fig. 1).

"Jimba" #2 is early flowering type which was selected by line breeding system. However, this line has many axillary buds. As a result of line selection, we obtained six lines for early flowering same as *"Jimba"* #2, which are derived from *"Aladdin"* (Fig. 1).

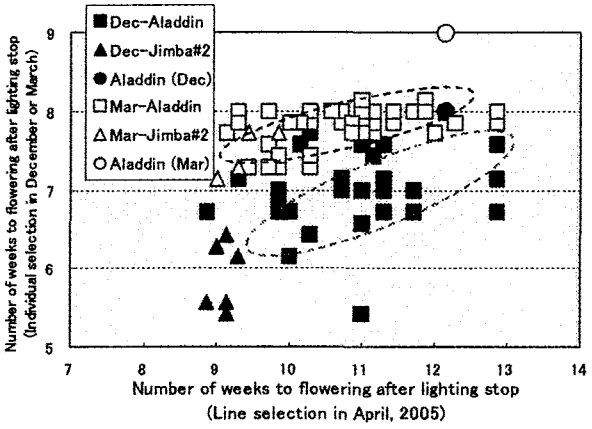

Fig. 1 Comparison of weeks to flowering in line selection.
Individual selection in December (*filled square* or *triangle*) or March (*open square* or *triangle*). Each selected mutants which are derived from *"Aladdin"* (*filled* or *open square*) and *"Jimba"* #2 (*filled* or *open triangle*). Weeks to flowering of original *"Aladdin"* in December (*filled circle*) and March (*open circle*).

3.2 Individual selection

We obtained approximately 6,000 regenerated M1 plants, which were derived from carbon ion re-irradiated leaf discs of *"Aladdin"* and B02-1-1. B02-1-1 is a selected line for few axillary bud, the numbers of blind nodes of this line were same as *"Imagine"*.

DNA contents of *"Aladdin"* and B02-1-1 were analyzed and compared with that of cv. *"Jimba"*. In *"Aladdin"* and B02-1-1, DNA contents did not show any decrease [1]. In M1 plants derived from leaf discs of *"Aladdin"* or B02-1-1, DNA contents remained almost the same level as in original "*Jimba*" [3].

In M1 plants derived from *"Imagine"*, DNA contents decreased more than 2% when ion beam were applied, then, almost all plants were lower plant height or poor growth than original plant of *"Imagine"* [3]. On the other hand, the M1 plants derived from *"Aladdin"* or B02-1-1 are vigorous growth and large volume. As a result of individual selection, we obtained 14 visible mutants for few axillary buds (Table 1). These mutants were same or higher levels of the numbers of blind nodes than *"Aladdin"*.

The flower characters of selected plants were shown in Fig. 2. In *"Aladdin"* or B02-1-1, the number of flower petals is more than that of *"Jimba"*. Also, the numbers of petals of the selected mutants are same levels of the original *"Aladdin"* or B02-1-1. These facts suggest that we are able to breed the additional improvement step by step by using ion beam re-irradiation.

From the screening of 4,265 controls or M1 plants, 46 visible mutants showing early flowering type were selected (Table 2). These mutants were flowering in seven to eight weeks after lighting stop even under low temperature of 10 to 12°C during 2 to 3 months.

When we have to use the re-irradiation technique for plant improvement, the materials/ mutants must be those with keeping original DNA contents. We hope next season to be able to select lines which still keep both selected characters.

References

1) K. Ueno et al., TIARA Ann. Rep. 2002 (2003) 52-54
2) S. Nagayoshi, Radiation & Industries 98 (2003) 10-16.
3) K. Ueno et al., TIARA Ann. Rep. 2003 (2004) 53-55
4) K. Mishiba and M. Mii, Cell Tech., (1988) Vol.17, No. 4: 609-615.

Table 1. The number of tested and selected plants in December 2004, which regenerated from leaf cultures re-irradiated by ion beam, for selection of few axillary buds.

Cultiver	Line	Number of tested and selected plants								
		non-irradiated	C220 (Gy) 1	C220 (Gy) 2	C320 (Gy) 1	C320 (Gy) 2	C320 (Gy) 3	meristem clone	non-treated	Total
Aladdin		663	269	205	0	195	234	17	19	1,602
Jimba	#1							0	19	19
	#2							0	19	19
	B02-1-1	47	15	4		120	195	10	13	404
	Total	710	284	209	0	315	429	27	70	2,044
Number of selected plants		3	1	2	0	5	2	1	0	14
(%)		0.4	0.4	1.0		1.6	0.5			0.7

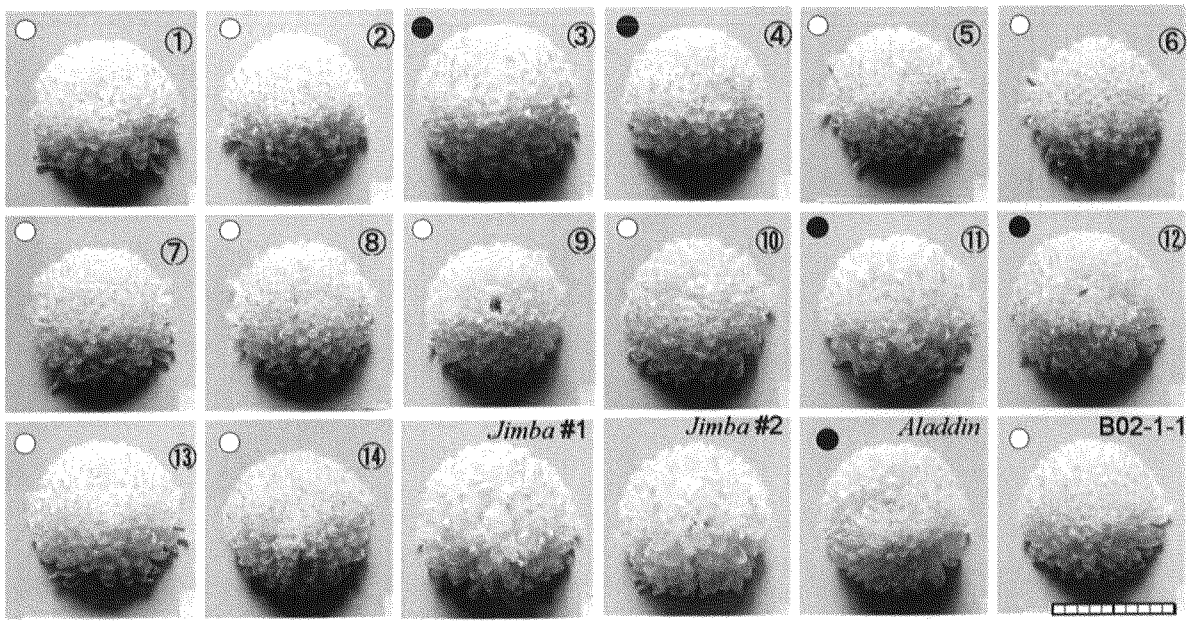

Fig. 2 Individual selected plants for few axillary buds mutants, which were derived from leaf of *"Aladdin"* or B02-1-1, and these are M1 plants after C ion beam re-irradiation.
●: *"Aladdin"*, ○: B02-1-1 (selected mutant line of few axillary buds), bar: 10cm

Table 2. The number of tested and selected plants in March 2005, which regenerated from leaf cultures re-irradiated by ion beam, for selection of early flowering type.

Cultiver	Line	Number of tested and selected plants								
		non-irradiated	C220 (Gy) 1	C220 (Gy) 2	C320 (Gy) 1	C320 (Gy) 2	C320 (Gy) 3	meristem clone	non-treated	Total
Aladdin		1,129	468	272	186	1,129	880	57	29	4,150
Jimba	#1							10	30	40
	#2							10	0	10
	B02-1-1							65	0	65
	Total	1,129	468	272	186	1,129	880	142	59	4,265
Number of selected plants		11	3	6	2	10	12	2	0	46
(%)		1.0	0.6	2.2	1.1	0.9	1.4			1.1

2.8 Effects of Ion Beam Irradiation on Mutation in Sugi Cedar (*Cryptomeria japonica*) and Hinoki Cypress (*Chamaecyparis obtusa*)

K. Ishii*, Y. Hosoi*, Y. Hase** and A. Tanaka**

Department of Molecular and Cell Biology, Forestry and Forest Products Research Institute*, Department of Ion-beam-applied Biology, JAERI**

1. Introduction

Sugi cedar (*Cryptomeria japonica* D. Don) and Hinoki cypress (*Chamaecyparis obtusa* Sieb. et Zucc.) are indigenous conifer species in Japan, and the most important plantation forest trees. They produce the sawn timber of the highest quality for house construction. In forest tree species with long life cycle, mutation is supposed to be promising in shortening the breeding time.

Ion beam is expected to increase the mutation frequency and wide spectrum, since it has a high LET (linear energy transfer). The combination of ion beam irradiation and tissue culture was beneficial for high frequent mutation induction[1)2)3)]. In the previous report, we have obtained the xantha (yellowish color) and wax rich mutants in Hinoki cypress by ion beam irradiation[4)]. We tried to detect not only leaf plastid mutation by observation but also the chromosomal level mutation by flow cytometer[5)].

In this study, we tried to induce the mutants by irradiation of the in vitro cultured buds of Sugi cedar and shoot primordia of Hinoki cypress with $^{4}He^{2+}$ and $^{12}C^{6+}$ heavy ion beams. Mutants such as male-sterile to solve the problem of pollinosis are promising in the future.

2. Experimental procedure

2.1 Plant materials and ion beam irradiation

In vitro cultured buds on half-strength LP medium[6)] of Sugi cedar originally collected from arboretum in Forestry and Forest Products Research Institute, Tsukuba, Ibaraki, were used. Shoot primordia of Hinoki cypress were also used for the experiments. They are cultured on CD medium[7)] supplemented with 10μM 6-benzylaminopurine and 0.03 μM naphthalene acetic acid (NAA). Fresh buds or shoot primordia were subcultured on the medium in petri dish (35 x 10 mm) which was covered with Kapton film. They were irradiated with 50 MeV $^{4}He^{2+}$ or 320 MeV $^{12}C^{6+}$ ion beams delivered from the AVF cyclotron at TIARA in JAERI-Takasaki. After irradiation the shoot primordia were subcultured to the new media for assessing the surviving rate and detecting mutation.

2.2 Treatments of GA on Sugi cedar and UV on Hinoki cypress

Regenerated Sugi cedar trees were grown in the greenhouse and treated with gibberellic acid at 100ppm to induce the formation of male flowers. After 3 months, male flower induction was checked with each tree.

Shoot primordia irradiated with He ion beam were further irradiated with 0.6 mW/cm^2 of UVB in the Raytron (Nippon Ikakikai, RTP-220-NC).

Surviving shoot primordia were subcultured to be checked the morphological characters.

3. Results and Discussion

Surviving rate of in vitro cultured buds of Sugi cedar and shoot primordia of Hinoki cypress irradiated with 5 to 20 Gy $^{4}He^{2+}$ and 1 to 5 Gy $^{12}C^{6+}$ ion beams decreased as the amounts of irradiation increased (Fig. 1,2). Five Gy $^{12}C^{6+}$ ion beams caused more damage to Hinoki shoot primordia than $^{4}He^{2+}$ in the same dose. There was plastid mutation like albino and partial light-green leaves in Sugi cedar (Fig. 3,4). Wax rich shoots appeared in Hinoki cypress culture. Shoot elongation from surviving buds was suppressed with irradiation of 2 and 5 Gy $^{12}C^{6+}$ ion beams. Among the regenerated plantlets which have been habituated and grown in a greenhouse for further assessing experiments to detect mutants, there were plantlets which did not survive. Preliminary assessing the sterile mutants by spraying gibberellic acid for inducing flowers indicated that male flowers were induced in Sugi cedar with 5 Gy but not with 10 and 20 Gy $^{4}He^{2+}$ ion treatment (Fig. 5).

Among the regenerated plantlets of Hinoki cypress after UVB treatment, wax rich mutants were observed. We described also the albino, xantha and wax rich mutants from irradiated shoot primordium of Hinoki cypress[4]. Wax rich mutants may have some resistance to UVB because wax absorbs UVB, however further study is needed for properly detecting the UVB resistant mutations by screening the UVB irradiation condition.

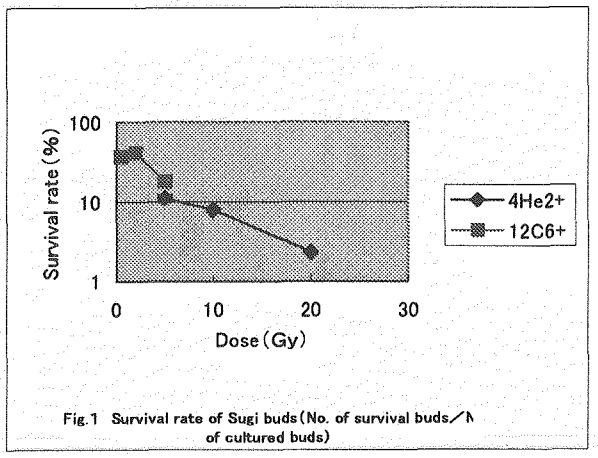

Fig.1 Survival rate of Sugi buds (No. of survival buds／N of cultured buds)

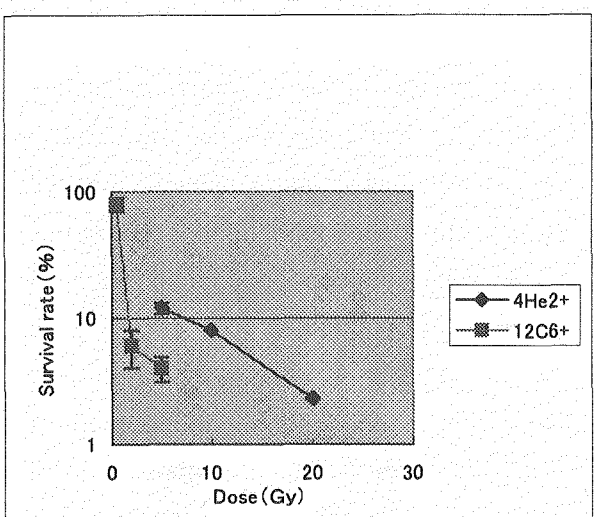

Fig 2 Survival rate of Hinoki shoot primordia (No. of survival sh primordia/No. of cultured shoot primordia)

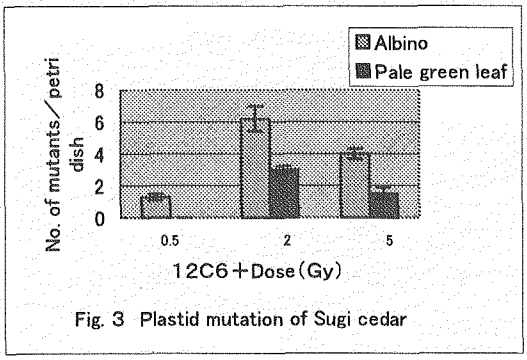

Fig. 3 Plastid mutation of Sugi cedar

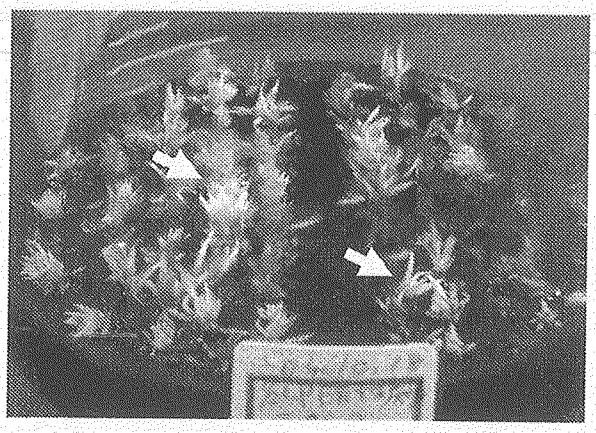

Fig. 4 Albino leaf of Sugi cedar (arrows)

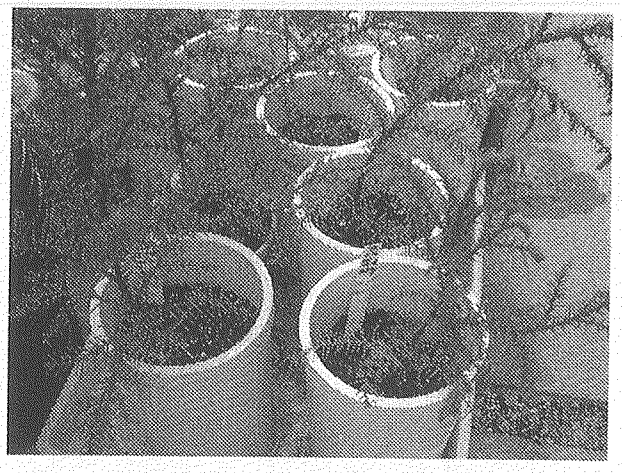

Fig. 5 Gibberellic acid treated Sugi cedar which was irradiated with $^{4}He^{2+}$ ion

References

1)S. Nagatomi, A. Tanaka, A. Kato, H. Watanabe and S. Tano, TIARA Annual Report 5(1996)50-52.

2)S. Nagatomi, A. Tanaka, H. Watanabe and S. Tano, TIARA Annual Report 6(1997) 48-50.

3)T. Nakahara, K.Hirashima, M. Koga, A. Tanaka, N. Shikazono and H. Watanabe, TIARA Annual Report 1998(1999)28-29.

4) K. Ishii, Y.Hase, N. Shikazono and A.Tanaka, TIARA Annual Report 2000(2001)55-56.

5)K. Ishii, Y.Hase and A.Tanaka, TIARA Annual Report 2003(2004)56-57.

6)J. Aitken-Christie and T.A. Thorpe, Cell Culture and Somatic Cell Genetics of Plants 1(1984)82-95.

7)K. Ishii, Plant Cell Tissue and Organ Culture 7(1986)247-255.

JP0650176

2.9 Effects of Ion Beam Irradiation on the Shoots Regeneration from Callus and Shoot Apex of Garlic (*Allium Sativum* L.)

T. Tashiro*, Y. Yamamoto**, A. Tanaka*** and Y. Hase***
Faculty of Horticulture, Chiba University*
Yokkaichi Agriculture Center, Yokkaichi City**
Department of Ion-beam-applied Biology, JAERI***

1.Introduction

We established a novel system of practical micropropagation for an enhanced plant propagation, which produced viable bulblets *in vitro*. This micropropagation system is an effective method to proliferate, select and plant in the field[1]. A combined method of ion beam irradiation with tissue culture resulted in a high frequent mutation. We supposed that the ion beams induced specific mutation not only on morphological characters, but also on the chemical composition of garlic. One of the irradiated materials was compact and granular embryogenic callus (hereinafter referred to as "callus")[2,3]. The other was thin sections of bulb basal plates (hereinafter referred to as "segment")[3,4]. Callus necessarily takes over four months culture period to produce bulblets, but the regenerated shoots can produce enough numbers to select mutants. Segment is induced directly from basal plates within two months culture period, but it is difficult to produce many regenerated shoots. The initial stage of contamination is low in the irradiated callus and it is high in the irradiated basal plates.

With an aim to solve the above-mentioned problems, we have been studying whether the irradiation to each callus stage had influences on the culture period and shoot regeneration rate. Also, the cultured shoot apex induces shoots and bulblets within a very short period of about two months and has less of the initial stage contamination. We have been studying this method to investigate the irradiation effect in a short-term. We have investigated the effects of ion beams on the mutation of volatile sulfur compounds of garlic as our last objective.

2.Materials and Methods

2.1 Shoots regeneration from callus classified by the growth stage

We classified the growth stages of callus into; stage Ⅰ, at the callus proliferation, stage Ⅱ, at the regeneration and stage Ⅲ, at the shoots induction. The callus, 1mm thick, was placed in a plastic petri dish containing MS medium supplemented with 2,4-D 0.5mg/l for stage Ⅰ and with BA 2mg/l and NAA 0.2mg/l for stage Ⅱ, Ⅲ. The dishes were covered with Kapton film, and then irradiated with 320MeV $^{12}C^{6+}$ or 50MeV $^{4}He^{2+}$ ion beam from the TIARA AVF cyclotron in JAERI. The irradiation dosages were 0.2Gy for each sample.

2.2 Shoots regeneration from shoot apex

The shoot apexes, 0.5mm square, were picked out under the stereomicroscope and then cultured on MS hormone free

medium. Five days later, they were transplanted to a plastic petri dish containing the same medium. Two days later, 70 shoot apexes were irradiated with 0.5Gy in 320MeV $^{12}C^{6+}$ and 53 shoot apexes were irradiated with 0.5Gy in 50MeV $^{4}He^{2+}$.

3.Results and Discussions

3.1 Effect of ion beam irradiation on the shoots regeneration from callus classified by the growth stage

The culture period was dependent on the different callus growth stage irradiated in carbon or helium ion beams (Table 1). The irradiated calluses in carbon ion beams need longer culture periods than the calluses in helium. The culture periods in the treatments were longer than the control in stages II and III (Table 1). In the control, it took 157 days to culture in stage I, 81 days in stage II and 45 days in stage III. The response of regeneration rate from different callus growth stage irradiated in carbon or helium ion beams is shown in Table 2. The regeneration rate in all callus growth stages was 100% in the control. The irradiated calluses in both carbon and helium ion beams in stage I reduced the regeneration rate. In stage II, the carbon irradiated callus reduced in regeneration, but the helium irradiated callus did not reduce in regeneration rate. The regeneration rate in the treatments were the same as the control in stage III.

The response of shoot regeneration from different callus growth stage irradiated in carbon and helium ion beams is shown in Table 3. The number of regenerated shoots was 3.4 in stage I, 132.7 in stage II and 132.6 in stage III using carbon ion beam, and 5.8 in stage I, 310.0 in stage II and 451.3 in stage III using helium ion beam, respectively. The number of regenerated shoots was 12.8 in stage I, 623.0 in stage II and 775.0 in stage III in the non-irradiated treatment.

These data indicated that there were difference among the sensitivity for ion beam irradiation in each callus growth stage and sensitivity tended to be higher as the callus growth stage progressed. The sensitivity for irradiated calluses was higher in carbon ion beam than in helium ion beam.

The fewer numbers of regenerated shoots in stage I in non-irradiated and

Table 1 The culture period[1] of the ion beam irradiated callus, which was classified by growth stage

Radiation	Callus growing stage		
	Stage I (days)	Stage II (days)	Stage III (days)
Carbon	165	101	101
Helium	154	90	88
Control	157	81	45

1) Culture days from radiation to acclimatization

Table 2 The regeneration rate[1] of the ion beam irradiated callus, which was classified by growth stage

Radiation	Callus growing stage		
	Stage I (%)	Stage II (%)	Stage III (%)
Carbon	51.7	78.3	100
Helium	71.4	100	100
Control	100	100	100

1) Percentage regenerated callus after irradiation and transplanting to the medium for regeneration

Table 3 The regeneration shoots[1] of the ion beam irradiated callus, which was classified by growth stage

Radiation	Callus growing stage		
	Stage I (No. of plants /callus g)	Stage II (No. of plants /callus g)	Stage III (No. of plants /callus g)
Carbon	3.4	132.7	132.6
Helium	5.8	310.0	451.3
Control	12.8	623.0	775.0

1) Number of regenerated shoots after irradiation and transplanting to the medium for regeneration

irradiated treatments strongly suggested that the cells were injured by the manipulation of the 1mm thick callus.

3.2 Effect of ion beam irradiation on the shoots regeneration from shoot apex

The response of morphological character of regenerated shoots irradiated with carbon and helium ion beams is shown in Table 4. The cultured shoot apex *in vitro* performed equally on ordinary shoot with normal leaf 3～5mm width. In the control, the rate of normal leaves was 54.8%, whilst it was 2.9% and 15.1% in carbon and helium respectively. The ion beam influenced leaf color, width and growing speed remarkably. The irradiation induced abnormal leaves such as about 1mm width and needle-like narrow leaves. Although there were no abnormal leaves in the control, narrow leaves were induced in the carbon and helium treatments at an induction rate of 17.1% and 13.2% respectively. This type of abnormal leaves is a revelation due to an induced irradiation of segments and calluses.

A single irradiated shoot apex induced multiple bulblets in both carbon and helium ion beams (Fig.1). The rate of induced multiple bulblets due to irradiation was almost the same in the control. The vitrified shoots occurred at a rate of 45.2% in the in the control. We inferred that this was because the whole apex was kept in the medium, even as it was transferred. The vitrified shoots occurred at a rate of 72.9% on carbon and 71.7% on helium. These percentage increases are a confirmation of the effect of the ion beam.

References

1) Y. Yamamoto and T. Tashiro, International Plant Propagatorrs'Society 7:17-18(2000).
2) T.Tashiro, Y.Yamamoto, A.Tanaka, N.Shikazono, and Y.Hase, TIARA Annual Report 2001, JAERI-Review 2002-035:49-51(2002).
3) T.Tashiro, Y.Yamamoto, A.Tanaka, N.Shikazono, and Y.Hase, TIARA Annual Report 2002, JAERI-Review 2003-033:60-62(2003).
4) T.Tashiro, Y.Yamamoto, A.Tanaka, N.Shikazono, and Y.Hase, TIARA Annual Report 2003, JAERI-Review 2004-025:58-60(2004).

Table 4 Variants regenerated from shoot apex cultures irradiated by ion beam

Morphological character	Carbon	Helium	Control
No. of irradiated shoot apex(a)	70	53	126
Normal shoots(%)	2.9(2)[2)]	15.1(8)	54.8(69)
Vitrified shoots(%)	72.9(51)	71.7(38)	45.2(57)
Abnormal shoots (%)	24.2(17)	13.2(7)	0(0)
Shoots with narrow leaves(%)	17.1(12)	13.2(7)	0(0)
Shoots with light green leaves(%)	7.1(5)	0(0)	0(0)
multiple bulblet(%)[1)]	26.3(5)	26.7(4)	26.1(18)

1) Percentage shooot apex with multiple bulblets regenerated from shoot apex cultures, except for vitrified shoot, irradiated by ion beam

2)Figures in parenthesis are the number of variants

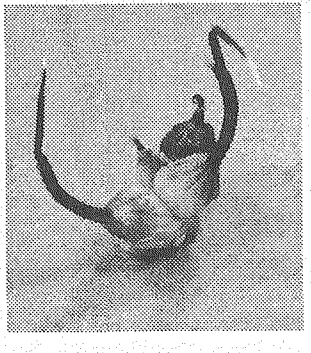

Fig.1 Multiple bulblet induced by shoot spex irradiated with 0.5Gy helium ion beam.

2.10 Selection of Low Oxalate Mutant in the M_2 Progeny Derived from Irradiated-seeds with Ion Beam and Gamma-ray in Spinach

K. Murakami*, N. Hata*, Y. Yoshida*, M. Masuda*, A. Tanaka**,
N. Shikazono** and Y. Hase**
Department of Applied Plant Science, Faculty of Agriculture, Okayama University*
Department of Ion-beam-applied Biology, JAERI**

1. Introduction

Spinach (*Spinacia oleracea* L.) is one of the most important vegetables grown worldwide for its high nutritious value. However, it accumulates large amounts of oxalate, which causes inhibition of calcium absorption and contributes to the formation of urinary stones in human[1]. Although several attempts to reduce oxalate content in spinach leaves have been made by cultivation techniques, there has been limited success. Furthermore, there has not been any improved cultivar or line with regard to reduced oxalate content[2]. A new approach through mutation breeding could provide an effective alternative solution.

In seed propagated crops, a mutant gene is generally recessive and easily identified in homozygous status in M_2 progenies of autogamous species. However, in cross fertilized species, mutant genes induced in M_1 plants remain heterozygous in M_2 progeny, making phenotypic detection of mutants difficult. Since spinach is a typical dioecious crop, mutant gene expression in M_2 progeny seldom occurs. However, occur spontaneously a few gynomonoecious plants with the ability to self-fertilize and their stable lines can be established by successive self-fertilization[3),4)]. Mutation breeding programs may be conducted effectively by employing such lines. We reported that temperature at 20-25 ℃ promoted the expression of gynomonoecy[5)].

In our previous report, we irradiated gynomonoecious spinach seeds with $^{12}C^{5+}$ and $^{4}He^{2+}$ ion beam and gamma-ray, and indicated that recessive mutants could be obtained in M_2 generation through self-fertilization of gynomonoecious plants in spinach[6)].

In this study, we measured the oxalate content of leaf blades in the M_2 progenies derived from ion beam and gamma-ray irradiated spinach seeds.

2. Experimental procedure

Spinacia oleracea L. cv. Shin-Nippon (Atariya Seed, Chiba) was used because relatively higher percentages of gynomonoecious plants had been observed in this cultivar than others. Self-fertilized seeds were harvested separately from three gynomonoecious plants. After removal of their pericarp, the seeds were irradiated with 100 Gy gamma ray, 5-30 Gy 220 MeV $^{12}C^{5+}$ and 50-300 Gy 50 MeV $^{4}He^{2+}$ ion beams. The M_1 seeds were sown and seedlings were planted in an open-sided plastic house. After bolting and just before anthesis, the plants were covered with transparent bags to prevent cross-pollination. Self-fertilized M_2 seeds from each M_1 plants were harvested separately from July to August.

On 15 September, 2003, 16 seeds per

each M_2 line (total 5392 seeds in 337 M_2 lines) were sown on cell flat (128 cells per tray, 30×60 cm) filled with vermiculite. At sowing time, these cell flats were put in a 60 cm wide-row with 5 cm interval in an open-sided plastic house, in which N, P_2O_5 and K_2O had been applied to ground at 20 $kg \cdot 10a^{-1}$. To enable root development into the ground from basal hole of the cell flats, the seedlings were irrigated thoroughly from the surface of cell flats for 2 weeks after sowing. Thereafter, further was done by supplying water between the rows.

On 15 August, 2003, leaf discs with 0.6 cm diameter were collected from the apical part of the largest leaf blades in each of 1607 M_2 plants at 6-8 leaf stage and put into tubes. At the first screening, a sample constituted two discs from two different plants. Two leaf discs from 2 plants were put into the 2 mL tube, 1.9 mL 1N-H_2SO_4 solution was added and the setup left for more than 24 hrs at room temperature. Then it was diluted to 1:10 with water and analyzed with a HPLC system (Shim-pack SCR-102H column; 3×30 mm, Shimadzu, Kyoto). Sample solution was not filtered. A sample of 10 μL was loaded. The flow rate was 1.5 ml/min and column temperature was 80℃. The mobile phase was 1% (v/v) phosphoric acid. Oxalate was determined by absorbance at 210 nm with UV–VIS Detector SPD-10A (Shimadzu, Kyoto). The resulting chromatograms were analyzed with a data processing program (BROWIN, JASCO, Tokyo).

In the first analysis of 813 samples, 9 samples with low oxalate content and 13 samples with high oxalate content were selected. At the second screening, one leaf disc with 6 mm diameter was sampled from the apical part of 4th-expanded leaf blades of selected 38 plants on 22 December, 2003. Then, the second analysis of total oxalate content was carried out in each selected plant. After measuring the fresh weights of the leaf disks, the oxalate concentration was determined as described above.

3. Results and Discussion

At the first screening, 1607 plants were tested. The variation of oxalate concentration ranged from 0.5 to 1.8 μmol/leaf disc and showed normal distribution (Fig. 1). There were no plants with extreamly low or high content. The samples whose oxalate concentration was lower than 0.7 μmol/leaf disc and higher than 1.7 μmol/leaf disc were selected, and re-analyzed. In the second analysis, plants selected as low in oxalate in the first screening also tended to contain lower oxalate than those selected as high in oxalate (Fig. 2). In this study, we did not obtain mutants with extreamly low oxalate content, but it was indicated that effective selection of low oxalate mutant from many M_2 plants could be achieved by the following two steps; the analysis of pooled leave of 2 plants in the first and the analysis of selected individuals in the second.

References

1) B. Libert and V. R. Franceschi, J. Agric. Food Chem. 35 (1987) 926-938.
2) Y. Kawazu, M. Okimura, T. Ishii and S. Yui, Scientia Hortic. 97 (2003) 203-210.
3) S. Sugiyama and C. Suto, Bull. Nat. Inst. Agr. Sci. D6 (1964) 211-329 (In Japanese with English summary).
4) T. Nishi and T. Hiraoka, Bull. Hort. Res. Sta. A4 (1965) 153-179 (In Japanese with English summary).

5) N. Hata, K. Murakami, Y. Yoshida and M. Masuda, J. Japan. Soc. Hort. Sci. 74 (2005) 228-233.
6) N. Hata, K. Murakami, Y. Yoshida, M. Masuda, A. Tanaka, N. Shikazono and Y. Hase, JAERI-Review 2004-025 (2004) 61-63.

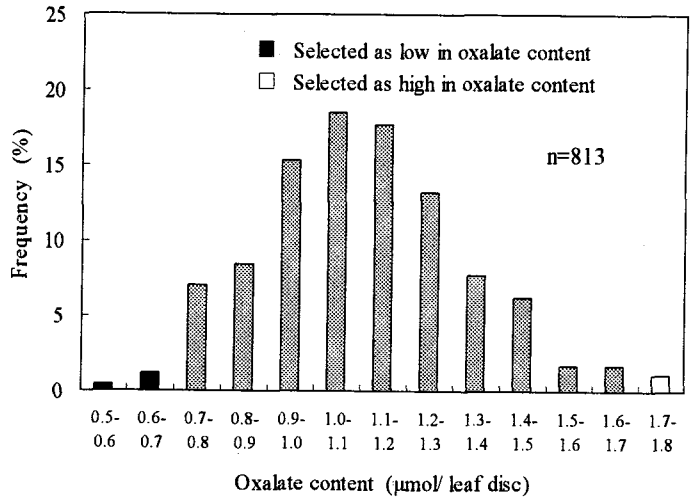

Fig. 1 Frequency distribution of oxalate content in the first analysis of pooled leaves of 2 plants.

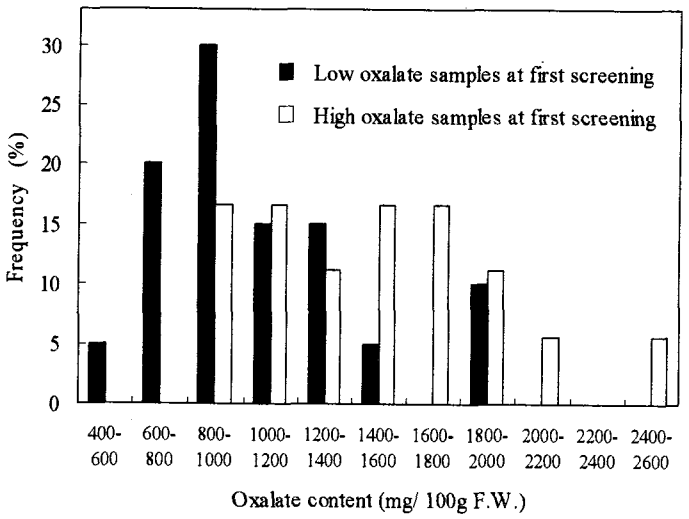

Fig. 2 Frequency distribution of oxalate content in the second analysis in selected plants.

2.11 Effect of Ion Beam Irradiation on Coloration of Fruit Skin of Eggplant (*Solanum melongena* L.)

N. Matsuzoe*, T. Umeda*, Y. Hase** and A. Tanaka**
Faculty of Environmental and Symbiotic Sciences, Prefectural University of Kumamoto*, Department of Ion-beam-applied Biology, JAERI **

Introduction

Fruit skin color of eggplant (*Solanum melongena* L.), depends on quantities of anthocyanin in fruit skin, is one of the important qualities when consumers choose which eggplants they buy. Then, Anthocyanin is also an important antioxidant for human health. Quality and quantity of light effects on the coloration of fruit skin of eggplants. We have reported the cultivars/lines of eggplant in the dark treatment, which were grouped into three pigmentation types (photoreceptive, non-photoreceptive and middle type) for photosensitivity to fruit coloration[1] (Fig.1). The major anthocyanin in the fruit skin of all the cultivars/lines, except cultivars in American group, was delphinidin 3-*p*-coumaroylrhamnosylglucoside-5-glucoside (Dp3*p*CRG5G); the ratio of the Dp3*p*CRG5G to the total anthocyanin ranged from 69.1 to 87.7% in these cultivars/line. The major anthocyanin of cultivars in American group was delphinidin 3-rhamnosylglucoside (Dp3RG), made up 79.5 of the total. We tried to obtain mutants of eggplants that have other major anthocyanins than Dp3*p*CRG5G or Dp3RG because of studying the synthetic pathway of anthocyanin. In this paper, we also describe effects of the ion beam irradiation on germination rate in M1 generation. As for M2 generation, we report individuals that change their photosensitivity to fruit coloration.

Materials and Methods

Solanum melongena cvs. 'Kitta', 'Black Beauty' and 'Kumamotonaga' were used for the experiments. Dry seeds of the cultivars were irradiated with ion beam (220 MeV $^{12}C^{5+}$) with the doses 25 and 50 Gy at TIARA. After irradiation, the germination rate was investigated in the greenhouse and the seedlings were transplanted in the field. M2 seeds derived from self-pollination of the M1 plants were germinated in the greenhouse and the seedlings were transplanted in the field. Changes of the fruit color and quantity of a major anthocyanin of those fruits were the main focus of this investigation. And furthermore, the photosensitivity to fruit coloration was assessed by color of the skin under the calyx, where is the absence of light (Fig.2).

Results and Discussion

The influences of ion beam irradiation on germination were shown in Table 1. The germination rates were 71-96 in all cultivars irradiated with 25 Gy. That of cv. 'Kitta' irradiated with 50gy was the lowest in those of all cultivars. After transplanting the M1 plants to the field, very few M2 plants were derived from self-pollination of the M1 plants irradiated with 50 Gy. These results suggest that the best dose to obtain mutants of eggplants is the vicinity of 25Gy in 220 MeV carbon (12C5+) ion beam.

In 62 plants in M2 generation (25Gy),

there was no mutant plant that had other major anthocyanin than Dp3*p*CRG5G or Dp3RG (data not shown). However, we found that 5 mutant plants changed their photosensitivity to fruit coloration in M2 generation (Fig.3). Three mutant plants were in cv. Kumamotonaga and 2 mutant plants were in cv. Kitta. We are currently researching the characteristics on coloration of the mutant plants and these selfed lines.

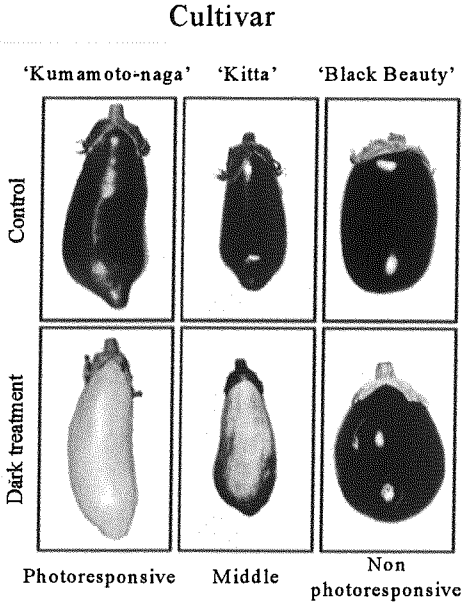

Fig.1 Color of fruit used to the experiment and effect of dark treatment to fruit on skin coloration.

Table 1. Effect of carbon ion beam on Germinations of eggplants.

Dose (Gy)	Cultivar	Germination rate (%)
25	Kumamoto-naga	96
	Black-beauty	71
	Kitta	91
50	Kumamoto-naga	89
	Black-beauty	80
	Kitta	50

References

1) N. Matsuzoe, M. Yamaguchi, S. Kawanobu, Y. Watanabe, H. Higashi and Y. Sakata, J. Japan. Soc. Hort. Sci. 68, 138-145 (1999)

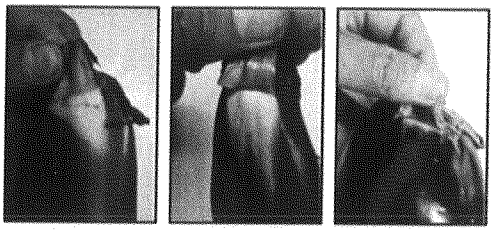

Fig.2 Color of fruit skin under calyx of eggplants before irradiation

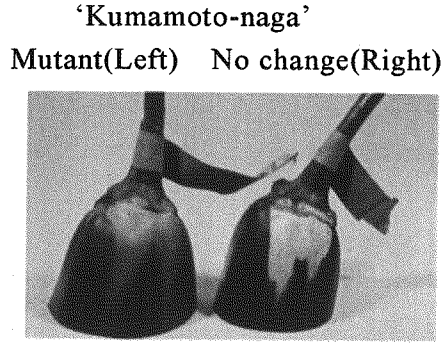

Fig.3 Mutants in color of fruit skin under the calyx.
Assessment of photosensitivity to fruit coloration.

2.12 Studies on Flower Color and Morphological Mutations from Chrysanthemum In Vitro Explants Irradiated with Ion Beams

T.Sato*, T.Ohya*, Y.Hase** and A.Tanaka**
Akita prefecture Agricultural experiment station.*
Department of Ion-beam-applied Biology, JAERI**

1. Introduction

Chrysanthemum is important flower in Akita prefecture. Especially chrysanthemum cultivar "Natsuyasumi" (purpulish red flower) is suited for the climate of Akita prefecture. However, grower, market and consumer were demanded for yellow or white color cultivar.

By the last year, we examined an adequate dose of Natsuyasumi flower culture materials[1]. As a result, whitish flower color mutants were obtained with 20Gy $^{12}C^{5+}$ ion beam irradiation (NPI-220-20-W-2 : NPIW2)[2].

However, some red remained at the center and the edge of a flower. Therefore, these white flower color mutants are not fulfilled the purpose.

In this study, we irradiated ion beam to NPIW2 again.

2. Materials and Methods

We used the explants of petal of NPIW2 on medium in petri dishes. The samples were irradiated with 10Gy 220MeV ($^{12}C^{5+}$) or 320MeV ($^{12}C^{6+}$) ion beams from the TIARA AVF cyclotron in JAERI. After the irradiation, the cultured materials were transferred to a new medium and obtained regeneration plants. After acclimation, we transplantated regeneration pants to field. In flowering time, we selected flower color mutant.

3. Results and Discussion

The flow of the obtaining of a flower color mutant was shown in fig.1.

Useful mutant were not obtained by the $^{12}C^{5+}$ ion beam irradiation.

In case of $^{12}C^{6+}$, the white (NPIW2-NPI320-10-W-1 and 2) and yellow (NPIW2-NPI320-10-Y-1) flower color variants were obtained (Fig. 2). The flower color was a white at NPIW2-NPI320-10-W-1 and 2 and the remainder of the tinge of red like NPIW2 wasn't observed. However, the falling of the plant length and the delay of the flowering time were observed.

On the other hand, in NPIW2-NPI320-10-Y-1, the flower color was vivid reddish yellow. It was suggested that, re-irradiation of the ion beam was effective to obtaining of a yellow flower color mutant from Natsuyasumi. However, the lowering of the plant length and disorder in the flower form were observed.

In this study, we were not able to get an useful mutants. However, re-irradiation of ion beam is effective for induction of flower color mutant in chrysanthemum. Therefore, we continue ion beam re-irradiation to selected white flower color mutant.

References

1) T.Sato, H.Naganoma, Y.Hase and A.Tanaka, JAERI-Review 2002-035 (2002).68-69.

2) T.Sato, Y.Torigoe, Y.Hase and A.Tanaka, JAERI-Review 2003-033 (2003) 81-82.

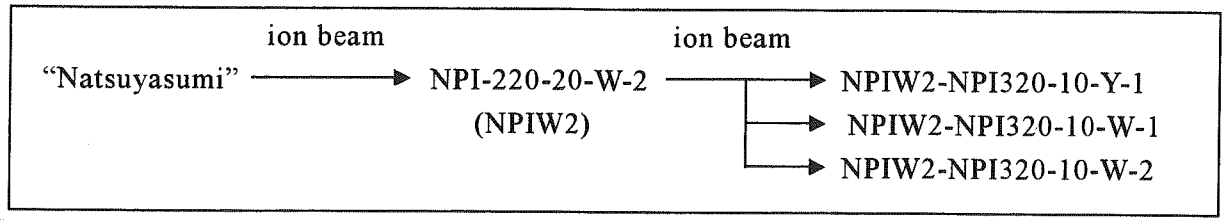

Fig.1 The flow of the obtaining of a flower color mutant.

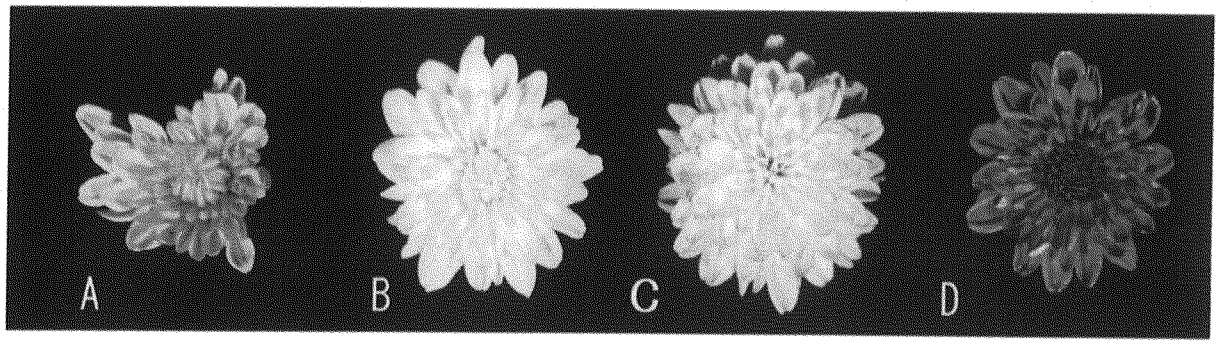

Fig.2 Selected white flower color mutants.
A : NPIW2-NPI320-10-Y-1 , B : NPIW2-NPI320-10-W-1
C : NPI-220-20-W-2(NPIW2), D: "Natsuyasumi" (Control)

Table Character of flower color mutants.

mutant	JHS Color chart (center, edge)	flowering time	diameter of flower (mm)	plant length (cm)
NPIW2-NPI320-10-Y-1	vivid reddish yellow vivid reddish yellow	8/6	3.8	81.5
NPIW2-NPI320-10-W-1	white white	8/4	5.5	84.5
NPIW2-NPI320-10-W-2	white white	9/7	3.5	62.5
NPI-220-20-W-2 (=NPIW2)	pinkish white pale pink	8/6	5.7	126.3
Natsuyasumi	vivid purplish red vivid purplish red	8/4	5.8	128.3

2.13 Induction of Mutations Affecting Bolting Time by Ion Beam Irradiation to Calluses of Japanese Bunching Onion (*Allium fistulosum* L.)

M. Kondo*, N. Hamato**, Y. Hoshi*, ****, K. Ogata*, H. Kobayashi*, Y. Hase***, N. Shikazono*** and A. Tanaka***

Department of Biotechnology, Niigata Agricultural Research Institute *

Horticultural Research Center, Niigata Agricultural Research Institute **

Department of Ion-beam-applied Biology, JAERI***

Agriculture Promotion Department, Toukamachi Regional Promotion Bureau ****

1. Introduction

The Japanese bunching onion (*Allium fistulosum L.*), as well as garlic and onion, are important allium crops in Japan. The flower-bud formation of Japanese bunching onion is induced by encountering low temperature and short-day in winter. And, the bolting and the blooming are induced by encountering high temperature during spring. The bolting lowers the market value of Japanese bunching onion, because the flower stalk is not only hard to eat but also ruin the appearance. Therefore, a mutant variety of Japanese bunching onion that bolts at early or late time is profitable for the producers.

The ion beam has been shown to be useful to improve one property such as flower color, flower shape, flowering time etc. Without inducing undesirable mutations together with them [1), 2)]. And, it has been reported that chimeric plants hardly regenerated from calluses after induction of mutation[3)]. Therefore, we adopted the calluses of Japanese bunching onion as the material for the ion-beam irradiation. We determined that the dose of 0.5 Gy of $^{12}C^{6+}$ was appropriate for obtaining mutants, which changed a single property[4)].

In this study, we selected 4 R1 plants, which showed precocious bolting time.

2. Materials and Methods

2.1 Plant material

The calluses were induced from the seed of Japanese bunching onion cultivar "Tokyo natsuguro nigou".

2.2 Ion beam irradiation

The calluses were crushed to about 1.0 mm diameter by squashing on stainless steel sieves of 0.98 mm mesh (the mesh size of 20 or less). The crushed calluses were covered with sterilized Kapton film (7.5 μm in thickness, Toray-Dupon, Japan), and exposed to 320 MeV $^{12}C^{6+}$ beam with the dose of 0.5 Gy.

2.3 Regeneration of R0 plants

The ion beam-exposed calluses were cultured in the liquid callus proliferation medium for 3-6 weeks and then on the regeneration medium for 2 months under 16 hr light/8 hr dark at 25°C. The regenerated shoots were acclimated in a greenhouse. About 5,000 of the acclimated R0 seedlings were planted in a field from June to July 2003.

In spring of 2004, we investigated the bolting time of those Japanese bunching

onions every 7 days. We selected 22 R0 plants, which bolted from March 13 to 19. These plants were self-pollinated to produce R1 seeds.

2.4 Investigation of R1 plants

Seedlings of 15 R1 lines were planted and grown in the field in September 2004. In the spring of 2005, we investigated the bolting time of them.

3. Results and Discussion

We selected 22 R0 plants, which showed precocious bolting time (Table 1). Seven of them did not produce seedlings.

The winter survival rates of the 15 R1 lines, which produced seedlings and passed through the winter of 2004-2005, were 29% - 100% (Table 2). Four of the 15 R1 lines bolted earlier than "Tokyo natsuguro nigou" in the spring of 2005 (Fig 1). Moreover, the winter survival rates of these lines were comparable to that of "Tokyo natsuguro nigou" (Table 2), and they showed normal appearance (data not shown). Therefore, we selected these 4 lines for further examination of the bolting time of the next generations obtained by self-pollination. Selection of late-bolting R1 lines is also now in progress.

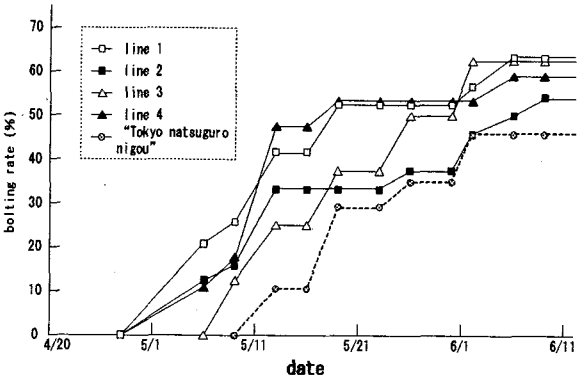

Fig. 1 Bolting time of ion beam-irradiated R1 lines and "Tokyo natsuguro nigou".
Line 1-4: Precocious bolting R1 line

Table 1 Bolting time of ion beam-irradiated R0 plants and non-irradiated plants.

Bolting time	Irradiated "Tokyo natsuguro nigou"	Non-irradiated "Tokyo natsuguro
3/13～3/19	22	1
3/20～3/26	121	1
3/27～4/ 2	733	13
4/ 3～4/ 9	587	5
4/10～4/16	1020	9
4/17～4/23	842	10
4/24～4/30	488	1
5/ 1～5/ 7	356	0
5/ 8～5/14	114	0
5/15～5/21	40	0
5/22～5/28	5	0
5/29～6/ 4	0	0
Total	4328	40

Table 2 Winter survival rates of R1 lines and "Tokyo natsuguro nigou".

R1 lines	Nnumber of surviving plants		Winter survival rate (%)
	Before winter	After winter	
1	19	19	100
2	31	24	77
3	9	8	89
4	23	17	74
5	30	26	87
6	15	7	47
7	9	3	33
8	16	13	81
9	35	22	63
10	30	18	30
11	25	13	52
12	13	11	85
13	14	4	29
14	13	13	100
15	17	15	88
Total	299	213	69
"Tokyo natsuguro nigou"	19	17	89

References

1)M. okamura, N. Yasuno, A. Tanaka and Y. Hase, TIARA Annual Report 2003 (2004) 51-52.
2)K. Ueno, S. Nagayoshi, Y. Hase, N. Shikazono and A. Tanaka, TIARA Annual Report 2003 (2004) 53-55.
3)S. Nagatomi, E. Miyahira and K. Degi, Gamma Field Symposia 35 (1996) 51-69.
4)M. Kondo, Y. Hoshi, H. Kobayashi, Y.Hase, N. Shikazono, A. Tanaka, TIARA Annual Report 2002 (2003) 83-85.

2.14 Characteristics of UV-Sensitive or -Resistant Rice (*Oryza sativa*) Mutants

J. Hidema*, Y. Takahashi*, M. Yamamoto*, Y. Hase**, A. Sakamoto**, A. Tanaka** and T. Kumagai*
Graduate School of Life Sciences, Tohoku University*,
Department of Ion-beam-applied Biology, JAERI**

1. Introduction

UV-B radiation can damage plants, decreasing growth and productivity[1]. We investigated the effects of supplementary UV-B radiation on the growth and yield of Japanese rice cultivars in the field in a cool rice-growing region of Japan[2), 3)]. The findings of those studies indicated that supplementary UV-B radiation markedly influenced not only the growth and grain development but also grain size and grain storage protein contents of rice. Furthermore, we investigated the sensitivity to UV-B radiation of rice cultivars of 5 Asian rice ecotypes, and found that (1) rice cultivars vary widely in UV-B sensitivity[4)], (2) among the Japanese rice cultivars, Sasanishiki exhibited resistance to UV-B radiation, while Norin 1 was less resistant, although these cultivars are closely related[5), 6)].

To date, we found that (1) two or more genes controlled the difference of sensitivity to UV-B between these rice cultivars[7)], (2) putative quantitative trait loci (QTL) associated with the resistance to supplementary UV-B radiation in rice were detected on chromosomes 1, 3 and 10 at least[8)], (3) Cyclobutane pyrimidine dimer (CPD), which is major DNA damages induced by UV-B, photolyase activity is a crucial factor for determining the UV-B sensitivity in rice cultivars[9), 10), 11)]. However, it is unclear the factors other than CPD photolyase contributing to UV resistance.

The aim of our study is to clarify the mechanisms of resistance to UV-B radiation for improving UV-B resistance in plants by bioengineering or breeding programs. In order to make it, identifying rice mutants with increased or decreased UV-B resistance can help our study powerfully. Heavy ion beams, such as carbon ions, are more effective in plants for inducing mutations compared with electron beam (Shikazono et al. unpublished data). Novel mutants have been obtained by the carbon ion irradiation in several plant species[12)].

The aim of this study is to isolate UV-B hyper resistant or hypersensitive rice mutants induced by carbon ion irradiation.

2. Experimental procedure

2.1 Plant material and irradiation method

Dry rice seeds of Sasanishiki (*Oryza sativa* L.) were used. About 150 seeds were placed upward embryo on petri dish. The irradiation apparatus for seed, connected to a vertical beam line of the AVF-cyclotron (JAERI, Takasaki), was used for the 320 MeV carbon-ion irradiation. We had found that the optimum radiation dosege for inducing mutations in rice "Sasanishiki" was 80 Gy[13)]. Thus, the carbon-ion irradiation with the doses of 80 Gy was performed under atmospheric pressure within 3 min.

2.2 Mutant isolation

About 4,500 M1 seeds were grown to maturity and harvested. Twenty M2 seeds derived from each M1 plant were used for the first screening of root bending assay, which method was described in detail elsewhere[14)]. The eight candidates that showed the longer root length than that of wild type "Sasanishiki" and the ten candidates that showed the shorter root length than that of wild type were isolated from 30,000 M2 plants. These lines were

further grown individually under normal conditions, self-pollinated and the M3 or M4 seeds of each candidate line were harvested. Second and third screening was carried out using 10 to 20 seeds of the M3 or M4 progenies by the methods of long-term exposure assay[14] and root bending assay. Growth analysis included the determination of the plant height, number of tillers and fresh weights of the aboveground parts of the plants.

2.3 CPD or (6-4)pp photorepair activity

The induction and repair of CPD and (6-4) photoproducts ([6-4] pp) were analyzed by ELIZA. CPDs and (6-4) pp were detected by the specific antibodies TDM-2 and 64M-2, respectively. To induce CPD, the detached third fully expanded leaves were placed on wet filter paper and irradiated with unfiltered UV-B radiation emitted from a UV-B-fluorescent tube (FL20SE; Toshiba, Tokyo, Japan) at a rate of 0 to 10 W m^{-2} for 15 min. For repair experiments, the detached leaves were exposed 4.5 kJ m^{-2} of UVB. Immediately after UVB exposure, the leaves were exposed to blue irradiation (60 μmol m^{-2} s^{-1}) from blue fluorescent tubes (20B-F, Toshiba, Tokyo, Japan) or kept in a light-tight box immediately after the UV-B exposure. After exposure of UV-B or blue radiation, the leaves were harvested immediately and stored in liquid nitrogen until being analyzed. All subsequent manipulations were carried out in red light to minimize uncontrolled photoreactivation. Rice DNA was extracted from each sample, fifty microliters of the extracted DNA was placed in each well. The DNA concentration was adjusted to 0.5 μg ml^{-1} for TDM-2 and 3 μg ml^{-1} for 64 M-2. The ELISA procedure was described in detail elsewhere[15].

3. Results and Discussion

A total of 4,500 dry rice seeds were irradiated with a carbon ion beam and then germinated. After flowering, the plants were self-pollinated and the M2 seeds were harvested. The eight candidates that showed the longer (less than 20%) root length than that of wild type "Sasanishiki" (UV-resistant) and the ten candidates that showed the shorter (less than 20%) root length than that of wild type (UV-sensitive) were selected by root bending assay from about 30,000 M2 plants. To confirm genetic stability of UVB sensitivity, each candidate of the M2 through M4 generation was tested for UVB sensitivity by both a long-term exposure assay and root bending assay. Among them, three UV-B hyper-resistant mutant lines and two UV-B hypersensitive mutant lines were established. Figure 1 shows the effects of supplementary UV-B radiation on the growth of UV-B resistant mutant (No. 319), UV-B hypersensitive mutant (No. 403), and Sasanishiki rice plants. These mutants are phenotypically wild type, Sasanishiki, in growth and development under visible radiation alone. When these mutants were grown under supplementary UVB radiation, plant length, tiller number and fresh weight of the UV-B hypersensitive mutant No. 403 was markedly retarded in comparison with wild type "Sasanishiki". In contract, the growth of No. 319 mutant was not affected by supplementary UV-B radiation.

We next examined to test whether the each mutant isolated in this experiment is deficient of CPD or (6-4) pp photorepair activity, which is thought to play a role in coping with UVB-induced DNA damage. First, we determined the susceptibility to CPD or (6-4) pp induction in the leaves of these mutants. There was no difference in the susceptibility to CPD or (6-4) pp induction between these mutants and Sasanishiki (data not shown). Our previous data showed that there was a significant correlation between the CPD levels induced by challenge UV-B exposure and the amount of UV-absorbing compounds in rice leaves. Thus, there are no significant differences in the levels of UV-absorbing compounds in leaves. Table 1 shows summary of the results of CPD or (6-4) pp photorepair abilities and dark repair abilities among these mutants. Interestingly, we found that there was

no difference in the ability of photorepair of CPD or (6-4) pp and dark repair ability of UV-B resistant mutants, No. 272 and 319, and UV-B sensitive mutant, No. 001, in comparison with wild type "Sasanishiki". These results indicate that the mutation of unknown factor(s) for determining UVB sensitivity could lead to UVB sensitivity in Nos. 272, 319 and 001. We are interested in what factors other than the CPD photolyase would effectively act to increase the UVB-sensitivity in rice, a question of which should be answered in the near future.

Acknowledgement

We thank Dr. T. Mori for providing the antibodies TDM-2 and 64M-2. This work was supported by Grants-in-Aid for Scientific Research from the Ministry of Education, Culture, Sports, Science and Technology, Japan (14704060, 15201010 and 17510037).

References

1) A. Teramura, Physiologia Plantarum 58 (1983) 415-427.
2) T. Kumagai et al. Agriculture, Ecosystems and Environment 83 (2001) 201-208.
3) J. Hidema et al. J. Rad. Res. 46 (2005) 143-149.
4) T. Sato et al. J. of Breeding 43 (1993) 61-68.
5) T. Kumagai et al. J. of Breeding 42 (1992) 545-552.
6) J. Hidema et al. Plant Cell Physiol. 37 (1996) 742-747.
7) T. Sato et al. Physiol. Plant. 91 (1994) 234-238.
8) T. Sato et al. Theoritical and Applied Genetics 107 (2003) 1003-1008.
9) J. Hidema et al.Plant Cell 12 (2000) 1569-1578.
10) M. Teranishi et al. Plant Cell Physiol. 45 (2004) 1845-1856.
11) J. Hidema et al. Plant J. 43 (2005) 57-67.
12) Y. Hase et al. Plant J. 24 (2000) 21-32.
13) J. Hidema et al. JAERI-Review 2003-33, (2003) 85-87.
14) J. Hidema et al. JAERI-Review 2004-025, (2004) 70-72.
15) Y. Takeuchi et al. Plant Cell Physiol. 37 (1996) 181-187.

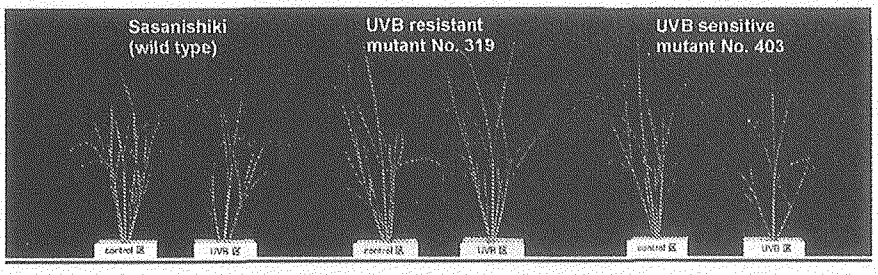

Fig. 1 Effects of supplementary UVB radiation on the growth of UV-resistant mutant, No. 319, UV-sensitive mutant, No 403, and wild-type Sasanishiki.

Table 1. The degrees of UVB resistance and the abilities of CPD or (6-4)pp photorepair and dark repair of Sasanishiki (wild type) and UVB sensitive nd resistant mutants of rice.

mutant	UVB resistance*	CPD photorepair activity **	(6-4)pp photo- repair activity **	Dark repair activity**
Sasanishiki	R (++)	++	++	++
No. 001	S (+)	++	++	++
No. 403	S (+)	++	++	-
No. 224	R (+++)	++	+	++
No. 272	R (+++)	++	++	++
No. 319	R (+++)	++	++	++

*R means UVB resistance, S means UVB sensitivity. The number of (+) means the degree of UVB resistance; + < ++ <+++
**The number of (+) means the degree of repair activities; (low) + < ++ <+++ (high), -; the repair activity could not be detected.

2.15 Induction of Dwarf Mutation in *Salvia coccinea* by Ion Beam Irradiation

M. Kato*, S.Kageyama*, T. Haketa*, M. Fukushima*,
Y. Hase** and A. Tanaka**
Takii Plant Breeding & Experiment Station*
Department of Ion-beam-applied Biology, JAERI**

1. Introduction

Ion beams have higher LET(linear energy transfer) and bring intensive RBE(relative biological effectiveness) than γ-rays and X-rays. By the irradiation with heavy ion beams, specific flower color, flower shape, leaf shape and male sterile mutants were induced in several flowers[1) 2) 3) 4)].

We reported the effect of ion beams and γ-rays on survival rate of *Salvia coccinea* seeds[5)].

In this study, we investigated the effect of ion beam irradiation on induction of dwarf mutants in *Salvia coccinea*.

2. Materials and Methods

Seeds of *Salvia coccinea* 'Lady in Red' were used in this study. They were irradiated with 320MeV carbon ion beam at 60Gy, 50MeV helium ion beam at 80Gy and γ-ray at 100Gy. The numbers of seeds irradiated with carbon ion beam, helium ion beam and γ-ray were 5000, 5000 and 1000 respectively.

After the irradiation, seeds were planted in a greenhouse and produced M_2 seeds by single seed descent method. All the seeds produced were planted.

The M_2 generations were investigated about main stem length, flowering date, flower numbers of spike and heading node. The numbers of plants investigated in carbon ion, helium ion, γ-ray and control regimes were 241,286,258 and 20 respectively.

3. Results and Discussion

Compared with the control, the averages of stem length of irradiated M_2 generation are elongated. And the deviations of the groups were extended. The order of a confidence limit ($p=0.001$) of the stem length of those plants was γ-ray, helium ion, carbon ion, control from short one (Table 1).

So we thought it was able to select dwarf mutants in those groups.

The heading nodes of irradiated M_2 generations were wider than control (Fig.1). And heading node affected stem length (Fig.2). The plants which had low heading node tended to have short stem, early flowering and many flowers. The order of frequency to induce plants which have low heading node was carbon ion, helium ion, γ-ray, control from high one (Table 2).

From these results, we concluded that selecting low heading node plants from M_2 generations being irradiated with carbon ion beam is the best method to obtain useful dwarf mutant.

We selected dwarf mutants from M_2 generations which reached flowering.

Now the progenies of selected plants are under investigation.

Table 1 Stem length of M_2 generations

Radiation	Average (mm)	Standard deviation	Confidence limit (p=0.001)
320MeV $^{12}C^{6+}$	185.5	24.0	111.3
50MeV $^{4}He^{2+}$	189.7	28.3	102.2
γ-ray	176.2	26.1	95.5
Control	175.1	15.4	127.5

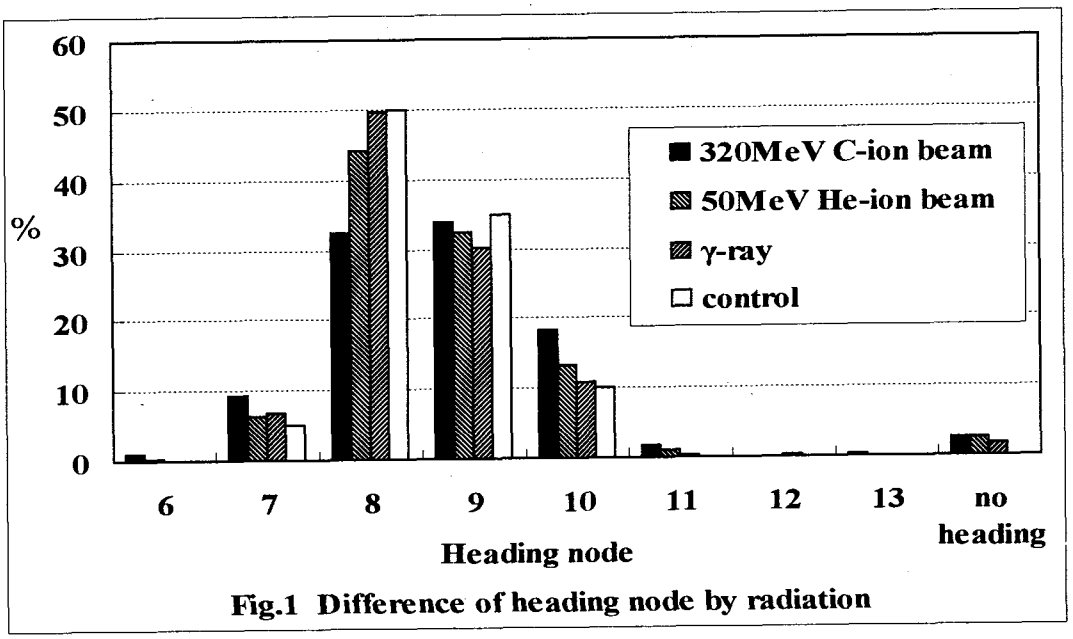

Fig.1 Difference of heading node by radiation

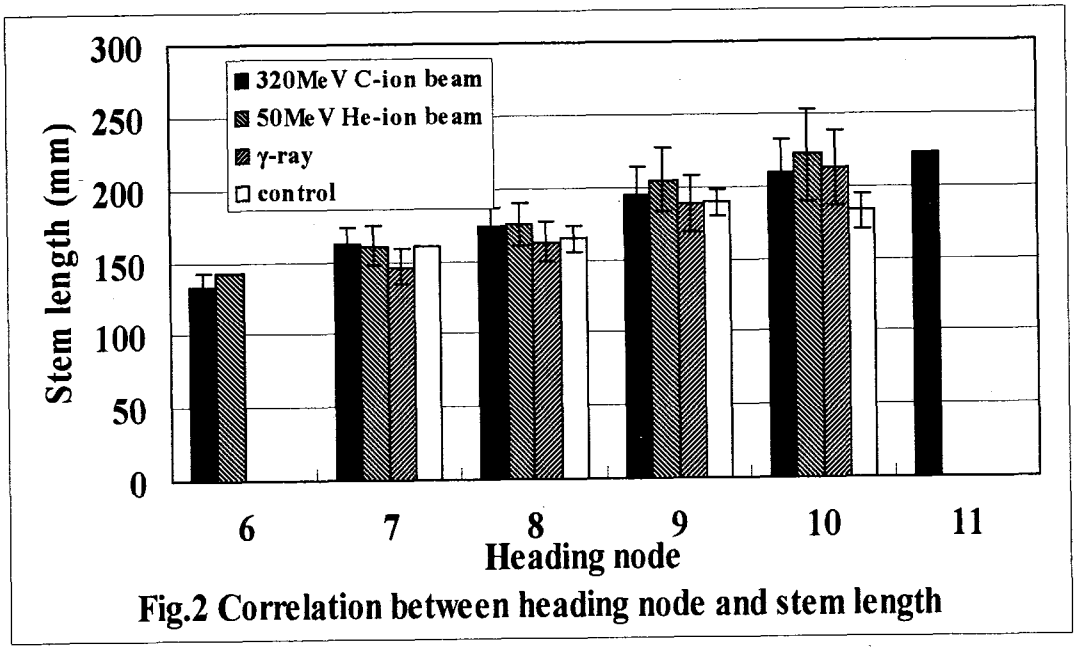

Fig.2 Correlation between heading node and stem length

Table 2 Heading node of M_2 generations

Radiation	Average	Standard deviation	Confidence limit (p=0.001)
320MeV $^{12}C^{6+}$	8.57	0.96	5.62
50MeV $^{4}He^{2+}$	8.57	0.83	6.00
γ-ray	8.43	0.78	6.01
Control	8.50	0.76	6.15

References

1) M.Okamura, M.Ohtsuka N.Yasuno, T.Hirosawa, A.Tanaka, N.Shikazono, Y.Hase and M.Tanase, JAERI-Review 2001-039(2001) 52-53

2) K.Suzuki, Y.Yomo, T.Abe, Y.Katsumoto, K.Miyazaki, S.Yoshida and T.Kusumi, RIKEN Accel.Prog.Rep. 35,129(2002)

3) H.Yamaguchi, S.Nagatomi, A.Tanaka N.Shikazono, T.Morishita and K. Degi, Jaeri-Review 2000-24(2000) 41-42

4) M.Kato, S.Kageyama, T.Haketa, M.Fukushima, Y.Hase and A. Tanaka JAERI-Review 2004-25,(2004)73-75

5) M.Kato, S.Kageyama, T.Haketa, M.Fukushima, Y.Hase and A.Tanaka JAERI-Review 2003-33,(2003)88-89

2.16 Research on Production of Mutant of *Cephaelis ipecacuanha* A. Richard which is a Source of the Expectorant used in First Aid

S. Isogai*, Y. Hase**, A. Tanaka** and K. Shimomura*
Graduate School of Life Sciences, Toyo University*
Department of Ion-beam-applied Biology, JAERI**

1. Introduction

Cephaelis ipecacuanha A. Richard (Rubiaceae) is one of the more important medicinal plants found in the Amazon rainforest, and its dried roots are commonly used as an expectorant, an emetic and an amoebacide. In recent years, ipecac syrup has been used as an emetic for first aid in Japan. Therefore a stable supply of ipecac is desirable. The efficient methods of propagation through tissue culture have been studied such as shoot multiplication[1], adventitious shoot formation on the internodal segment[2] and adventitious root formation[3].

Since ipecac is a tropical plant, it is difficult to cultivate this plant in Japan except for the warm districts in winter[4]. Therefore, it is important to improve the characteristics of the ipecac plant for cultivation in Japan. We have started to produce mutants, such as low temperature tolerant clones and high-alkaloid producing clones, using ion beam irradiation.

2. Experimental procedure

2.1 Plant material

Cephaelis ipecacuanha shoots used for the experiment were maintained on phytohormone free (HF)-Gamborg B5[5] (B5) solid medium. In order to obtain sufficient shoot material for the experiment, the shoots were transferred onto B5 solid medium supplemented with 0.5 mg/L GA_3, and cultured at 25 °C under the dim light for 4 weeks.

2.2 Medium and culture condition

The media used for the experiments, for proliferation of shoots and for induction of adventitious buds, were adjusted to pH 5.7 before the addition of 0.2 % Gelrite, and then was autoclaved at 121 °C for 15 minutes. The cultures were incubated at 25 °C under 14 h/day dim light (7- 8 $\mu Em^{-2} S^{-1}$).

2.3 Induction of adventitious shoot formation and ion beam irradiation

Internodal segments (*ca.* 6 mm in length) of shoots cultured on B5 solid medium supplemented with or without 0.5 mg/L GA_3 were placed horizontally on WP solid medium supplemented with 0.01 mg/L N^6-benzyladenine (BA) and cultured at 25 °C under 14 h/day dim light.

After 3 weeks of culture, internodal segments were exposed to 320 MeV C ion beams of 0.5 to 200 Gy using the AVF cyclotron in TIARA. Before the

irradiation, the plastic covers of the petri dishes were replaced with kapton film. Internodal segments were then exposed to C ion beams and were transferred onto fresh medium and cultured. Twelve weeks after the ion exposure, adventitious shoots formed on the internodal segments were isolated and cultured on HF-B5 solid medium at 25 °C under 14 h/day dim light. After 6 weeks of culture, all leaves developed were used for quantitative analysis of emetic alkaloids by HPLC.

2.4 Shoot culture at 4 °C

Adventitious shoots regenerated on the surface of internodal segments exposed to C ion beams were cultured at 4 °C under 14 h/day dim light. After 4 weeks of culture, induction of adventitious shoot formation from internodal segments of shoots cultured at 4 °C was carried out as mentioned above.

2.5 Alkaloid extraction

Extraction method reported by Yoshimatsu and Shimomura[7] was slightly modified to quantify the emetic alkaloids by HPLC. Briefly, samples (*ca.* 5 mg) lyophilized individually were accurately weighed and crushed in the small test tube. The samples thus prepared was mixed with 100 μl of 10 % NH_4OH for 1 min then extracted with 3 ml of ether for 5 min using a vortex mixer. The extract was filtrated with the cotton plug and concentrated under a N_2 gas stream, then further dried *in vacuo*.

2.6 HPLC analysis

The extract prepared as mentioned above was dissolved in 100 μl of MeOH and quantitatively analyzed by HPLC according to the method reported[7]. Analytical conditions were as follow, TSK gel ODS-120A (4.6 i.d. x 250 mm) with 10 mM1-heptanesulfonic acid sodium salt (adjusted to pH 4.0 with 2 % phosphoric acid)-CH_3CN (67: 33) as mobile phase, monitoring absorbance at 285 nm. The flow rate was 1.0 ml/min throughout the analysis.

3. Results and discussion

As a result of the experiments last year, it was considered that C ion beams ranging from 5 to 10 Gy was suitable for inducing mutation. Therefore, the internodal segments were exposed to C ion beams of 5 and 7.5 Gy. Survival rate, adventitious shoot formation rate and No. of adventitious shoots formed per internodal segment at 7.5 Gy were as high as those at 5 Gy. Consequently, 7.5 Gy exposure was employed for further experiments.

In preliminary experiments, some adventitious shoots regenerated on the surface of internodal segments exposed to 0.5- 10 Gy when cultured at 4 °C. However, all segments including the untreated shoots showed browning and adventitious shoot regeneration did not occur.

Emetic alkaloid contents of the regenerated shoots were analyzed by HPLC. Some shoots exhibited higher or lower alkaloid contents compared to the control. Among the clones examined, the clone of interest is the one showing high content of emetine compared to that of the control. However, the regenerated shoots exhibited different levels of alkaloid contents compared to that of the

control. Unfortunately these shoots showed the same contents as the control after the subculture (Fig. 1). Variation of alkaloid content found before the successive subculture was thought to be transient.

It would be necessary to obtain more adventitious shoots to find the target mutants.

Investigation of the shoots having different characteristics is in progress.

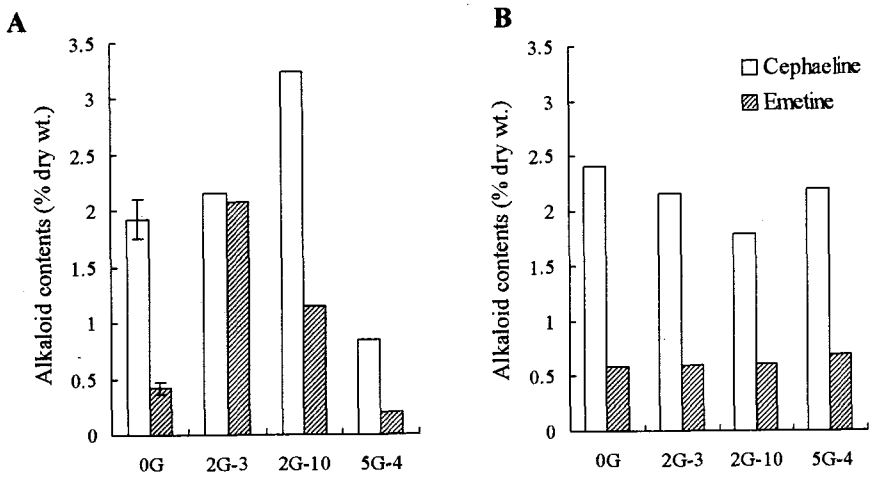

Fig. 1 Emetic alkaloid contents of leaves of regenerated shoots after exposure to heavy ion beam
A: Before subculture
B: After subculture (2 times)

References

1) K. Yoshimatsu and K. Shimomura, Plant Cell Reports, **7**: 288-291 (1998)
2) K. Yoshimatsu and K. Shimomura, Plant Cell Reports, **9**: 567-570 (1991)
3) K. Yoshimatsu and K. Shimomura, Plant cell Reports, **14**: 98-101 (1994)
4) K. Yoshimatsu, K. Aoi and K. Shimomura, J. Plant Physiol., **144**: 22-25 (1994)
5) O. L. Gamborg, R. A. Miller and K. Ojima, Exp. Cell Res., **50**: 151-158 (1968)
6) Lloyd, G. and McCown, B., Int. Plant Propag. Soc. Combd.Proc., **30**: 421-427 (1980)
7) K. Yoshimatsu and K. Shimomura, Phytochemical Analysis, **4**: 217-219 (1993)

2.17 Research on Production of Mutants in Plants Used for Food Additives and Materials: Development of High-anthocyanin Producing Clone and Low-bad Smell Clone

M. Sato*, S. Isogai*, F. Betsui**, K. Touno**
Y. Hase***, A. Tanaka*** and K. Shimomura*, **
Graduate School of Life Sciences, Toyo University*
Plant Regulation Research Center, Toyo University**
Department of Ion-beam-applied Biology, JAERI***

1. Introduction

Red cabbage *Brassica oleracea* var. *capitata* L. and red radish *Raphanus sativus* L. (Cruciferae) are annual and biennial plant. Main pigments of red cabbage and red radish are cyanidin acylglycosides and peralgonidin acylglycosides[1], respectively. These pigments are used for food additives and materials. However, there is a problem that dimethylsulfide remains after purification process, and it requires much money to removal from those pigment extracts. In addition the content of red cabbage pigment possibly extracted is only 1 % of fresh weight. In order to prepare these important red pigments of red cabbage and radish for the food additives, these problems have to be solved. Nowadays, the anthocyanin pigments attract much attention. Although red cabbage is used for the cook, the leaf is waxy and relatively hard compared to the green cabbage. Therefore we attempt to produce the mutant as soft as the green cabbage. We started to establish the mutants, such as high-anthocyanine producing clone and low-bad smell clone by ion beam irradiation.

2. Experimental procedure

2.1 Plant materials

Red cabbage shoots used for the experiment were maintained on phytohormone free (HF)-Linsmaier and Skoog (LS)[2] solid medium.

Red radish cultivers used for the experiment were Ten-ankoushin and FA-30. These radish shoots were maintained phytohormone free (HF)-Murashige and Skoog (MS)[3] solid medium.

2.2 Medium and culture condition

The media used for the experiments, proliferation of shoots and induction of adventitious buds, were adjusted to pH 5.7 before addition of 0.2 % Gelrite, and then autoclaved at 121 °C for 15 minutes. The cultures were incubated at 25 °C under 14 h/day light.

2.3 Preparations of red cabbage shoots and ion beam irradiation

Petioles of *in vitro* red cabbage were cut into ca. 1 cm in length. Petiole segments were placed horizontally on LS solid medium supplemented with 4 mg/L of indole-3-butyric acid (IBA) and 0.25 mg/L of N^6-benzyladenine (BA) (Φ90 mm,

petri dish) and cultured at 25 °C under 14 h/day dim light.

After 2 weeks of culture, the induced calluses were cut into 2 mm thickness, and placed on MS solid medium. Thereafter, the lids of petri dish were replaced with kapton film, and the next day, calluses were exposed to 320 MeV C ion beams ranging 0.5 - 200 Gy using the AVF cyclotron in TIARA. The next day of the exposure, the exposed calluses were transferred onto fresh medium and cultured for 25 °C under 14 h/day dim light.

2.4 Preparations of red radish shoots and ion beam irradiation

Apical shoot segments (ca. 5 mm) of Ten-ankoushin removed petioles were placed horizontally on HF-MS solid medium (Φ60 mm, petri dish).

Stemsegments with bud clump of FA-30 were cut into 2 mm thickness. These discs were placed horizontally on MS solid medium supplemented with 5 mg/L kinetin (Φ60 mm, petri dish).

The exposure was performed as the same as the cabbage mentioned above, and the treated segments and discs exposed to ion beams were transferred onto fresh medium and cultured at 25 °C under 14 h/day dim light.

3. Results and discussion

3.1 Red cabbage

After exposed ranging 0 – 5 Gy, roots formed on the surface of calluses of all segments. However, adventitious bud was not formed on the rooted calluses after 8 weeks of inoculation on fresh medium. Since the regeneration rate of petiole segments was not satisfied, the condition was reexamined. Leaf segment (ca. 5 x 5 mm) was excised as the main vein was

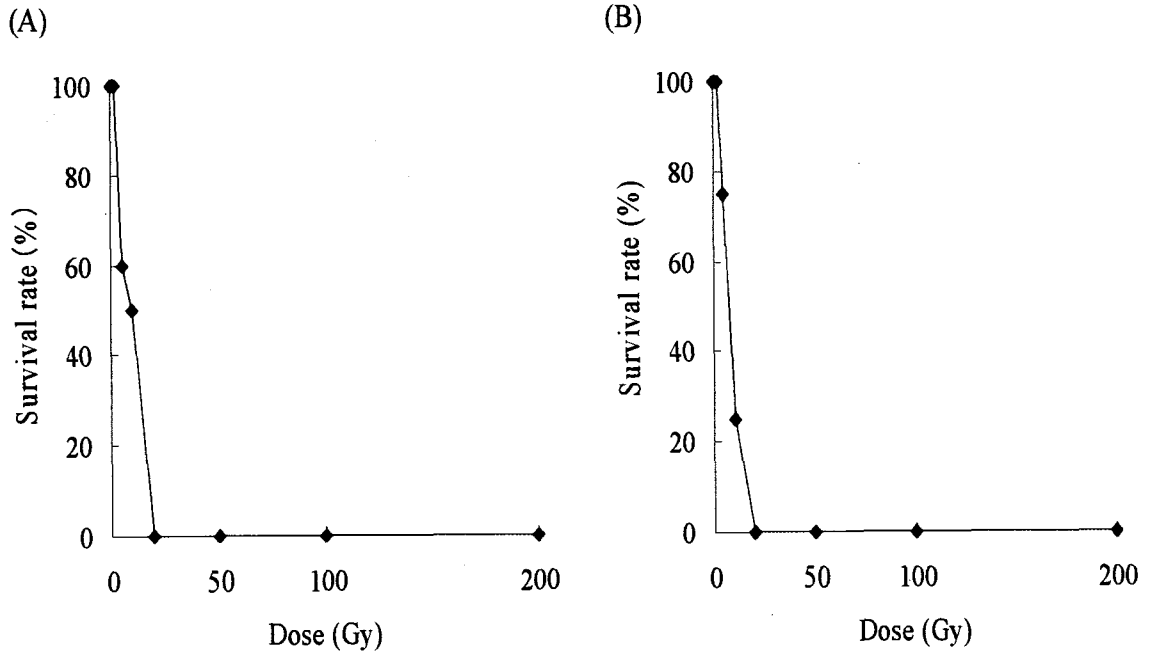

Fig. 1 Survival rate on leaf segments (A) and petiole segments (B) exposed to different doses of C ion beam

placed in the center of the segment. Petioles of red cabbage shoots were cut into 1 cm in length. Leaf and petiole segments were placed horizontally on LS solid medium supplemented with 1 mg/L 1-naphthaleneacetic acid (NAA) and 2 mg/L BA[4] (Φ90 mm, petri dish) and cultured at 25 °C under 14 h/day dim light. In a preliminary experiment, at week 8 after inoculation, adventitious shoots were formed on only leaf segments (16-41 %), but not on petiole segments. Therefore the leaf segments and petiole segments were exposed to 320 MeV C ion beams ranging 0.5 to 200 Gy. Leaf segments exposed to C ion beams of more than 10 Gy died after browned (Fig. 1A). The petiole segments exposed to C ion beams of more than 10 Gy also died (10 Gy). One adventitious shoot was formed on the leaf segment exposed at 0.5 Gy. Since the frequency of explants responded was low (16 – 41 %) mentioned above, the method of regeneration is necessary to reexamine for obtaining more adventitious shoots.

3.2 Red radish

In Ten-ankoushin, apical buds developed in all exposure range (0 – 200 Gy). Although 200 Gy is actually lethal dose, the buds grew after the high exposure. Therefore it was thought that C ion beam did not reach terminal buds.

In FA-30, lateral buds developed on disk in range at 0 and 0.5 Gy. The upper part of disk turned brown, whereas the lateral buds developed at 100 and 200 Gy. The material for the C ion beam exposure should be considered since the preparation of the disks in 2 mm thickness was not investigated whether suitable size or not.

Therefore the investigation of regeneration condition for the petiole and leaf segments is in progress.

References

1) F. Betsui, N. Tanaka-Nishikawa and K. Shimomura, Plant Biotechnol., **21** (5), 387-391 (2004)
2) E.M. Linsmaier, F. Skoog, Physiol. Plant., **18**, 100-127 (1965).
3) T. Murashige, F. Skoog, Physiol. Plant., **15**, 473-497 (1962)
4) E. Pua, G. Sim, G. Chi, and L. Kong, Plant Cell Reports, **15** : 685-690 (1996)

2.18 Analysis of Mutation Induced by Carbon Ion Beams in *Saccharomyces cerevisiae*

Y. Matuo*, S. Nishijima*, Y. Hase**, A. Sakamoto**,
A. Tanaka** and K. Shimizu***
Graduate School of Engineering, Osaka University*
Department of Ion-beam-applied Biology, JAERI**
Radioisotope Research Center, Osaka University***

1. Introduction

The breeding technology using the mutation induced by the ion beam irradiation has been greatly developed, and has been applied to the various fields. However, the detailed molecular mechanism has not been proven considerably. In this study, the budding yeast *Saccharomyces cerevisiae* was used as a model eukaryotic organism. This study is intended to elucidate the molecular mechanism of the mutagenesis caused by ion beam. The mutation sites caused by ion beams were determined and the mutation spectrum were compared with those induced by gamma ray.

2.Materials and methods

2.1 Strains

S. cerevisiae strains used in this study are S288C(*RAD*$^+$), X36B-3C (*rad3*), JG-18(*rad18*), and G160/2b(*rad52*).

2.2 Sample preparation

Appropriate diluted yeast culture was filtrated through nitrocellulose membrane filter (HA, Millipore). The filter was put on petri dish (50 mm) and covered with kapton® film (7.5 μm thick).

2.3 Irradiation methods

The yeast samples were irradiated with carbon ions ($^{12}C^{5+}$; 220 MeV) with the dose 10 to 300 Gy, and LET is 107 keV/μm. Carbon ion beam was generated from AVF cyclotron in JAERI. The angle scanning is carried out for the uniform irradiation. The samples were incubated at 30°C for 2-3 days.

2.4 Measurement of cell survival and mutation frequency

The survival rates following irradiation were determined on the basis of colony-forming ability. The mutation frequencies on *URA3* locus were determined using 5-FOA method [1]. Briefly, the yeast bearing *URA3*$^+$ gene cannot grow on the medium containing 5-FOA, but when *URA3*$^+$ gene changes to *ura3*$^-$ by the mutation, the yeast can grown on it.

2.5 Sequence analysis of mutation sites

The mutation sites of *ura3* mutants were determined by DNA sequencing. *URA3* regions of obtained *ura3* mutants were amplified by PCR and sequenced by primer extension using ABI model 3100.

3.Results and Discussion

3.1 The mutation frequency

The results show that the optimum dose for mutagenesis by carbon ion beams is 100 Gy. The ion beams at 100 Gy generate mutations 168.5-fold more than spontaneous mutation (Fig.1). Moreover, the ion beams are more than 11.6-fold more effective in generation of mutations than gamma ray.

3.2 sequence analysis

We obtained the *URA3*→*ura3* mutants at a dose of 100 Gy, *URA3* gene region (804 bp) of *ura3* mutants were amplified by PCR method, and the mutation site were determined by the sequencing.

The result shows that mutations caused by ion beam irradiation have remarkable features. Mutations of spontaneous generation are usually transition, whereas mutations generated by ion beams are dominantly transversion. The transversion / transition ratio in the *WILD* type was 5.0, and the ratio in the *rad52*$^{-}$ type was 4.0 (Table 1).

Moreover, the fact that GC→TA substitutions were largely observed suggests that the mutations by ion beams resulted from oxidative damage such as formation of 8-oxodGTP (8-hydroxydeoxyguanosine5'-triphosphate) mainly [2,3].

Further, the mutation sites are localized on several regions with 170bp to 186bp interval. This interval may correspond to nucleosome structure. The nucleosome core particle of budding yeast contains histone proteins and 147 base pairs of superhelical DNA with 15-20 bp linker (Fig.2,3).

To elucidate the relationship between nucleosome structure and hotspot, we are going to analyze the *URA3* gene on the plasmid not on chromosome. Additionally, we obtained single base deletion mutations, whereas the analysis of mutations in *Arabidopsis* showed that the deletion of large region and inversion were predominant in mutations [4,5]. In the yeast, we could not obtain the large deletion mutation. The reason is not clear, but the analysis of diploid strain may give us some information.

References

1) D. Burke, et al., in 'Methods in Yeast Genetics' Cold Spring Harbor Laboratory Press (2000) pp7-15

2) H. Kamiya et al., ucleic Acids Research **28** (2000) 1640-1646.

3) H. Kasai, et al., Mutat Res. **387** (1997) 147–163.

4) N. Shikazono, et al., Genetics **163** (2003) 1449-1455

5) S. Kitamura, et al., TIARA. Ann. Rep. **2002** (2003) 44-46

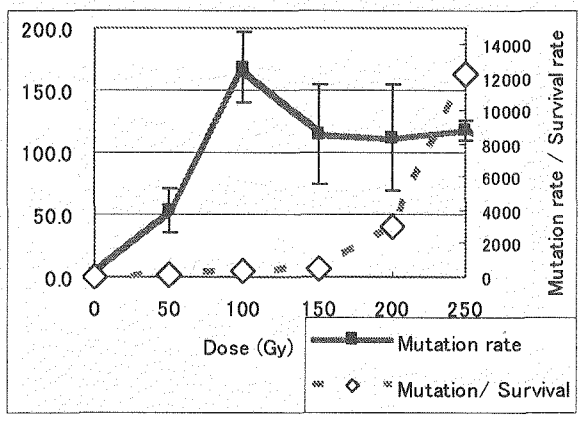

Fig.1 Induction fold and Survival curve of the Mutation on ion beams in *RAD*$^{+}$ type

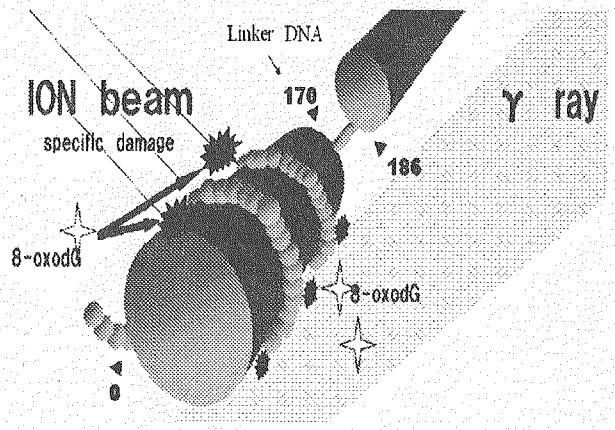

Fig.2 The model of a hotspot by ion beam and Gamma ray

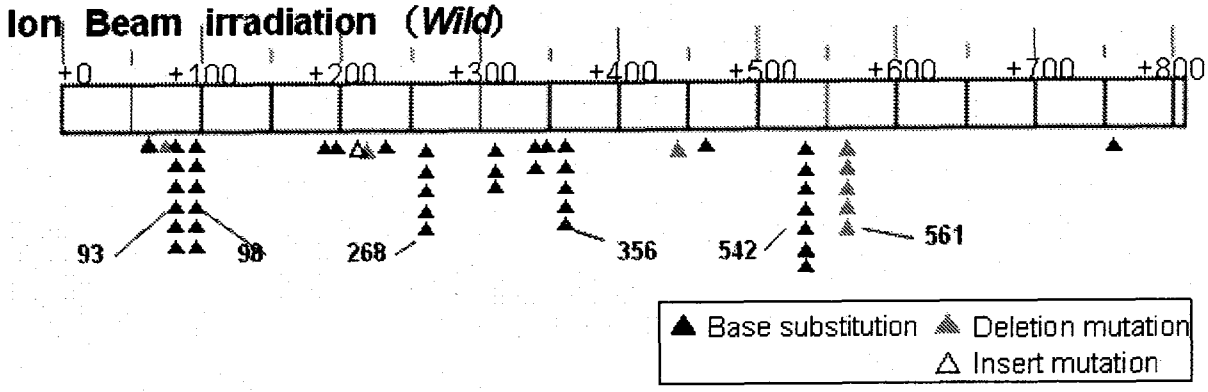

Fig.3 The mutation sites of *ura3* mutants caused by ion beam

Table 1 Mutational spectrum of irradiation – ion beam and gamma ray

Mutations class	Ion Beam *Wild* type		Ion Beam *rad52* type		Gamma ray *Wild* type	
	Number	Percentage	Number	Percentage	Number	Percentage
Total	**51**	**100.0%**	**32**	**100.0%**	**30**	**100.0%**
Base substitution						
Transitions	**7**	**13.7%**	**6**	**18.8%**	**6**	**20.0%**
GC : AT	**7**	**[100%]**	**6**	**[100%]**	**6**	**[100%]**
AT : GC	0	[0%]	0	[0%]	0	[0%]
Transversions	**35**	**68.6%**	**24**	**75.0%**	**20**	**66.7%**
GC : TA	**21**	**[63%]**	**19**	**[79%]**	**13**	**[65%]**
GC : CG	**12**	**[31%]**	**3**	**[13%]**	**3**	**[15%]**
AT : CG	1	[3%]	1	[4%]	4	[20%]
AT : TA	1	[3%]	1	[4%]	0	[0%]
Del. And Insertion	**9**	**17.6%**	**2**	**6.2%**	**4**	**13.3%**

2.19 The Frequency of Rooting and the Growth of In Vitro Shoots of Hybrid Limonium 'Moon Light' Irradiated with Ion Beams

T. Enomoto*, K. Tokuhiro*, K. Nakatsubo*, M. Amano*, Y. Hase** and A. Tanaka**
Kaneko Seeds LTD.*
Department of Ion-beam-applied Biology, JAERI**

1. Introduction

The color of petals in hybrid Limonium, which is interspecific hybrids consisted of L. latifolium and L. bellidifolium and so on, is purple in several tones and the variation of the flower color is limited. The color of 'Moon Light' which is Kaneko Seeds LTD original variety is purple too. To extend the variation of the flower color of 'Moon Light', we irradiated with ion beams to shoots cultured in vitro.

2. Experimental procedure

Independent shoots with 4 to 6 leaves cut out from multiple shoots cultured on the multiple medium for hybrid Limonium. Shoots were placed up the meristem in petri dish containing MS medium supplemented with 0.5 mg/l IBA, 30 g/l sucrose and 9 g/l agar (rooting medium). The pH of the medium was adjusted to 5.7. Petri dishes were covered with polyimide film and irradiated with 320 MeV carbon-ion beam from the TIARA AVF cyclotron (JAERI, Takasaki). After irradiation, shoots were transferred onto the fresh rooting medium and cultured at 25℃under a 16 hour photoperiod by using white fluorescent lamps (27 μmol·m^{-2}·S^{-1}). The frequency of rooting and the growth of shoots was examined one month after transferring.

3. Results and Discussion

Shoots were irradiated with the dose from 0.5 Gy to 12 Gy. The frequency of rooting decreased with increasing the dose (Table 1). The growths of roots and shoots were strongly inhibited in doses more than 4 Gy and more than 2 Gy respectively. In the case of 1 Gy, although the growth of shoots was somewhat inhibited, the frequency of rooting was high. There was no difference between 0.5 Gy and the control. Therefore, the suitable dose was estimated to be around 1 Gy.

Table 1 The frequency of rooting and the growth of in vitro shoots irradiated by 320 MeV carbon ion beams

Dose (Gy)	Frequency of rooting (%)	Growth of roots*	Growth of shoots*
0	75	Normal	normal
0.5	85	Normal	normal
1	82	somewhat inhibited	normal
2	58	somewhat inhibited	strongly inhibited
4	40	strongly inhibited	strongly inhibited
8	43	strongly inhibited	strongly inhibited
12	35	strongly inhibited	strongly inhibited

*by observation

2.20 Development of an Efficient Method for Mutation Induction

Y.Hase, C.Suzuki and A.Tanaka
Department of Ion-beam-applied Biology, JAERI

1. Introduction

The ion beam is widely used for plant breeding as a mutagen. In order to increase the efficiency of ion-beam mutagenesis much more, the relationship among the factors such as the irradiation dose, the physical properties of ion beams, the mutation frequency, the mutation spectrum and a kind of materials used for the experiment have to be investigated.

Nagatomi *et al.* exposed the petals and leaves of chrysanthemum to the ion beams to obtain flower-color and -shape mutants. They succeeded to screen many mutants from the regenerated plants[1]. In addition, they reported that the mutation spectrum was wider in case of the petals as compared to the leaves. Similar result was observed in another chrysanthemum breeding experiment (unpublished result). These results suggest that the mutation spectrum might be different when different types of tissue are used. In order to examine this hypothesis, we designed an experiment to detect deletion-type mutations induced in somatic cells. Here, we describe about the deletion-type mutation found in the leaf cells exposed to the carbon ions.

2. Experimental procedure

The 7-day-old seedlings of Arabidopsis thaliana (ecotype Columbia) were exposed to the carbon ions. The genomic DNA was extracted from each leaf of the first leaf pair at three days after irradiation. The nested-PCR was carried out using the primer sets that amplify the coding region of the At3g54890 gene. The PCR primers were designed to amplify 9,166 bp fragment after the 2nd PCR. The extension time required for amplification of the wild-type fragment was first checked, and then, the PCR was performed with the extension time that suppressed the amplification of the wild-type fragments. The PCR products were separated on agarose gel and the amplified fragment was sequenced.

3. Results and Discussion

The genomic DNA was individually isolated from 24 leaves exposed to the carbon ions. We succeeded to detect one deletion-type fragment with the length of around 4.7 kb (Fig.1). The sequencing analysis revealed that the deletion of 4,433 bp and the insertion of 15 bp were involved (Fig.1). Our results show that the deletions induced by ion beams can be detected by the method described here. The difference in the mutation spectrum by the kind of tissue (for example, leaf vs root) will be analyzed.

References

1) Nagatomi *et al.*, TIARA Annual Report 1995 Vol.5 (1996) 50-53.

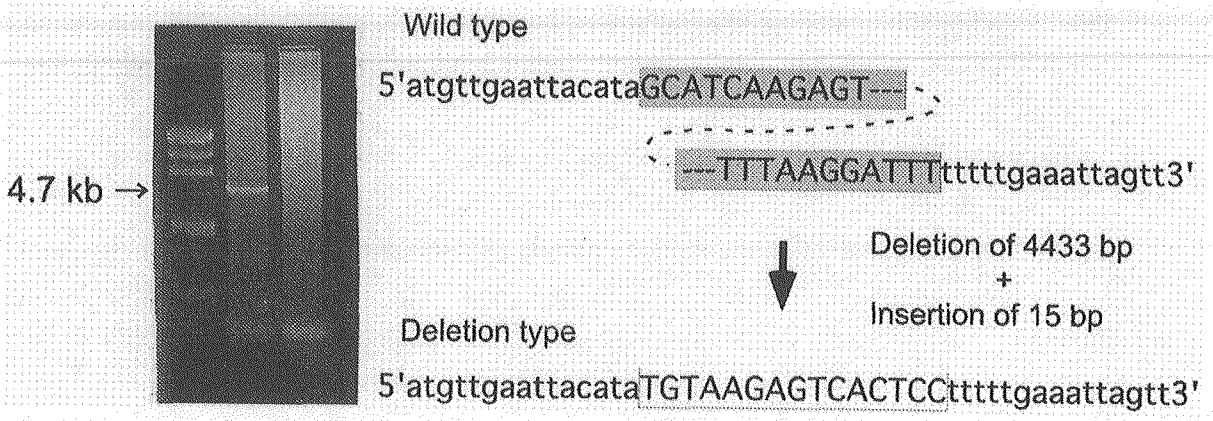

Fig. 1 The amplified deletion-type fragment and the DNA sequence around the rejoined site.

2.21 Development of New Commercial Strains in Functional Mushrooms (*Lyophyllum decastes*) by Ion Beam Irradiation

Y. Kawashima*, K. Nakajima*, T. Matsumoto*, Y. Hase** and A. Tanaka**
Gunma Prefectural Forestry Experiment Station*
Department of ion-beam-applied Biology, JAERI**

1. Introduction

In mushrooms, the varieties have been improved through clonal selection from natural genetic resources and crossing among strains. As these methods require long terms and result in low efficiency, it is essential to establish a more effective method of mutation breeding in mushroom.

The Institute of Radiation Breeding in cooperation with Agricultural Technology Institute of Nagano Farmer's Federation, has developed a radiation breeding method and selected a pure-white mutant variety in *Flammulina velutipes* [1] . It was confirmed that the optimum radiation dose to induce mutation in *F. velutipes* was ranging from 800 to 1200 Gy. This is the first example of commercial variety in mushroom induced by gamma ray. The method is applicable to not only *F. velutipes* but the other kinds of mushroom.

Ion beams, which have a higher linear energy transfer (LET) than X and gamma rays[2], are one of efficient mutagenic agents, and applicable to mutation breeding of many horticultural and ornamental crops[3]. However, there have been few studies on the effects of ion beam irradiation on induction of mutation in mushroom[4].

The basidiomycete *Lyophyllum decastes* (Fr.:Fr)Sing. grows in hardwood and coniferous forests, in grassy places, alongside paths or streets, in parks or gardens, on humusy soils, rarely also in cellars. That's mushroom is found in the northern regions of northern hemisphere such as, North America, Europe, Asia, North Africa. *L.decastes* is superior edible mushroom. But cultivating this mushroom has not been popular yet.

In this study, we investigate the efficiency of mutation generation by ion beam breeding and the new varieties in *L.decastes*.

2. Materials and Methods

L.decastes were used as registration variety GLD-17 and wild variety GLD-89. GLD-17 was named "Gunma GLD-17" and applied for a new variety in June, 2002.

The fresh fruit body segments or spore were cultured on modified Potato Dextrose Agar (PDA) medium in a 5cm petri dish.

The samples covered with Kapton film were irradiated with carbon ion beam (320 MeV $^{12}C^{6+}$) at various doses (5 to 1200 Gy). After irradiation the fruit body segments were transferred to the fresh PDA medium and cultured at 22 °C. Mycelial growth or regeneration rate was investigated after 50 days of culture.

3. Results and Discussion

When the dosage of irradiation increased, the regeneration rates of the mycelial growth decreased. At the dose of more than 600 Gy in $^{12}C^{6+}$ ion beams, the regeneration rate decreased (Fig.1,2). At the dose of more than 350 Gy $^{12}C^{6+}$ ion beams, few spore was germinated (Fig.3). Till now, no morphological changes was observed in the fruit bodies(Fig.4).

We are performing cytological studies to investigate horticultural values of the regenerated fruit bodies.

References

1) S. Nagatomi, Ins. Radiat. Breeding Technical News 50 (1995).

2) A. Tanaka et. al., Int. J. Radiat. Biol 72 (1997) 121-127.

3) N. Kudo et. al. TIARA Ann. Rep. 16(1998) 62-64.

4) H.Akaishi et. al. TIARA Ann. Rep. 18(2000) 56-57.

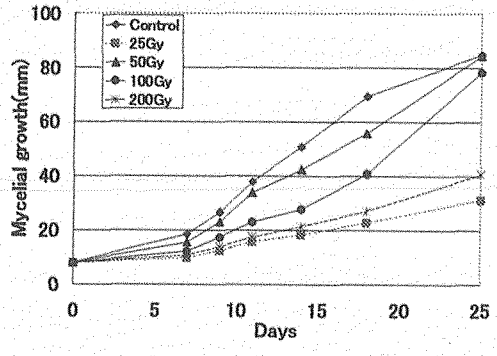

Fig.1 Effect of $^{12}C^{6+}$ ion beam on the mycelial growth of *L.decastes*

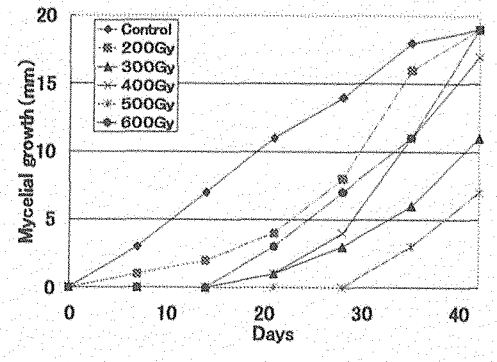

Fig.2 Effect of $^{12}C^{6+}$ ion beam on the mycelial growth of *L.decastes*

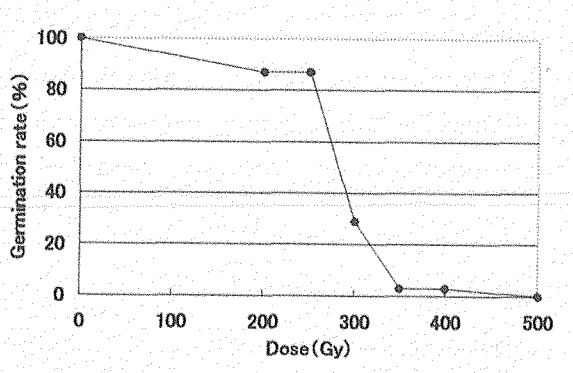

Fig.3 Effect of $^{12}C^{6+}$ ion beam on the regeneration of *L.decastes*

Fig.4 Fruit body of *L.decastes*, ion beam irradiation(left) and control(right)

2.22 Induction of Mutation by Carbon Ion Irradiation to Rice

T. Tsukamoto*, H. Nakanishi*, M. Suzuki*, Y. Hase**, A. Tanaka**,
N. K. Nishizawa* and S. Mori*
Faculty of Agricultural and Life Sciences, The University of Tokyo*,
Department of Ion-beam-applied Biology, JAERI**

1. Introduction

Iron (Fe) is required for many functions in plants, including heme and chlorophyll biosynthesis, photosynthesis, and as a component of Fe-S cluster containing enzymes. Although abundant in soils, Fe forms highly insoluble ferric-hydroxide precipitates under oxidative or alkaline conditions that limit its availability for plants. Therefore, plants have evolved mechanisms to solubilize and to take up Fe efficiently. Graminaceous plants release mugineic acid family phytosiderophores (MAs) into the rhizosphere that bind Fe(III) ion and are then taken up into the roots.

We have been studied the mechanism of Fe absorption by plants to enhance tolerance to low Fe availability in alkaline soils. Especially, we isolated the genes of the synthetic pathway of MAs and produced transgenic plants expressing these genes[1]. In addition, the *OsYSL* genes, which encode Fe^{3+}-MAs complex transporters[2], and the *OsIRT1* gene, which encodes an Fe^{2+} transporter[3] were isolated. We produced the transgenic tobacco expressing the Fe^{3+}-chelate reductase of yeast[4,5]. These transgenic plants showed enhanced tolerance to low Fe availability in alkaline soil. However, the growth of these plants in alkaline soils was inferior to that of plants growing in normal soils.

In this study, we investigated the optimum radiation dosage for producing Fe-deficiency resistant rice mutants induced by carbon ion irradiation.

2. Materials and methods

2.1 Plant material

Dry rice seeds of rice (*Oriza sativa* L. cv. Nipponbare) were used. About 100 seeds were placed upward embryo on petri dish. The irradiation apparatus for seeds, connected to a vertical beam line of the TIARA AVF cyclotron, was used for the 320 MeV carbon ion irradiation. The carbon ion irradiation with the doses of 20, 40, 60, 80, 100, 120, 140, 160, 180 and 200 Gy were performed under atmospheric pressure within 3 min.

2.2 Growth condition

After irradiation, 100 seeds in each lot were germinated at room temperature (ca. 24°C) on paper towels soaked with distilled water. After germination, the plantlets were transferred to a plastic tray in fertilized soil in a growth chamber under a mixture of incandescent and fluorescent lamps with a 12 h light (27 °C)/12 h dark (17 °C) regime and a photon flux density of 320 μmol m^{-2} s^{-1}. The germination rate was measured at 2 days after planting in tray. The survival rate was measured by counting the viable plants at 3 weeks after germination. After 30 days, the growth rate (the ratio of the value for the plant length of unirradiated plant) was measured.

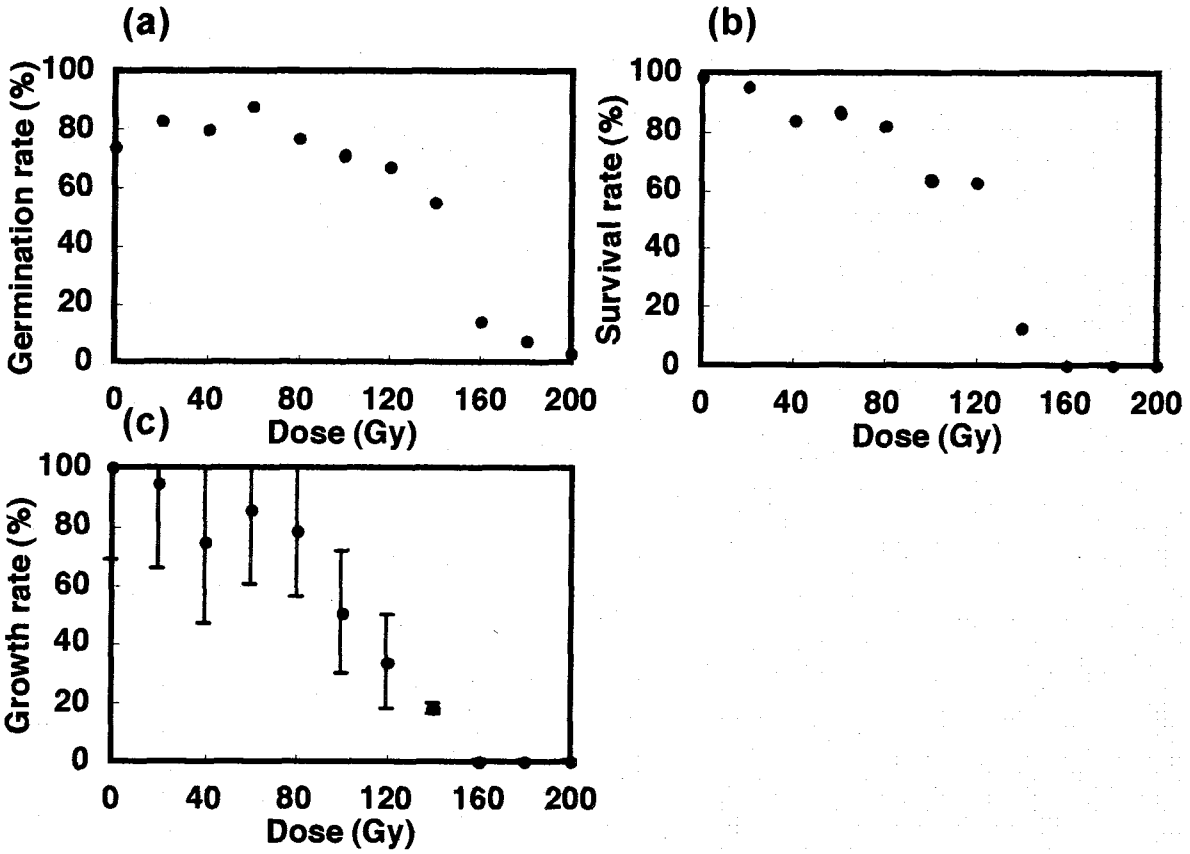

Fig. 1 Dose-response curves for germination rate (a), survival rate (b) and growth rate (c) following irradiation by 320 MeV carbon ion beams with different dose.

3. Results and discussion

Figure 1 shows the effects of 320 MeV carbon ion beams on germination rate (Fig. 1a), survival rate (Fig. 1b) and growth rate (Fig. 1c) in nipponbare rice cultivar. The germination rates were more than 55% in the range of 0-140 Gy. A remarkable reduction at doses of 160 Gy was observed. The survival rates were more than 60% in the range of 0-120 Gy. A remarkable reduction at doses of 140 Gy was observed. The growth rates were more than 74% in the range of 0-80 Gy and gradually decreased at doses of 100-160 Gy.

Significant differences in the sensitivity of rice seeds to carbon ion dose were observed for germination rate, survival rate and growth rate. The shoulder of dose-response curve was 80 Gy (Fig. 1c). We adopted 50 Gy as the adequate dosage for 320 MeV carbon ion beams to obtain mutants efficiently.

References

1) Takahashi et al., 2001, *Nat. Biotechnol.* 19: 466-469.
2) Koike et al., 2004, *Plant J.* 39: 415-424.
3) Bughio et al., 2002, *J. Exp. Bot.* 53: 1677-1682.
4) Ohki et al., 1999, *Plant Soil* 215: 211-220.
5) Oki et al., 2004, *Soil Sci. Plant Nutr.* 50: 1159-1165.

2.23 Carbon Ion Beam Breeding of Rice Suitable for Low Nitrogen Input

H. Kitamura*, M. Mori*, D. Sato*, J. Nakagawa*, T. Yoshida*,
K. Yoshizawa*, T. Kawai* Y. Hase** and A. Tanaka**
Shiga Prefecture Agricultural Technology Promotion Center*
Department of Ion-beam-applied Biology, JAERI**

1. Introduction

In Shiga Prefecture, eutrophication of Lake Biwa caused by nitrogen is a serious problem.

The data estimated by Shiga Prefectural Government at 2000 was reported that 16% of nitrogen flowing into Lake Biwa is caused by agricultural drainage.[1)]

Therefore reduction of applied nitrogen to agriculture field is an important subject of Shiga Prefecture office.

Enacting the ordinance for promotion of harmony between agricultrue and natural environment could decrease fertilizers and pesticides.

Breeding the rice plants that maintain stable yield under low input of nitrogen fertilizer greatly can contribute to the agricultural administration of Shiga Prefecture.

Recently, it has been reported that ion beam causing novel mutations on genome is a promising mutagen for crop breeding.

Therefore, we have started to breed the rice cultivar suitable for growing in low nitrogen condition. Here, we show the dose response of carbon ions for hulled rice seeds and callus.

2. Experimental procedure

2-1. Optimization of radiation dose of ion beam for hulled rice

The hulled rice seeds (*Oryza sativa* cv. Akinouta and Daiiku-1743) were exposed to 320 MeV carbon ions with the dose range of 0 ~ 180 Gy. The irradiated seeds were surface sterilized and sown in 128-cell tray filled with soil. Germination rate and ripening rate were examined.

2-2. Optimization of radiation dose of ion eam for culture cell of rice

The hulled rice seeds were cultured on N6 medium to induce calli for 27 days or 42 days.

The calli were crushed into 1-mm diameter by squashing them on a stainless sieve, and were continued to culture on N6 medium for one week. They were exposed to 320 MeV carbon ions with the doses range of 0 ~ 20Gy.

The calli were transferred to regeneration medium at 37 ~ 44 days after exposure.

The regeneration rate was examined 49 ~ 56 days after transfer.

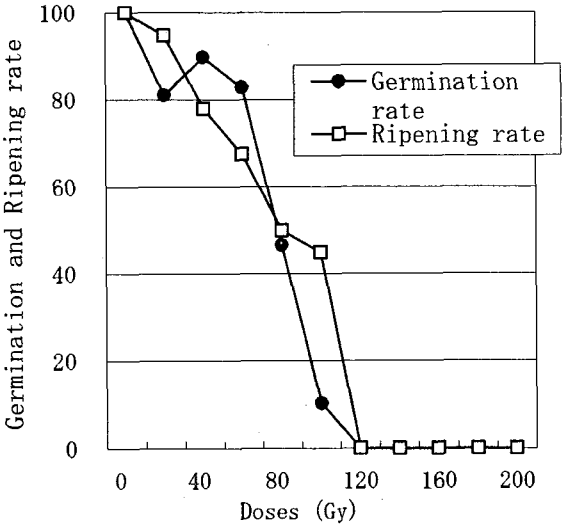

Fig. 1 Dose-response curves for germination rate and ripening rate following irradiation by Carbon ion (12C6+, 320MeV) with different dose.

3. Results and discussion

Table 1 and Fig. 1 show the effects of carbon ions on germination and ripening of the hulled rice cv. Akinouta. The germination rate and ripening rate were decreased as the dose increased. The seeds irradiated with more than 120 Gy did not germinated. The similar dose response was observed in case of the Daiiku-1743 (data not shown).

From these results, we concluded that the suitable dose for our rice cultivars is 40 Gy.

Since the dose response for regeneration rate of callus was not clear, we could not conclude the suitable dose for them (Table 2). More than 10,000 seeds of "Akinouta" and "Daiiku-1743" irradiated with 40Gy were planted in the paddy fields to obtain M2 generation. The mutants that show different nitrogen absorption ability will be screened.

References

1) Biwako Environment Division; Shiga Prefecture, Environment of Shiga.,21(2002)

Table 1. Effects of carbon ion beam * irradiation to hulled rice seeds (cv. Akinouta) on the germination and ripening

Doses (Gy)	0	20	40	60	80	100	120	140	160	180	200
Number of seeds (a)	100	100	100	100	100	100	100	100	100	100	100
Number of germination (b)	58	47	52	48	27	6	0	0	0	0	0
Percentage of germination (b/a)	58	47	52	48	27	6	0	0	0	0	0
Germination rate **	(100)	81	90	83	47	10	0	0	0	0	0
Number of ripening (c)	43	33	30	24	10	2	0	0	0	0	0
Percentage of ripening (c/b)	74	70	58	50	37	33	0	0	0	0	0
Ripening rate **	(100)	95	78	67	50	45	0	0	0	0	0

* Carbon ion beam : $^{12}C^{6+}$, 320MeV

** Number of ratios when germination rate and ripening rate at 0 Gy are assumed to be 100

Table 2. Effects of carbon ion beam * irradiation on the regeneration of calli

Variety name/Line name	Callus instruction period(days)	Doses(Gy)	No. of irradiated calli (a) **	No. of regenerated calli (b)	Regeneration rate (b/a %)	No. of shoots
"Akinouta"	42	0	80	9	11	11
		5	20	6	30	7
		10	40	13	33	19
		15	80	16	20	23
		20	20	1	5	1
	27	0	80	26	33	36
		5	80	23	29	33
		10	80	9	11	11
		15	80	14	18	19
		20	80	12	15	16
"Daiiku 1743	42	0	60	4	7	4
		5	80	1	1	1
		10	80	13	16	17
		15	80	2	3	4
		20	80	11	14	15
	27	0	80	8	10	10
		5	40	0	0	0
		10	80	7	9	9
		15	60	3	5	3
		20	80	11	14	17

* Carbon ion beam: $^{12}C^{6+}$, 320MeV

** 20 calli /9cm petri dishes

2.24 Analysis of Cellular Radiation Response and Local Damage Induced by High LET Heavy Ions

S. Wada*, T. Funayama*, T. Sakashita*, Y. Yokota*, N. Hamada**, T. Kakizaki***, Y. Hase* and Y. Kobayashi*
Department of Ion-beam-applied Biology, JAERI*
Subdivision of Quantum Biology, Gunma University Graduate School of Medicine**
Department of Veterinary Medicine, Kitasato University***

1. Introduction

High linear energy transfer (LET) radiation, such as heavy ion beam, has greater biological effectiveness than low LET radiation. Thus, heavy ion therapy is thought to provide more effective for radioresistant tumors against low LET radiation. Now, clinical trials of carbon ion beam have started.

Higher biological effectiveness of high LET radiation is probably a consequence of local damage like clustered DNA damages that contain locally multiple oxidized bases, single strand breaks and double strand breaks (DSB), because it is considered that the clustered DNA damages is non-repairable or more difficult to repair than a lesion sparsely induced. However, much less is known about the yield and reparability of clustered DNA damages.

Recently, to clarify the induction of DNA damage induced by high LET heavy ions, we established a method of simultaneous detection of ions traversing the cellular nuclei and DNA damage in the individual cells[1]. By the method it was clarified that the induction of DNA damage per one particle increased with LET and depended on the local ionization distribution (track structure)[2].

Mammalian cells have evoked two pathways for repairing DSB, homologous recombination (HR) and nonhomologous end joining (NHEJ). The major pathway in mammalian cells is NHEJ. Many proteins involved in NHEJ include Ku70/80 heterodimer, DNA- PKcs, XRCC4 and ligaseIV. First, Ku bind to the ends of a DSB and DNA end binding by Ku initiates a cascade of molecular events that leads to joining of the broken DNA ends. In addition to DNA repair, Ku protein plays a role in multiple nuclear processes, such as chromosome maintenance and trans-cription regulation.

In this study we investigated NHEJ pathway of DNA repair by exposure to high LET heavy ions, by analyzing responses of Ku protein to DNA damage induced by high LET heavy ions.

2. Materials and methods

pGFP and pGFP-Ku80 were transfected into xrs-5 cells (mutated in Ku80). These cells (xrs5-GFP cell and xrs5-GFP-Ku80 cell) were grown in MEM-alpha medium supplemented with 10% serum and were incubated at 37 ℃ in humidified atmosphere of 5% carbon dioxide and 95% air.

Accelerated ions of 20 MeV H^+ (2.7 keV/μm), 50 MeV He^{2+} (16 keV/μm), 220 MeV C^{5+} (108 keV/μm), 350 MeV Ne^{8+} (321 keV/μm), 260 MeV Ne^{7+} (437 keV/μm), 460

MeV Ar^{13+} (1610 keV/μm) were provided by the AVF cyclotron at TIARA JAERI-Takasaki. Cells were irradiated with ion beams or gamma rays.

To examine the cell survival rates, colony formation assay was preformed. About 10 days after irradiation, colonies were stained and counted.

To evaluate DNA damage and NHEJ pathway induced by heavy ion beams, immunohistochemistry was applied. Cells were attached on the CR-39 plate that is a particle track detector. After irradiation (10-30 min) the cells were fixed by 1% paraformalehyde in PBS. The cells were incubated with anti-γH2AX for 1 hr at the room temperature. Thereafter the cells were washed in phosphate-buffered saline (PBS) and incubated with fluorescent -conjugated secondary anti- body for 1 hr at room temperature. The cells on the CR-39 were stained with DAPI and the opposite side of the CR-39 plate was etched with KOH-ethanol solution at 37°C. Using a conforcal microscope, we took a image of the cell, and then the microscope was focused on ion pits etched on the CR-39 plate, and the image were stored. By merging both images, hit-ions and the fluorescent signal (γH2AX and GFP) were simultaneously detected. The relationship between the location of hit-ions and the site of DNA damage, and NHEJ pathway was investigated.

3. Result and discussion

The sensitivity of xrs5-GFP cells and xrs5-GFP-Ku80 cells to ion beams and gamma rays were determined by survival curves. xrs5-GFP-Ku80 cells were radioresistant to gamma rays and all ion beams, in comparison with xrs5-GFP cells. This result indicates that GFP-fused Ku80 proteins function in the Ku-dependent DSB repair process. To evaluate lethal effects per one particle, the inactivation cross section was calculated using 37% survival dose. The inactivation cross section increased with LET for xrs5-GFP cells and xrs5-GFP-Ku80 cells. The inactivation cross section of xrs5-GFP-Ku80 cells was always larger than that of xrs5-GFP cells for the all LET ranges. However, with increasing LET, the difference of inactivation cross section between xrs5-GFP cells and xrs5-GFP-Ku80 cells became smaller. This suggests that the number of non-repairable DSB by Ku -dependent DSB repair system increases with increasing LET.

To detect the site of DNA damage induced by heavy ion beams, γH2AX signal was observed in xrs5-GFP-Ku80 cells. The site of that signal and the site of etched pits were coincident. And when GFP foci were observed on the nuclei, GFP-Ku80 co-localized with γH2AX. This indicates that Ku80 proteins localizes to DNA damage induced by ion beams. The GFP foci were observed from 10 min to 30 min after C ion and Ne ion irradiation. While the foci were observed for 10 min after Ar ion irradiation, were not observed for 20 min.

These results indicate that the difference of LET values of ion beams influence NHEJ responses.

Reference

1) S. Wada et al., Journal of Radiation Research, 43: (2002) S153-156
2) S. Wada et al., TIARA Annual Report, 2003: (2004) 91-92

2.25 Effects of Heavy Ions on Associative Learning of *Caenorhabditis elegans*

T. Sakashita*, D. D. Ikeda**, N. Hamada*, ***, S. Wada*, T. Funayama* and Y.Kobayashi*
Department of Ion-beam-applied Biology, JAERI*
Molecular Genetics Research Laboratory, The University of Tokyo**
Graduate School of Medicine, Gunma University***

1. Introduction

Since the 1950's, there have been many reports about effects of ionizing irradiation (X-rays, γ-rays) on learning and memory. Many of those reports focused on learning ability using a maze-learning experiment of a mouse, and the conclusion of them as a phenomenon agreed with the deterioration of learning ability by ionizing irradiation. At present, it is generally thought that the main factor of deterioration of learning ability is the suppression of the newborn-neurogenesis in hippocampus. However, it is still unknown about the response of neuron network itself to ionizing irradiation. Thus, we used *C. elegans*, which is well known as a model organism of neuron development and network, at an adult stage without newborn neuron. The present study aims to investigate the response of associative learning and neuron network of *C. elegans*. *C. elegans* normally moves towards NaCl, but animals show avoidance of NaCl after they experience starvation and NaCl simultaneously. This behavior is termed "associative learning".

Our study aims at (1) the investigation of the dose response of associative learning to heavy-ions irradiation, (2) a search of radio-specific response location by local irradiation of heavy ions and (3) a simulation of heavy-ion irradiation experiment using neural network analysis. In 2004, we investigated the dose response of associative learning to C ions and constructed the irradiation plate of *C. elegans* for micro-irradiation with C ions.

2. Experimental procedure

2.1 Heavy ions

$^{12}C^{5+}$ (220 MeV) ions from AVF cyclotron accelerator at TIARA in JAERI-Takasaki were used for heavy-ion irradiation experiments.

2.2 "Broad-field" irradiation experiment

Associative learning was analyzed as follows; (1) well-fed animals were placed onto the food-/NaCl+ conditioning plate for 2 hrs before C-ion irradiation, (2) the conditioning was continued up to 4 hrs after irradiation, and (3) chemotaxis assay was carried out after 4-hr conditioning. On the other hand, the influence of C-ion irradiation on chemo-attraction behavior was examined using food-/NaCl- plates as a control. Chemotaxis index (C. I.) is the index of chemotaxis assay and evaluated by the distribution of animals after 15-min free movement on the assay plate with NaCl-concentration gradient. It was calculated as C. I. = [(number of animals within a 1.5-cm radius of the NaCl spot) - (number of animals within a 1.5 cm radius of the control spot)] / (total number of animals on the assay plate). When all animals exist in a NaCl spot, C.I. is equal to 1.

2.3 Localized -irradiation experiment

Anesthetic restraint of animals is needed to hit a local part of *C. elegans* by C ions. To anesthetize animals and to keep uniformity of sample thickness, we used the original irradiation plate whose base is a 150-μm-thick

micro-coverslip , and a 250-μm-thick slide seal with an empty square for animals and buffer is attached to the base, and the upper part is sealed by a plastic seat. A plate including 20 - 30 animals was irradiated at once.

3. Results and Discussion

3.1 "Broad-field" irradiation experiment

Figures 1 (a) and (b) show the results of the chemo-attraction and associative learning on C ions irradiation experiments. There were no significant changes in both results. Thus, it might be concluded that there is no relation between associative learning of *C. elegans* and C ions irradiation. However, we observed the enhancement of associative learning of *C. elegans* by Co-60 gamma-ray irradiation at the dose of less than 500 Gy. Therefore, we tried to test the effect of C-ion irradiation at the time point of 2 hrs during 4-hr conditioning, i.e., the transitional state of associative learning. As a result, although it was a preliminary result, the tendency of enhancement on associative learning was observed in animals irradiated with C ions (Fig. 2). Further study will be needed to confirm reproducibility, and reconsideration will also be needed to avoid artifact effects.

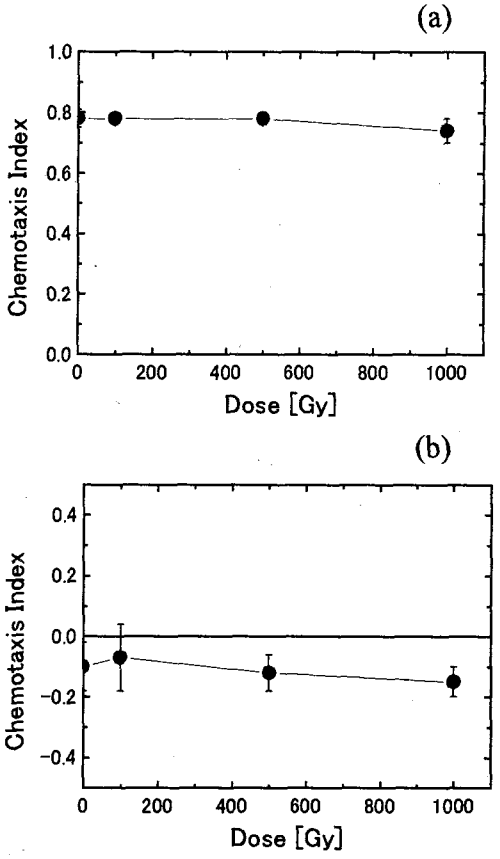

Fig. 1 Dose responses of chemo-attraction (a) and associative learning (b) on C ions irradiation experiments.

3.2 Localized-irradiation experiment

We constructed the experimental procedure that setting animals onto the irradiation plate, making the database of animal positions, hitting them with a precise number of C ions, and transportation of animals to the conditioning plates are carried out within one hour when anesthesia is kept effective. We will accumulate data on effects of localized-irradiation with C ions about chemo-attraction and push forward experiment of associative learning of *C. elegans* before long.

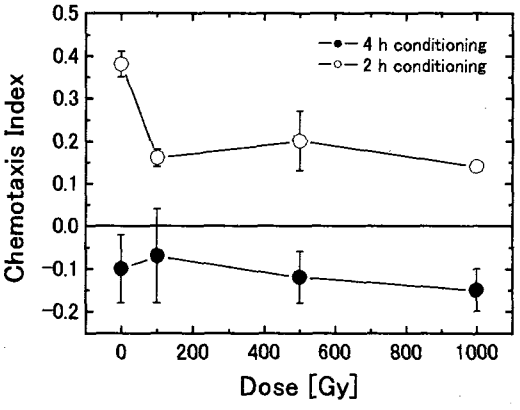

Fig. 2 Dose response of associative learning under 2 hrs conditioning on the food-/NaCl+ plates.

2.26 Effect of Heavy-ion Microbeam Irradiation on Phosphorylation of Histone H2AX

T. Funayama*, S. Wada*, N. Hamada*, **, T. Kakizaki*, ***, Y. Yokota*, T. Sakashita* and Y. Kobayashi*, **
Department of Ion-beam-applied Biology, JAERI*
Subdivision of Quantum Biology, Gunma University Graduate School of Medicine**
Department of Veterinary Medicine, Kitasato University***

1. Introduction

Analyzing the biological effect of heavy-ion beam is important for utilization of heavy-ion radiation on biological applications, like plant breeding and cancer therapy. Moreover, discovering the mechanisms of biological response to heavy ion will become important information for assessing the risk of space radiation.

1.1 Bystander effect

Bystander effect is a phenomenon that radiation effect induction arises in non-irradiated cells by intercellular signaling from irradiated cells.

Considering a low-fluence broad-field irradiation of heavy ion, bystander effect is considered to be important in assessing radiation effect of cell population, because of its dense energy deposition along with the projectile. As the dense energy deposition makes the distribution of energy into the irradiation target inhomogeneous, this un-uniform dose distribution forces the co-existence of non-hit cell within an irradiated cell population. Under these circumstances, bystander effect will take a part to enhance radiation effects when observed them in the total cell population.

1.2 Heavy-ion microbeam

To analyze the bystander effect, it is required to distinguish irradiated cells from non-irradiated cells. However, as far as conventional broad-field irradiation is employed, it is difficult to distinguish them .

Applying microbeam for targeted irradiation of particular cells is a good way to solve this issue. Therefore, we constructed the irradiation system of heavy-ion microbeam generated from the ion accelerated by AVF cyclotron of JAERI-Takasaki. The system was designed for rapid, automatic irradiation of heavy-ion on the specific region of the biological organisms. Using the system, we established the experimental system for target irradiation of individual cells, and discovered that heavy-ion hit on Chinese hamster ovary cell resulted in growth inhibition not only in ion-hit cells but also in non-hit bystander cells [1]. However, molecular analysis of bystander mechanism requires another endpoint that reflects the status of molecules inside the cell.

1.3 Phosphorylation of histone H2AX

Phosphorylation of histone H2AX is known as a modification marker of DNA chromatin structure, and frequently used for detection of chromatin structural changes induced by DNA double strand break. In addition the method for detecting

phosphorylation is rapid and easy when using the specific antibody to a phosphorylated H2AX molecule (γH2AX). Therefore, we employed a phosphorylation of histone H2AX as an endpoint of radiation effect. We analyzed the effect of heavy ion microbeam irradiation on phosphorylation of histone H2AX in Chinese hamster ovary cell line CHO-K1 last year.

2. Materials and Methods

2.1 Preparation of sample holder

A glass-based dish without coverslip (Asahi Techno Glass Corp.), which is a cell culture dish of 35-mm in diameter with a 12-mm hole in the center of its bottom, was used as a base of sample holder for microbeam irradiation. A 100-μm-thick film of CR-39 (TNF-1, Fukuvi Chemical Industry), in which center the 5 mm x 5 mm square mark was engraved as a fiducial mark, was used as a bottom of the sample holder. Paraffin was used to adhere CR-39 film on the bottom of the glass-based dish.

2.2 Cell line

Chinese hamster cell line, CHO-K1, were kept in an exponential growth phase with a culture medium (F12, Invitrogen Life Technologies) containing 10% FBS. The cells (approx. 2500-3000 cells) were inoculated within the area of 5 mm x 5 mm in the center of the sample holder.

2.3 Microbeam irradiation

Among the inoculated cells, less than 1% of whole cell population (25 cells) were selected and their positional data were stored into the database. Cell irradiation was carried out according to this positional data using heavy-ion microbeam system of TIARA. Every cell, of which position was stored in the database, was targeted and then irradiated with 5 count of $^{40}Ar^{13+}$ ion microbeam (11.5 MeV/u, LET = 1260 keV/μm).

2.4 Immunofluorescent staining of γH2AX

The irradiated cells were post-incubated up to 6 hours, then fixed by 2% paraformaldehyde in PBS solution. Phosphorylation of histone H2AX was detected by immunofluorescent staining using specific antibody to γH2AX. Stained sample was observed under fluorescent microscopy, then the both the numbers of cell nuclei positive and negative with fluorescent signal of γH2AX (γH2AX positive cell) were scored. Thereafter γH2AX-positive fraction was calculated from each sample and the effect of microbeam irradiation on H2AX phosphorylation was evaluated.

3. Results and Discussion

Fluorescent signal was observed in the sample stained with anti-γH2AX antibody (Fig.1). The frequency of γH2AX-positive nucleus in a non-irradiated sample, and in a sample of which medium but not cells was irradiated, was around 5%. These signals of γH2AX were considered not from radiation-induced DNA strand break but from some intracellular effect that modify the chromatin structure.

In the samples immediately fixed after cell irradiation, the γH2AX-positive frequency was also around 5%. The result indicated that phosphorylated form of H2AX did not necessarily reflect the status of DNA chromatin structure in the irradiated cells immediately after

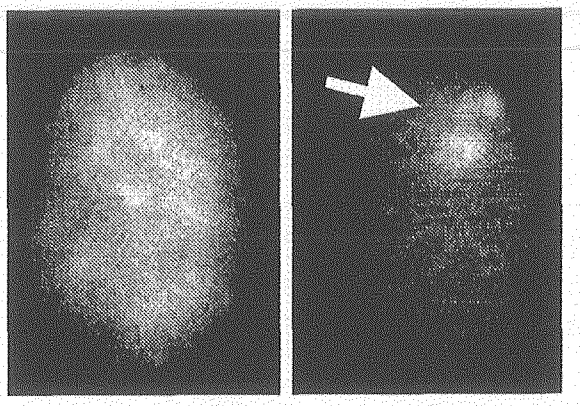

Fig. 1. *In situ* immunofluorescent staining of phosphorylated histone. The fixed cells were reacted with specific antibody against phosphorylated H2AX proteins and were observed under fluorescent microscope. Left panel: counter staining by DAPI; Right panel; immunofluorescent staining by anti-γH2AX antibody. Arrow indicates foci of γH2AX.

irradiation.

On the other hand, the frequency of γH2AX positive cells was around 10% in the samples with the post-irradiation incubation of more than 30 minutes. We irradiated less than 1% of total cell population. Nevertheless, more than 1% increase of the frequency of γH2AX positive nucleus was observed in the post-incubated sample. This result indicated H2AX phosphorylation was triggered from non-irradiated cells. Therefore, we concluded that heavy-ion irradiation induces the changes in choromatin structure that were able to be detected as γH2AX in non-hit cells by transmission of inter-cellular radiation signal.

This result suggested that the heavy-ion -induced bystander effect on the phosphorylation of histone H2AX in CHO-K1 cells. As the structural change of chromatin by DNA double strand break result in the H2AX phosphorylation, this γH2AX induction could be the induction of DNA double strand break in bystander cells.

It was reported that heavy-ion microbeam irradiation induces micronucleus in bystander cells[2]. Formation of micronucleus is considered to require DNA breaks in its very early step. Therefore, it was considered that the bystander effect inducing γH2AX might be a first step of micronucleus formation in non-irradiated bystander cells.

To unveil the whole mechanisms of bystander effect, we need further analysis of intracellular signal transduction in bystander cells. We consider that a potent candidate for further analysis is the molecules involved in a pathway of DNA damage signal transduction. Analysis of the response of these pathways, like p53/p21 induction and phosphorylation of ATM gene product, using heavy-ion microbeam will give us a clue to discover the complete signal transduction pathway of bystander effect.

References

1) T. Funayama, S. Wada, Y. Kobayashi, H. Watanabe, Radiation Research 163 (2005), 241–246.

2) C. Shao, Y. Furusawa, Y. Kobayashi, T. Funayama, S. Wada, Bystander effect induced by counted high-LET particles in confluent human fibroblasts: a mechanistic study, FASEB J., 17 (2003), 1422-1427.

2.27 Disappearance of Knob-like Protuberances in a Dermal Mutant (Knobbed) of the Silkworm, *Bombyx mori*, in Response to Heavy-ion Beam Irradiation

K. Kiguchi*, K. Fukamoto*, T. Sakata*, K. Shirai*, R. Kanekatsu*,
Y. Kobayashi**, T. Funayama**, T. Sakashita** and H. Watanabe**
Department of Applied Biology, Faculty of Textile Science and Technology, Shinshu University*
Department of Ion-beam-applied Biology, JAERI**

1. Introduction

Heavy-ion micro-beams are extremely useful radio-surgical tools for studying bio-function and differentiation of various cells and tissues in insects. Locally targeted irradiation of heavy-ion beams of silkworm larva had no deleterious effects on survival, but induces marked functional disruption of the irradiated tissues or organs [1,2,3]. For example, in instances where larval epidermis was locally irradiated with heavy-ions, scale development did not occur to various degrees in the irradiated area of the adult moths depending on the dose of irradiation [1,3].

A large number of geographical and mutant stocks of the domestic silkworm, *Bombyx mori*, are maintained, not only for practical breeding, but also for biological research. One such mutant, Knobbed (*K*), is one of body-shape mutants and is characterized by the appearance of dermal protuberances (knobs) on the crescent and star-spot larval markings (Fig. 1)[4]. Knob formation is believed to be due to the abnormal proliferation of epidermal cells, but the reason is still unknown. In order to clarify this mechanism, we investigated the effects of heavy-ions on the corresponding epidermal cells of newly hatched larvae and found that the knob protuberances disappeared after the local irradiation.

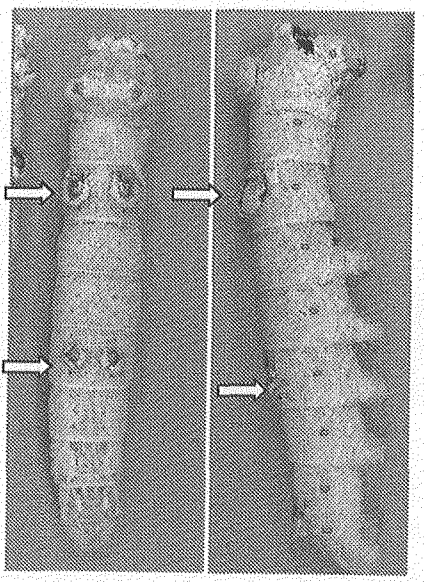

Fig. 1 Typical "knob" characters (arrows) on a silkworm mutant

2. Materials and Methods

The Knobbed (*K*) mutant strain of the silkworm, *B. mori*, was used for this experiment. The newly hatched larvae were exposed to localized heavy-ion micro-beams of carbon ion ($^{12}C^{5+}$, 220 MeV, 18.3 MeV/u, range in water=1.2 mm) of the AVF-cyclotron in TIARA. Movement of the highly mobile newly hatched larvae was restricted by confinement in a rectangular chamber (3.15 mm×0.95 mm ×1.50 mm) of an aluminum plate sandwiched between 100 μm OHP(overhead projector) films (Fig. 2). Given the beam depth (1.2 mm

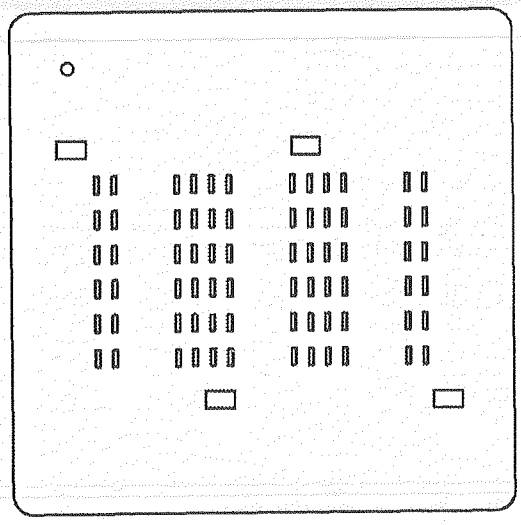

Fig. 2 A fixing holder devised for ion-beam irradiation of newly hatched silkworm larvae

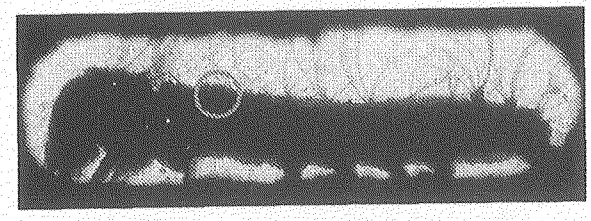

Fig. 3 Targeting a newly hatched larva for ion-beam irradiation using a 180 μm ϕ aperture

in water), 3 sheets of 100-μm mylar (polyimide) film were used in conjunction with the OHP films to avoid an ion-penetration into internal tissues such as intestines. Test larvae were locally irradiated with 100 to 500 Gy (surface dose) of carbon ions using an aperture of 180 μm ϕ (Fig. 3). Only the left dorsal region of the 5th larval segment was subjected to beam treatment, with the right half of the segment used as control. After irradiation, larvae were routinely reared on mulberry leaves at 25℃, and the larval integuments were cut off and fixed in Carnoy's fixative upon preparation for microscopic examination. The paraffin sections were prepared and examined using a light microscope. Some larvae were allowed to develop, and morphology of the irradiated sites was observed at each developmental stage under a dissecting microscope.

3. Results and Discussion

Using the aluminum holder sandwiched between OHP film (Fig. 2), newly hatched larvae could be irradiated with the desired beam size and dose. However, because some of larvae moved back and forth during irradiation, irradiated sites were occasionally off target and such cases were excluded from observations. Improvements to the fixing method in caterpillars are necessary to facilitate irradiation with a higher accuracy.

When the newly hatched larvae were irradiated with 100 Gy of carbon ions, minor morphological change was observed in the "knob" characters. However, irradiation at levels exceeding 350 Gy resulted in the protuberances disappearing at a high frequency (Fig. 4). Light microscopy revealed that the epidermal cells of protrusions are composed of

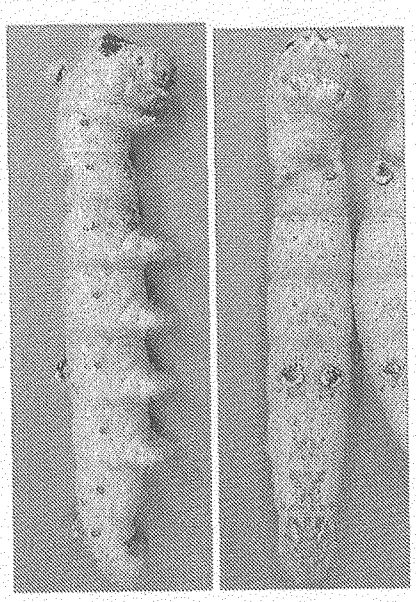

Fig. 4 Disappearance of protuberances (arrow) in the irradiated larva (5th instar, Day 3) with ion beams at 350 Gy.

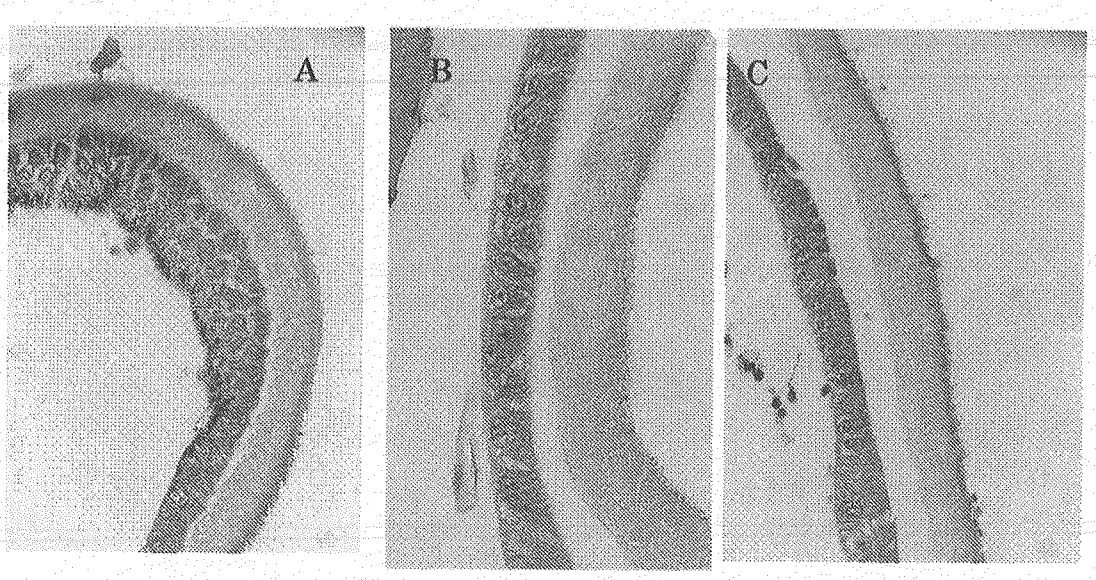

Fig. 5 Cross sections of the integuments from the "Knobbed" mutant strain (5^{th} instar, Day 3).
A: Section of a protuberance.
B: Section of a normal integument.
C: Section of a previous protuberance after ion-beam irradiation.

two or more layers (Fig. 5a), with only one epidermal layer found at non-knobbed areas of the mutant (Fig. 5b). Interestingly, reversion to a single epidermal layer at the sites of previous bumps accompanied the disappearance of the protuberances (Fig. 5c). These results indicate that irradiation of ions inhibits the differentiation of "knob" characters. Based on these findings we are studying the mechanism of knob formation with special emphasis on the effect of ion-beams on cell division and ploidy of the epidermal cells.

References

1) Z.-L. Tu, S. Yamasaki, K. Shirai, R. Kanekatsu, K. Kiguchi, Y. Kobayashi, M. Taguchi, H. Watanabe, J. Seric. Sci. Jpn., 68 (1999) 443-453.
2) E. Ling, K. Fukamoto, S. Xu, K. Shirai, R. Kanekatsu, Y. Kobayashi, Z.-L. Tu, T. Funayama, H. Watanabe, K. Kiguchi, J. Insect Biotech. & Sericol. 72 (2003) 95-100.
3) K. Kiguchi, K. Fukamoto, K. Shirai, R. Kanekatsu, Y. Kobayashi, T. Funayama, T. Sakashita, and H. Watanabe, JAERI-Review, 2004-025 (2004) 85-87.
4) H. Aruga, Bull. Seric. Exp. Sta. Jap. 9 (1939) 295-304.

2.28 Dose Dependency of Bystander Effects and Radiation Quality of the Beam

Y. Furusawa*, Y. Matsumoto*, M. Aoki*, R. Hirayama*, Y. Kobayashi**, T. Funayama**, T. Sakashita**, S. Wada** and N. Hamada**
Heavy-Ion Radiobiology Research Group, NIRS*,
Department of Ion-beam-applied Biology, JAERI**,

1. Introduction

It has been thought that the heritable biological effects of radiation requires an interaction of the radiation with DNA either by direct ionization or by the production of OH radicals. Presumably, no effect would be expected in cells that received no direct exposure. Recently, evidence has been demonstrated that low doses particles lead to the sister chromatid exchange (SCE) in many cells in a population even though only a few cells have been traversed by an alpha particle[1]. This phenomenon has been called the "bystander effect," through which cells in the vicinity of directly targeted cells can respond to the radiation. By the use of several experimental approaches, it is reported that the bystander effect have appeared with multiple biological end-points, including cell killing, inductions of micronucleus, mutation, genomic instability, and so on.

Although the gap junctional intercellular communication (GJIC) is an important pathway for the production of bystander responses[2,3], but it is not always required. By irradiating nonconfluent cells with a precise number of particles, the findings that targeting of a single cell led to additional 10s of cells being damaged[4] give direct evidence of non-GJIC involved but the likelihood of medium mediated bystander responses.[5-8].

To clarify the mechanisms of transduction of bystander signal through the GJIC, an LET dependency of bystander effect were studied using microbeam facilities at TIARA/JAERI, PF/KEK and SPICE/NIRS.

2. Materials and Methods

2.1. Cells

AG01522 normal human skin fibroblasts purchased from Coriell Cell Repositories were cultured at 37°C in humidified atmosphere of 95% air and 5% CO_2 with Eagle's minimum essential medium (Sigma M5650) supplemented with 2 mM L-glutamine and 18% fetal bovine serum (Lenexa) plus streptomycin and penicillin. Cells destined for heavy-ion irradiation were seeded in the specially made dish at a density of 1.4×10^5 cells per dish 4 days before the irradiation. The medium was changed at day 2, so that at the time of irradiation the cells were in full confluence.

2.2. Irradiations

A charged particle microbeam apparatus installed below a vertical beam line of the cyclotron at TIARA was used to deliver precise number of heavy ions of 220 MeV ^{12}C-, 260 MeV ^{20}Ne-, and 360 MeV ^{40}Ar-beams. The calculated LET values were 120 keV/μm, 430 keV/μm, and 1260 keV/μm, respectively. The cells were irradiated with 2.6 MeV proton beam

having 13.5 keV/μm as the LET at SPICE/NIRS, and 5.39 keV monochromatic soft X-rays with LET of 5.3 KeV/μm at PF/KEK. Particles traversing through the Kapton films and a cell were detected by photomultiplier tube (PMT) with plastic scintillator at TIARA and SPICE.

Just before irradiation, a thin Kapton film (8 μm) was floated on the medium surface, and the medium was removed to cover the cell surface by the film, except PF. This process kept the cells fully hydrated during irradiation, which was 30 min. After the irradiation, by adding new medium in the dish, the film was floated again in the medium surface and could remove the film safely without gives any damage to the cells.

Cells at 49 (=7x7) different positions in the confluent culture were irradiated with 1 to 6 particles at TIARA. Cells in 4 different 53 x 53 μm^2 square areas that consist approximately 50 cell at PF, or approximately 100 x 100 μm^2 single area at SPICE. After the irradiation, 2 ml medium was immediately supplied to each (or just changed the medium at PF) dish and cells were subsequently cultivated for 15 h until the micro nuclei (MN) assay to start growing. Un-irradiated control dishes were treated with the same protocol except for irradiation.

2.3. MN assay

The formation of MN was assayed by using the cytokinesis block technique. Cells in each irradiation dish were harvested, re-seeded in a 60 mm dish, and incubated in the presence of 2.5 g/ml cytochalasin-B. After 48 h, the cells were harvested again, treated with a 75 mM KCl hypotonic solution at 37°C for 10 min, and fixed by methanol at −30°C overnight. The fixed cells were spread on a slide grass and stained with 10 mg/ml acridine orange.

After this cytochalasin-B treatment,

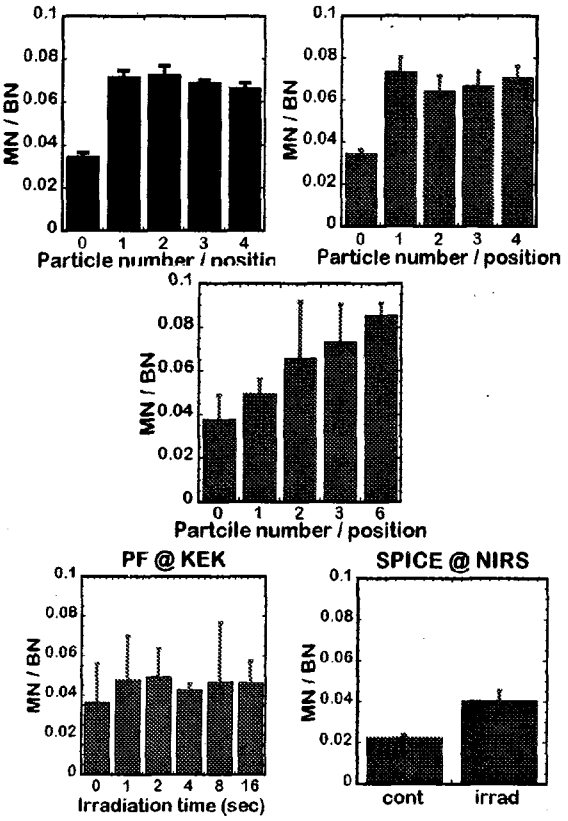

roughly 20% of the cells became binucleated (BN) cells when the cells were sub-cultured in a new Petri dish. The MN in BN cells were counted by fluorescence microscopy.

3. Results and Discussion

Efficiency to produce MN in BN cells were not affected by the number of traversals at the cells in each position for higher LET beams (upper panels); i.e., ^{20}Ne (left) or ^{40}Ar (right) ion-beams having 430 or 1260 keV/μm, respectively. When cells were irradiated with ^{12}C-ion beams having LET of 120 keV/μm (center), clear particle

dependent increment of the MN induction was found up to 6 particles at each position. It is a preliminary experiment and there are no enough data at SPICE yet, we could find some bystander effect for proton beams. The dependency of particle number will be observed soon. There must be a particle number dependency of the Bystander effects. However, when cells irradiated with low energy photon beams at PF, we could not find bystander effect in this dose range tested.

References

1) H. Nagasawa, and B. J. Little, Cancer Res 52 (1992) 6394-6396.
2) C. Shao, Y. Furusawa, et al., FASEB J 17 (2003) 1422-1427.
3) C. Shao, Y. Furusawa, et al., Radiat Res 160 (2003) 64-69.
4) C. Shao, V. Stewart, et al., Cancer Res 63 (2003) 8437-8442.
5) H. Matsumoto, S. Hayashi, et al., (2000) Internat J Radiat Biol **76** (2000) 1649–1657.
6) C. Shao, M. Aoki, and Y Furusawa, J Radiat Res **42** (2001) 305–316.
7) C. Shao, Y. Furusawa, et al., Int J Radiat Res 78 (2002) 837-844.
8) C. Shao, M. Aoki, Y. Furusawa, J Radiat Res 45 (2004) 97-104.

2.29 The Presumption of Proton Beam Relative Biological Effectiveness for Mammalian Tumor Cells

T. Sano*, S. Wada**, M. Kaneko*, Y. Imaoka*, N. Yamada*, T. Kakizaki*, K. Suzuki*, M. Hosoya*, A. Kaihotsu*, M. Natsuhori*, N. Itoh* and Y. Kobayashi**

Department of Veterinary Medicine, Kitasato University*

Department of Ion-beam-applied Biology, JAERI**

1. Introduction

Recently, the incidence of tumor patients has been increasing, accompanied by a prolongation of the life spans of companion animals[1]. There are several treatment methods for tumors, which have become the primary cause of death. The chance of application of radiation therapy is now increasing in veterinary medicine, the same as in humans, because of its numerous advantages, including being bloodless and relatively non invasive, as well as maintaining the form and function of organs[2, 3, 4]. However, even tumors of the same origin and pathology, can show radiosensitivity over quite a wide range, and therefore, understanding the radiosensitivity of an individual tumor and an individual patient is of great importance in clinical situations[5]. Knowledge of the intrinsic radiosensitivities of cells from a tumor biopsy can help to produce an optimized radiotherapy protocol for individual patients[6]. It is thought possible to match treatment plans to individual patients if the differences in radiation sensitivity can be known before beginning treatment[5].

The purpose of this study was to evaluate the relative biological effectiveness of proton-beam irradiation compared with X-ray irradiation for three cell lines derived from canine spontaneous tumors.

2. Experimental procedure

2.1 Cell culture

Fibrosarcoma (F), Squamous cell carcinoma (S), and Hemangiopericytoma (H) derived from canine spontaneous tumors were used. Each cell lines was grown in Minimum Essential Medium Eagle (Sigma, St.Louis, U.S.A) supplemented with 10% fetal bovine serum (FBS) (Cansera International Inc., Canada), and 0.1 mg/ml kanamycin in 6-cm diameter culture dishes. All cells were incubated at 37℃ in a humidified atmosphere of 5% CO_2 and 95% air. All cells were irradiated at the logarithm proliferation phase.

2.2 Irradiation

Cells were irradiated with an X-ray beam from the Kitasato University orthovoltage X-ray irradiation machine and a 20-MeV proton beam from the TIARA AVF cyclotron. Each cell was irradiated by 0, 2, 4, 6, and 8 Gy X-ray (250 kVp, 6 mA, 1.6 Gy/min, LET 1.0 keV/ μm) and at the same dose of proton beam (20 MeV, 6 Gy/min, LET 2.7 keV/μm).

2.3 Survival

After irradiation, cells were plated at a density of approximately 100 surviving cells per 6 cm diameter culture dish. Approximately 10 days later, cells were fixed and stained with 0.5% crystal violet. Colonies of more than 50 cells were counted as survivors. The survival data were fitted to the linear-quadratic model.

$$\ln S = -\alpha D - \beta D^2$$

where S is the survival fraction and D is the radiation dose.

2.4 Data evaluation

A multiple regression analysis was used to calculate the means and standard deviations for the α and β values of each cell line. The doses required for reducing the survival fractions to each ratio and survival fractions at 2 Gy (SF2; %) for each cell line were calculated by using these α and β values. The relative biological effectiveness (RBE) values were calculated by comparing each survival ratio of the proton beams with those of the X-rays.

3. Results and Discussion

The dose-response curves as clonogenic survival curves in the three kinds of cell lines after X-ray and proton irradiation are shown in Figs. 1 and 2, respectively. Each survival curve is well-fitted to the linear-quadratic model, and the simulation curves correspond well with the measurement values. The parameters from the linear-quadratic model and SF2 are shown in Tables 1 and 2. The α values after X-ray irradiation of H were found to be higher than those of F and S. The survival curve after X-ray irradiation of H was linear, while those of F and S were linear-quadratic. SF2 of S, F, and H were 74%, 50%, and 30%, respectively. H was the most radiosensitive to X-rays. F possessed curvilinear survival curves with moderate radiosensitivity.

The dose responses after proton-beam irradiation were similar to those after X-ray irradiation. Similar to the X-ray irradiation results, the α values after proton-beam irradiation of H were higher than those of F and S. SF2 of S, F, and H were 68%, 44%, and 14%, respectively.

All RBE values of proton-beam irradiation exceeded 1.0. For S, RBE values tended to decrease with increases in the survival rate; in contrast, RBE of F tended to increase, wile those of H remained stable (Fig.3).

For survival rates of 20% or less, the RBE values of H were the highest, followed by those of S and F.

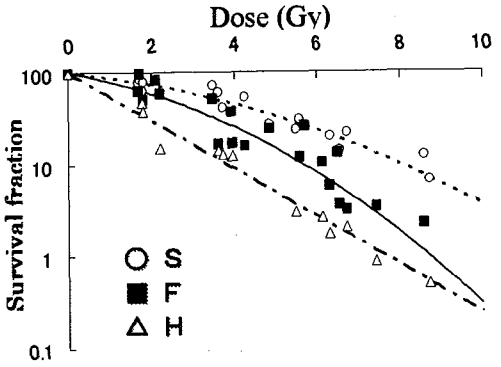

Fig.1 Survival curves of the three tumor cell lines (F, S, and H) after X-ray irradiation. The survival fraction was measured as the number of colonies formed after X-ray irradiation. Data were fitted using a linear quadratic model.

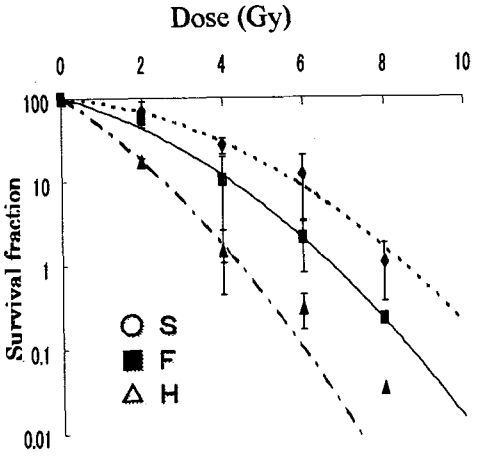

Fig.2 Survival curves of the three tumor cell lines (F, S, and H) after proton-beam irradiation. The survival fraction was measured as the number of colonies formed after proton-beam irradiation. Each data point is the mean ± the standard division (S.D.) of four independent examinations. Data were fitted using a linear quadratic model.

These results suggest that the RBE values of each cell type show different tendencies with regard to the survival rate.

It is therefore considered that the presumption of radiation sensitivity for proton-beam irradiation and establishment of a proton-beam irradiation protocol will become possible if the experimental frequency, the number of cells, and the varieties of cells are further increased, and if circumstantial information continues to accumulate.

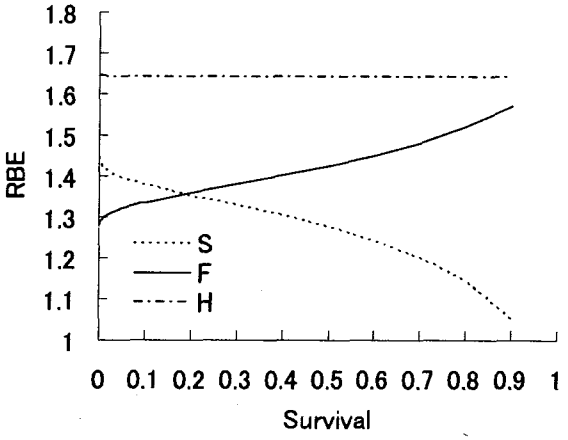

Fig.3 Transition of RBE to survival rate. RBE values were calculated by comparing The survival ratios for the individual proton-beams with those of X-rays.

Table 1

Parameters from the linear quadratic model fitted to the survival data after X-ray irradiation.

	α [a)]	β [a)]	SF2(%) [b)]
S	0.106±0.003	0.023±0.006	74
F	0.181±0.068	0.040±0.014	59
H	0.604±0.072	0.0002±0.02	30

a) α and β values were determined from the linear quadratic equation.

b) Survival fraction at 2Gy.

Table 2

Parameters from the linear quadratic model fitted to the survival data after proton-beam irradiation.

	α [a)]	β [a)]	SF2(%) [b)]
S	0.089±0.052	0.054±0.011	68
F	0.299±0.064	0.058±0.009	44
H	0.992±0.029	0.0006±0.0001	14

a) α and β values were determined from the linear quadratic equation.

b) Survival fraction at 2Gy.

References

1) D. J. Waters and D. M. Cooley, Iams Nutrition Symposium Proceedings, 3 (2000) 415-426.

2) R. L. Burk, T. Giel, Vet Clin North Am Small Anim Pract, 27(1) (1997) 7-20.

3) D. Harris, G.K. King, P.J. Bergman, Vet Clin North Am Small Anim Pract, 27(1) (1997) 37-46.

4) E. A. McNiel, S. M. LaRue, Clin Tech Small Anim Pract, 13(1) (1998) 33-37.

5) M. Bergqvist, D. Brattstrom, M. Stalberg, H. Vaghef, O. Brodin, B. Hellman, Cancer Lett, 133 (1998) 9-18.

6) S. Wada, H. Kuruhashi, Y. Kobayashi, T. Funayama, K. Yamamoto, M. Natsuhori, N. Ito, J. Vet. Med. Sci, 65(4), (2003) 471-477.

2.30 Ion Beam Irradiation has Different Influences on Glutathione Peroxidase of Retinal Pigment Epithelial Cells among ^{20}Ne, ^{12}C, and ^{4}He

K. Akeo*, T. Funayama**, Y. Kobayashi**, Y. Akeo*** and K. Tsubota*
Department of Ophthalmology, Keio University School of Medicine*
Department of Ion-beam-applied Biology, JAERI**
Akeo Eye Clinic***

INTRODUCTION

Glutathione peroxidase (GPX), a selenium-dependent and lipid peroxide-scavenging enzyme that effectively reduces lipid peroxides with the concomitant oxidation of glutathione is distributed in mitochondria [1]. We have shown that short-term incubation with linoleic acids (LA) increased the thiobarbituric acid-reactive substance (TBARS) in the retinal pigment epithelial (RPE) cells, which indicated the level of lipid peroxides [2]. Photoreceptor outer segments are susceptible to lipid peroxidation because of their high content of polyunsaturated fatty acids (PUFA) [3]. The pathogenesis in the Royal College Surgeon (RCS) rats is a failure of phagocytotic activity by RPE cells of the photoreceptor outer segments [4] that contain PUFA [3]. In the RCS rats after 3 weeks of birth, we can see strong positive-staining with anti-rat αGPX in the degenerating photoreceptor outer segments. We postulate that the degeneration and peroxidation of unphagocytized photoreceptor outer segments of the RCS rats was progressive because the eyelids of all these rats were open and light passed through their eyes 2 weeks after birth [5]. When the unphagocytized photoreceptor outer segments undergo oxidation by exposure to light [6], the PUFA is changed into lipid hydroperoxides, the antioxidative system in the photoreceptor cells, and the RPE cells may then malfunction.

The gamma ray (^{60}Co) causes ionization uniformly in the whole irradiated tissue. We previously reported that high dose of gamma irradiation prevented programmed cell death regulated by p53 and bcl-2 genes in the ciliary body dissected from living body, and was useful for preservation of organ after culture by the protective influence of inflammatory reaction. The irradiation resulted in a dose-dependent decline in the activities of GPX in the skin of mice [7]. Furthermore, the ion beam is an ionization radiation that is induced by acceleration of the ionizing atom of ^{20}Ne, ^{12}C, ^{4}He and so on, but has a characteristic to lose energy and stop at the constant depth of tissue. The reaching depth to the tissue depends on the ion species and the acceleration energy. The reaching depth in water is 1.64 mm in $^{4}He^{2+}$ (50MeV), 1.08 mm in $^{12}C^{5+}$ (220MeV), and 0.57 mm in $^{20}Ne^{8+}$ (350MeV). Gamma ray penetrates into the tissue, but an ion beam has higher energy and a maximum influence at a point inside the tissue. Moreover, the ion beam is supposed to have a bystander effect around the irradiated tissue. We investigate how these ion beams with the different reaching depth in tissue influence GPX, antioxidative enzymes in mitochondria of the RPE cells. We compared

the effects among the species of the ions.

METHODS

Confluent bovine RPE cells were exposed to an ionization radiation that is induced by acceleration of the ionizing atom of ^{20}Ne, ^{12}C, and ^{4}He. We obtained the RPE cells after 4, 8, 24, 48 hours of the irradiation and extracted total cellular RNA. We used an Internet web site, Primer3, to design the primers (5'-gcccaactttatgctcttcg-3' and 5'-ggacagcagggtttcaaatgt-3') for RT-PCR amplification of the cDNA of GPX and 18s ribosomal RNA. Reverse-transcribed polymerase chain reactions (RT-PCR) with cDNA, primer, and Cyber-green were carried out at 95°C for denaturation, 60°C for annealing, and 72°C for extension for 17–27 cycles. LightCycler technology is the most innovative and rapid possibility for carrying out and simultaneously evaluating PCR experiments. Fluorimetric analysis of the PCR products is performed as real-time measurement either continuously or at a specifically defined time during each PCR cycle. The experimental protocol contains four cycle programs: Program 1: Reverse transcription of the template RNA. Program 2: Denaturation of cDNA/RNA hybrid. Program 3: Amplification of cDNA. Program 4: Melting curve analysis (for product identification). Program 5: Cooling of the rotor and thermal chamber.

RESULTS AND DISCUSSION

The expression of GPX in RPE cells declined by the exposure to gamma ray after 4, 8, 24, 48 hours of the irradiation (Table 1), and increased after ion beam irradiation (Table 2, 3, 4). Gamma ray irradiation damaged the expression of GPX in the RPE cells and it might be possible for the ion beams to induce the expression in order to protect from the damage of cell membrane due to the accumulation of energy at narrow areas.

Table 1. Gamma Irradiation

F1/Cycle	RNA		GPX		GPX/RNA	
Gamma ray	(-)	(+)	(-)	(+)	(-)	(+)
0 hr	11.0	12.5	8.5	8.50	0.77	0.68
4 hr	11.0	13.0	10.5	9.50	0.96	0.73
8 hr	11.0	13.0	10.0	9.00	0.91	0.69
24 hr	13.0	13.0	10.0	8.00	0.77	0.62
48 hr	11.0	13.5	9.0	6.50	0.82	0.48

Table 2. $^{4}He^{2+}$ Irradiation

F1/Cycle	RNA		GPX		GPX/RNA	
$^{4}He^{2+}$	(-)	(+)	(-)	(+)	(-)	(+)
0 hr	11.5	13.0	13.5	16.0	1.17	1.23
4 hr	16.5	17.5	15.0	18.0	0.91	1.03
8 hr	16.0	16.0	17.5	22.5	1.09	1.41
24 hr	14.0	15.5	19.0	19.5	1.36	1.26
48 hr	16.5	17.0	19.5	17.5	1.18	1.03

Table 3. $^{12}C^{5+}$ Irradiation

F1/Cycle	RNA		GPX		GPX/RNA	
$^{12}C^{5+}$	(-)	(+)	(-)	(+)	(-)	(+)
0 hr	18.5	19.0	2.5	4.5	0.14	0.24
4 hr	21.5	21.0	6.5	5.0	0.30	0.24
8 hr	20.0	21.0	8.0	6.5	0.40	0.31
24 hr	24.0	22.5	5.5	7.5	0.23	0.33
48 hr	22.0	22.0	7.0	7.0	0.32	0.32

Table 4. $^{20}Ne^{8+}$ Irradiation

F1/Cycle	RNA		GPX		GPX/RNA	
$^{20}Ne^{8+}$	(-)	(+)	(-)	(+)	(-)	(+)
0 hr	11.5	16.5	4.5	5.5	0.39	0.33
4 hr	13.0	17.0	3.0	5.5	0.23	0.32
8 hr	16.5	14.0	5.0	5.0	0.30	0.36
48 hr	15.0	13.5	6.0	6.0	0.40	0.44

Referrences

1) K. Watanabe, Tran.Soc Pathology Jpn 76 (1986) 39 –74.
2) K. Akeo, and T. Hiramitsu, Pigment Cell Res 11 (1998) 320-326.
3) W.L. Stone, C.C. Farnsworth and E.A Dratz, Exp Eye Res 28 (1979) 387 –397.
4) M.H. Chaitin, and M.O. Hall. Invest Ophthalmol Vis Sci 24 (1983) 812-820.
5) K. Akeo, H. Tsukamoto, S. Okisaka, T. Hiramitsu and K. Watanabe, Pigment Cell Res 12 (1999) 107-117.
6) R.D.Wiegand, C.D. Joel, L.M. Rapp, J.C. Nielsen, M.B. Maude and R.E. Anderson Invest Ophthalmol Vis Sci 27 (1986) 727-733.
7) J.G. Chandra, G.K. Rajanikant, S.K Rao, and B.M. Shrinath, Clin Chim Acta 332 (2003) 111-121.

2.31 Molecular Mechanisms for Radiation-induced Bystander Effects

H. Matsumoto*, M. Hatashita*, A. Takahashi**, Y. Kobayashi***,
T. Funayama***, S. Wada*** and T. Sakashita***
Department of Experimental Radiology and Health Physics, Faculty of Medical Science, University of Fukui*
Department of Biology, Nara Medical University**
Department of Ion-beam-applied Biology, JAERI***

1. Introduction

Efficiency on damage formation of the various types at sub-cellular, cellular and supra-cellular level induced by low doses, where experimental data are difficult to be available, is generally based on linear back-extrapolations from data at higher doses. However, a large amount of data produced during the last decade seem to indicate higher yield about the damage than expected, possibly due to the so-called "bystander effect" (i.e. the induction of damage in cells that were not directly hit by radiation). In any case, the various forms of cellular communication seem to play a key role, since damage in indirectly hit cells may represent a response to signals coming from cells that were directly hit by radiation. On the other hand, it is well known that an adaptive response is induced by the priming low-dose or low-dose rate irradiation prior to exposure to the ionization radiation at a high dose. Namely pre-exposure to radiation increases radioresistance, i.e. sub-linear response at low doses. As another biological response to low dose radiation, we can find the hormesis, defined as a "stimulatory effect caused by low levels of toxic agents". Although the mechanisms underlying these effects are still unknown, several similarities between radiation-induced adaptive responses and bystander effects can be found in recent our experimental results. Here, we propose the possibility that radiation-induced advantageous bystander effects, which are brought about through nitric oxide (NO) radical generations, contribute the induction of adaptive response by the priming irradiation prior to the challenge irradiation with the ionization radiation.

2. Materials and Methods

2.1. Cells

Human non-small cell lung cancer H1299 cells and normal fibroblast AG1522 cells were kept in an exponential growth phase with a culture medium (Dulbecco's modified Eagle medium, Sigma) containing 10% and 15% FBS and 20 mM HEPES, respectively. Two days before irradiation, cells were spotted to make five colonies (1000 cells per spot) into the sample holder, 35 mm dish in diameter with bottom made with 100 μm CR-39 in thickness and then cells were cultured under the conventional conditions.

2.2. Irradiation with $^{20}Ne^{7+}$ beams

Just before irradiation, the medium was removed to make ions penetrate both the cells and the bottom of the sample holder.

During irradiation, cells were covered with an 8 μm-thick polyimide film (Kapton, Toray Industries). The number of ions having traversed the sample was counted with a constant fraction discriminator coupled to a preset counter/timer. A pulse-chopper in the injection-line of the cyclotron was used as a fast beam switch. A cell of the center colony was irradiated with 5 ~ 10 count of $^{20}Ne^{7+}$ beams[1].

Immediately after irradiation, the sample holder was refilled with the medium, and then cells were cultured under the conventional conditions.

2.3. Detection of phosphorylated H2A.X (γH2A.X) by immunochemical fluorescence staining

Cells were fixed for 5 min in a 1:1 methanol: acetone solution prior incubation with anti-phosphorylated H2A.X monoclonal antibodies (clone JBW301, Upstate, NY, USA) for 60 min at room temperature. Alexa Fluor 488-conjugated goat anti-mouse IgG (A-11029, Molecular Probes, OR, USA) was used as secondary antibodies. Cells were counter stained with 4',6-diamidino-2-phenyl-indole (DAPI) for 15 sec, mounted, and viewed with a Nikon ECLIPSE E600 fluorescence microscope using a 40 × objective. Images were processed using Adobe Photoshop and Microsoft PowerPoint software.

3. Results and Discussion

3.1. Detection of γH2A.X in the target colony by immunochemical fluorescence staining

The formation of γH2A.X foci was examined by immunochemical fluorescence staining. Thirty minutes after irradiation with 10 counts of $^{20}Ne^{7+}$ beams, the foci of γH2A.X were found in the irradiated cell in the target center colony. The foci of γH2A.X were also found in the unirradiated cells in the target center colony. These foci found in the unirradiated cells in the target colonies were abolished by the addition of NO radical scavenger, c-PTIO to the medium. These findings suggest that one of the bystander factors is NO radical.

3.2. Detection of γH2A.X in the bystander colony by immunochemical fluorescence staining

Six hours after irradiation with $^{20}Ne^{7+}$ beams, the foci of γH2A.X were found in the unirradiated cells in the bystander colonies. These foci found in the unirradiated cells in the bystander colony were abolished by the addition of NO radical scavenger, c-PTIO to the medium. These findings also suggest that one of soluble bystander factors excreted from the irradiated cells in the target colony is NO radical, which affect the unirradiated cells in the bystander colonies to form the foci of γH2A.X.

Collectively, our findings suggest that NO radicals as soluble bystander factors excreted from the irradiated cells in the target colony can induce single and double strand breaks of DNA in the unirradiated cells of the target and bystander colonies. We have previously reported that nitric oxide excreted from the irradiated cells with X-rays or carbon beams is an initiator and mediator of the radiation-induced bystander effect[2,3]. Further, we must elucidate the bystander factors induced by microbeams of $^{20}Ne^{7+}$ in the present study.

References

1) Funayama T, Wada S, Kobayashi Y, Watanabe H: Irradiation of mammalian cultured cells with collimated heavy-ion microbeam. *Radiat Res*, **163**: 241-246, 2005.

2) Matsumoto, H., Hayashi S., Hatashita M., Shioura H., Ohtsubo T., Kitai R., Ohnishi T., Yukawa O., Furusawa Y., Kano E.: Induction of radioresistance to accelerated carbon-ion beams in recipient cells by nitric oxide excreted from irradiated cells of human glioblastoma. Int. J. Radiat. Biol., 76: 1649-1657, 2000.

3) Matsumoto H., Hayashi S., Hatashita M., Ohnishi K., Shioura H., Ohtsubo T., Kitai R., Ohnishi T., Kano E.: Induction of radio-resistance by nitric oxide-mediated bystander effect. Radiat. Res., 155: 387-396, 2001.

2.32 Relationships between RBE and LET in Larvae of an Anhydrobiotic Insect, *Polypedilum vanderplanki*

M. Watanabe*, T. Kikawada*, Y. Nakahara, D. Horikawa*, T. Okuda*, T. Sakashita**, S. Wada**, T. Funayama** and Y.Kobayashi**
Department of Physiology and Genetic Regulation, National Institute of Agrobiological Sciences*
Department of Ion-beam-applied Biology, JAERI**

1. Introduction

Anhydrobiosis is the state in which an organism can tolerate complete desiccation and can survive for an extended period[1]. An African chironomid, *Polypedilum vanderplanki*, is the highest and largest multicellular animal entering anhydrobiotic state. The anhydrobiotic larva can survive, even in exposure to extreme temperatures such as –270 or 103℃, prolonged dry preservation for 17 years, high dose gamma-ray irradiation up to 7,000 Gy, and vacuum [2), 3), 4)].

These facts suggest that the desiccated larvae can survive also in outer space, where ionizing radiation, especially high-LET radiation (heavy ion beams), causes death of unprotected life. To investigate the resistance of *P. vanderplanki* to heavy-ion beams in the present study, we compared impacts of gamma ray and three kinds of high-energy ion-beams on larval survival and the following metamorphosis

2. Experimental procedure

2.1 Insect rearing and preparation for irradiation

P. vanderplanki was reared for successive generations under controlled light (13 h light: 11 h dark) and temperature (27 °C). The detail methods for rearing were described in Watanabe et al. (2002) [5)]. Last instar larvae around 1 mg wet body weight were used for all irradiation experiments. The larvae that had never experienced desiccation (Wet samples) were placed in a group on a moistened filter paper (diameter 4.7 cm) in a plastic Petri dish (diameter 5 cm, height 1 cm). The dish containing larvae was covered by a polyimide film (7 μm in thickness, Kapton®, Dupont-Toray, Tokyo). The anhydrobiotic larvae that had completely desiccated (Dry samples) were put between two pieces of polyimide film and covered on a Petri dish. These dishes were sealed with a Parafilm (Pechiney Plastic Packaging, Inc., Chicago, IL).

2.2 Irradiation

Wet and dry samples were exposed to $^{4}He^{2+}$ (50 MeV), $^{12}C^{5+}$ (220 MeV) or $^{20}Ne^{8+}$ (350 MeV) ion-beams from AVF cyclotron accelerator at TIARA or gamma rays from the Co-60 source at Food irradiation facility in JAERI-Takasaki. The liner energy transfer (LET) was 0.2 keV/μm in ^{60}Co gamma rays, 16.2 keV/μm in $^{4}He^{2+}$ beam, 116 keV/μm in $^{12}C^{5+}$ beam and 321 keV/μm in $^{20}Ne^{8+}$ beam. The irradiation dose ranges from 1 to 9000 Gy on gamma ray and from 1 to 7000 Gy on ion-beams.

2.3 Evaluation of biological effects

Wet samples were submerged in distilled water soon after irradiation, and examined their survival at 48 h after irradiation. Irradiated dry-samples were put in distilled water within 8 hours after irradiation, and checked their survival at 48 h after rehydration. The survivors

were reared on milk (2% w/v)-agar (1% w/v) in a glass container (ca. 600 ml), and examined their fate.

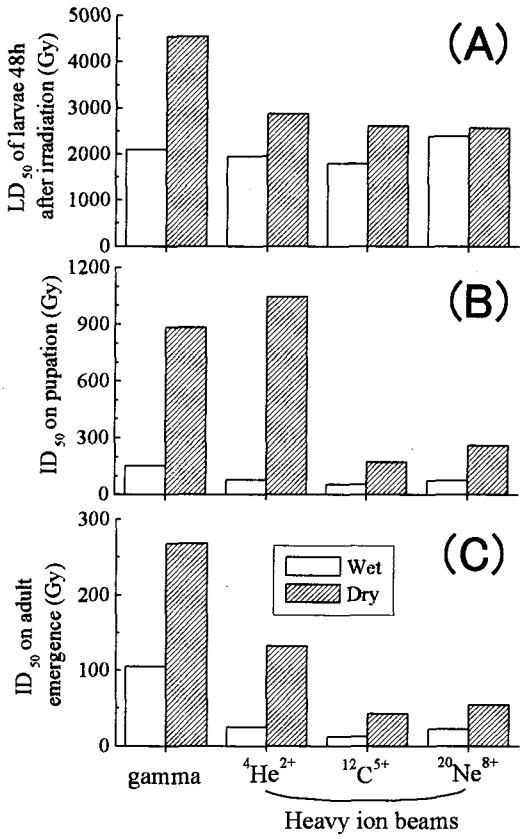

Fig.1 Biological effects of gamma and three kinds of heavy-ion beams on *P. vanderplanki*. 50% lethal dose (LD50) of larvae (A), 50% inhibitory dose (ID50) of pupation (B) and adult emergence (C).

3. Results and Discussion

Results of irradiation were shown in Fig. 1. Overall, dry samples were more tolerant against both gamma rays and high-energy ion beams in larval survival than wet ones. Such trends became prominent in pupation and adult emergence.

Based on these data, relative biological effectiveness (RBE) values for larval survival, pupation and adult emergence were estimated by using gamma rays as a standard radiation (Table 1). In all cases, regardless of dry or wet, the RBE values increased as liner energy transfer (LET) rose up to 116 keV/μm, and decreased at 321 keV/μm. This result coincides with general tendency that RBE peaks around 100 keV/μm of LET [6].

RBE values typically increased as the developmental stage progressed. For example, the RBE values obtained by $^{12}C^{5+}$ ion beam (LET: 116 keV/μm) were 1.6 and 1.7 in larval survival, 2.9 and 5.1 in pupation, and 6.3 and 8.1 in adult emergence of wet and dry samples. During metamorphosis, insects undergo tissue remodeling from developmental phase to reproductive phase, which is accompanied by active gene-expressions and vigorous cell differentiation and proliferation[7]. On the other hand, de novo protein synthesis and cell proliferation seem to be unnecessary during revival from anhydrobiosis of *P. vanderplanki*

Table 1 Relationships between LET and RBE in *P. vanderplanki*

	LET	RBE					
		Larval survival		Pupation		Adult emergence	
	(keV/μm)	Wet	Dry	Wet	Dry	Wet	Dry
gamma	0.2	1	1	1	1	1	1
$^{4}He^{2+}$	16.2	1.1	1.6	1.9	0.8	4.3	2.0
$^{12}C^{5+}$	116.0	1.6	1.7	2.9	5.1	8.1	6.3
$^{20}Ne^{8+}$	321.0	0.9	1.7	2.0	3.4	4.6	4.9

larvae. Therefore, it is suggested that gene expression and cell cycle are more susceptible to damage by high LET radiations.

Whereas the half inhibitory dose for adult emergence of wet samples was similar to those of the other non-anhydrobiotic insects[8], anhydrobiosis provided radioresistance to *P. vanderplanki* larvae (Fig. 1), suggesting that *P. vanderplanki* has higher possibility to survive exposure of cosmic ray than the other non-anhydrobiotic insects. It might be concluded that extremely low water content (ca. 3%) and extremely high content of trehalose (ca. 20%) in the anhydrobiotic larvae contribute to increase of radiation tolerance; low generation of free radicals in the former and an effective radiation protectant on DNA break in the latter[9]. As *P. vanderplanki* will not be exposed so high dose of radiation in nature, why and how they have acquired the higher radioresistance is an open question. Further studies are needed to understand the biological significance of the character in the anhydrobiotic *P. vanderplanki* larvae.

References

1) Clegg, J. S., Comp. Biochem. Physiol. B. 128 (2001) 613-624.

2) Hinton, H. E., J. Insect Physiol. 5 (1960) 286-300.

3) Adams, S., Antenna 8 (1985) 58-61.

4) Watanabe, M., T. Okuda, A. Fujita, T. Kikawada, T. Sakashita, S. Wada, T. Funayama and Y. Kobayashi, JAERI-Review 25 (2004) 103-105.

5) Watanabe, M., T. Kikawada, N. Minagawa, F. Yukuhiro, T. Okuda, J. Exp. Biol. 205 (2002) 2799-2802.

6) Hall, E. J. Radiology for the Radiologist, Medical Department, Harper & Row Publishers, New York (1978).

7) Riddiford, L. M., K. Hiruma, X. Zhou, C. A. Nelson, Insect Biochem. Mol. Biol. 33 (2003) 1327-1338.

8) Hirano, T. Shokubutsu Boeki 18 (1964) 189-195.

9) Yoshinaga K., H. Yoshioka, H. Kurosaki, M. Hirasawa, M. Uriytani, K. Hassegawa, Biosci. Biothech. Biochem. 61 (1997) 160-161.